Continuous Monitoring of Mechanical Properties of Plantar Soft Tissue Using Wearable Ultrasonic and Force Sensors for Diabetic patients

By

Fatemeh Zabihollahy

A thesis submitted to the Faculty of Graduate Studies and Research in partial fulfillment of the requirements for the degree of

Masters of Applied Science in Biomedical Engineering

Ottawa-Carleton Institute for Biomedical Engineering

Department of Systems and Computer Engineering

Carleton University

Ottawa, Ontario, Canada

August 2016

The undersigned recommend to the Faculty of Graduate Studies and Research acceptance of the thesis

Continuous Monitoring of Mechanical Properties of Plantar Soft Tissue Using Wearable Ultrasonic and Force Sensors for Diabetic patients

Submitted by Fatemeh Zabihollahy

in partial fulfillment of the requirements for the degree of Master of Applied Science in Biomedical Engineering

Thesis Supervisor Dr. Yuu Ono,

Chair, Department of Systems and Computer Engineering

Dr. Yvan Labiche

2016, Carleton University

Abstract

Diabetic foot ulceration is one of the complications of diabetes mellitus. 15% of diabetic patients will develop foot ulcer in their lifetime and 85% of all amputations are the result of a non-healing diabetic foot ulcer. One of the reasons of diabetic ulcers is neuropathy in which the nerves of foot are damaged and diabetic patients cannot feel the pain. Since pain is not a common symptom in those patients it is probable that they injure their feet and never know that, which leads to foot ulcer formation. Researches indicate that ulcers begin from the underlying tissue where soft tissues become stiffer. Thus tissue stiffness monitoring may be useful and important in preventing ulcer formation. In this research a wearable sensor for continuous monitoring of mechanical properties of plantar soft tissue at heel region was developed and tested. Thin and flexible force and ultrasonic sensors were used for measuring applied pressure to the plantar soft tissue and its resulting displacement respectively. The performance of the developed sensor was first evaluated using soft tissue mimicking phantoms, and then *in-vivo* experiment was conducted while the participant was stepping. The applied pressure and its resulting displacement of plantar soft tissue at the heel of a healthy subject were measured simultaneously over a period of time. Pressure-displacement curve for one load-unload cycle of plantar soft tissue was successfully extracted where certain tissue mechanical properties such as Young's modulus and stiffness are computable. This study offers a method for continuous monitoring of plantar soft tissue mechanical properties in diabetic patients with neuropathy. Although the focus of this research was on the diabetic foot, the proposed method can be used for continuous monitoring of any pressurized soft tissue in the body.

Acknowledgements

I would first like to thank my thesis supervisor Dr. Yuu Ono, Associate Professor of Systems and Computer Engineering, Carleton University for his wonderful collaboration. I appreciate his time and effort that he provided me throughout my graduate studies and his assistance in writing thesis.

Besides, I would like to thank Dr. Edward Lemaire, Full Professor of Physical Medicine and Rehabilitation, University of Ottawa for his insightful comments, which incented me to widen my research from various perspectives.

I would also like to express my gratitude to Dr. Bruno M. Trindade, a postdoctoral fellow of System and Computer Engineering, Carleton University who provided me with direction and technical support. I am gratefully indebted to him for his very valuable comments on this thesis.

I am grateful to my colleagues Zhen Qu, Ibrahim AlMohimeed and Andy Huang for their help and time during the years of study. They were always willing to share their knowledge and experiences.

I would also like to acknowledge Carleton University and Natural Sciences and Engineering Research Council of Canada (NSERC) for the opportunity and financial support provided for the research.

Finally, I must express my very profound gratitude to my husband and daughter and to my parents for providing me with unfailing support and continuous encouragement throughout my years of study and through the process of researching and writing this thesis. This accomplishment would not have been possible without them.

Table of Contents

List of Tables

List of Figures

List of Abbreviations

Abbreviation	Definition
2-D	Two-dimensional
A-Mode	Amplitude Modality of ultrasound imaging
ARFI	Acoustic Radiation Force Impulse Imaging
ARM	Advanced RISC Machines
B-Mode	White Gaussian Noise Brightness Modality
CPU	Central Processing Unit
DSP	Digital Signal Processing
GBWP	Gain Bandwidth Product
M-Mode	Maximum Motion Modality of ultrasound
MR	Magnetic Resonance
MRE	Magnetic Resonance Elastography
MRI	Magnetic Resonance Imaging
PSF	Point Spread Function
PVDF	Polyvinylidene Fluride
PZT	Lead Zirconate Titanate
RF	Radio Frequency
RMS	Root Mean Square
R-Square	Coefficient of Determination
RSD	Relative Standard Deviation
sd	Standard Deviation
SNR	Signal to Noise Ratio
SSI	Supersonic Shear Imaging
SWE	Shear Wave Elastography
SWEI	Shear Wave Elasticity Imaging
TUPS	Tissue Ultrasound Palpation System

List of Symbols

Abbreviation	Definition	SI Units
A	Area	Square Meter (m^2)
A_0	Amplitude of Reflected RF Ultrasonic Signal	
A_z	Initial Amplitude of RF Ultrasonic Signal	
c	Speed of Ultrasound Wave	Meter per second ($m.s^{-1}$)
d	Distance	Meter (m)
Δd	Displacement	Meter (m)
Δl	Displacement	Meter (m)
E	Young's Modulus	Pascal (Pa)
E(t)	Envelope of Signal	
ε	Stress	Pascal (Pa)
F	Force	Newton (N)
I	Electric Current	Ampere (A)
K	Stiffness	Newton per meter ($N.m^{-1}$)
μ	Amplitude Attenuation Coefficient	
P_n	n^{th} Position	
ϱ	Density	Kilogram per cubic meter ($Kg.\ m^{-3}$)
R	Coefficient of Reflection	-
R_F	Feedback Resistance	Ohm (Ω)
R_S	Sensor Resistance	Ohm (Ω)
σ	Strain	-
t	Time	Second (sec)
T	Coefficient of Transmission	-
V	Electric Potential	Volt (V)
V_T	Drive Voltage	Volt (V)
V_{DD}	Positive supply voltage	Volt (V)
V_{out}	Output Voltage	Volt (V)
y(t)	Signal	
$\hat{y}(t)$	Hilbert Transform of y(t)	
Z	Acoustic Impedance	Kilogram per second per square meter ($Kg.\ s^{-1}.m^{-2}$)

Chapter 1: Introduction

In this chapter an overview of the thesis is provided along with its objectives. In addition thesis contribution and organization is outlined.

1.1 Overview

For centuries physicians have used palpation for medical examination because often tissue are going to be stiffer in disease conditions and the elastic moduli of abnormal soft tissue may increase up to several times [1], [2]. As an example the difference in stiffness of plantar soft tissue in diabetic patients with neuropathy in comparison with healthy people are significant and diabetic people with neuropathy tend to have stiffer plantar tissues ($p<0.01$) [3]. It implied the necessity of precise and accurate method for measuring the stiffness of tissue in human bodies. In this thesis a stiffness measurement system including wearable force and displacement sensors were developed and its performance for tissue displacement measurement was evaluated. In addition continuous monitoring of mechanical properties of plantar soft tissue at heel part was performed over a period of time. In this thesis work, *in-vivo* measurements were done on the plantar soft tissue at heel region because the focus of this study is on diabetic patients where the heel is a high-risk area for foot ulceration but monitoring of soft tissue mechanical properties could be beneficial for other applications such as prosthetic and orthotic fitting, sport performance monitoring, bedsore and other skin injury prevention and detection.

1.2 Problem Statement

Diabetic foot ulceration is one of the complications of diabetes mellitus. Diabetic foot ulcers treatment is challenging and costly and mostly wound healing takes long time. Fifteen percent of diabetic patients will develop a foot ulcer in their lifetime and 85% of

all amputations are the result of a non-healing diabetic foot ulcer [4]. Anyone who has diabetes may develop a foot ulcer during his/her lifetime. This skin breakdown originates in microvascular disease and forms due to a combination of factors such as, poor circulation, foot deformities, lack of feeling in the foot, and irritation (such as pressure or pressure in combination with shear and/or friction). People who have had diabetes for many years may develop neuropathy, a reduction or loss of the ability to feel forces on the skin due to nerve damage caused by elevated blood glucose levels over time [5]. Since many people with neuropathy cannot feel pain in their feet, non-detected plantar tissue injuries may lead to foot ulceration over time.

It is also known that plantar soft tissue mechanical properties in people with diabetes change and become stiffer in certain areas, which are under pressure [6]. According to the research that has been done in 2010 [7] the total thickness of plantar soft tissue is increased by 8% in diabetic individuals at certain sites ($p<0.05$) include the big toe, the third and fifth metatarsal heads; and the heel pad while Sun *et al*. [3] showed that the thickness of plantar soft tissue does not change significantly in diabetic subject in comparison with healthy group and the difference of stiffness is significant ($p<0.01$). Therefore, it is useful and important to monitor stiffness of plantar soft tissues for diabetic people, verify changes in mechanical properties during daily activities, and warn them regarding the probability of foot ulcer formation.

Several investigations have been conducted to develop methods for soft tissue stiffness measurements that will be described in detail in the section 2.3.2. All of these methods are in-clinic procedures and the measurement is not continuous. Since pain is not a common symptom in foot ulcers in diabetes with neuropathy, continuous monitoring of

plantar soft tissue mechanical properties could be a good option to warn patients regarding the potential of ulcer formation.

1.3 Objectives

The main goal of this thesis is to develop a wearable ultrasonic stiffness sensor for monitoring the mechanical properties of soft tissues using thin and flexible force and displacement sensors and to evaluate its performance using some tissue-mimicking phantoms. While this research focused on the diabetic foot, the investigated technology can be used to monitor the mechanical properties of any soft tissue in the body, such as within a prosthetic socks or a cast.

1.4 Proposed Method

In this study, plantar soft tissue mechanical properties are estimated using wearable sensors. A polyvinylidene fluoride (PVDF) piezoelectric polymer film ultrasonic sensor [8] along with a pressure sensor was used to estimate strain and stress, respectively. Sensors were placed beneath the heel since the heel is a high-risk area for foot ulceration in diabetes.

A thin and flexible force sensor (FlexiForce, 0.203 mm thick, TekScan, South Boston, USA) was calibrated and integrated into this measurement system for pressure examination.

A PVDF ultrasonic sensor was used to estimate tissue displacement due to the body weight by means of an ultrasonic pulse echo method. Tissue displacement was obtained from a time delay change of ultrasonic RF signals reflected from a desired tissue boundary. The PVDF ultrasonic sensor is light and thin, thus non-invasive continuous

monitoring of plantar soft tissue thickness may be possible during walking, which is difficult using a conventional ultrasonic probe [9].

A pressure-displacement curve for plantar soft tissue was extracted, which represents tissue mechanical behavior. Before conducting *in-vivo* tests, phantom simulation experiments were conducted to investigate the performance of the developed measurement system. Phantom experiments helped to choose a proper digital signal processing (DSP) method for continuous monitoring of tissue mechanical properties. In addition DSP techniques were applied to remove outliers in displacement measurement.

By continuous monitoring of mechanical properties of plantar soft tissues, it may be possible to predict the foot ulcer formation in the early stages. In other words, this proposed method may be preventive, which is valuable and efficient because treatment of foot ulceration takes so long and in most cases ulcers will not heal and become a chronic wounds [10]. Also, this method does not impose any risk to the patient because in this method ultrasound wave is used for tissue displacement observation, which does not have any radiation exposure. Furthermore, this technique is non-invasive and does not irritate the patients. The sensors used are very thin and flexible, and should not cause any harm to the patient's foot.

1.5 Thesis Contributions

The following is a list of main contribution of this thesis and will be explained in details further:

- A wearable ultrasonic stiffness sensor using a combination of thin and flexible force and displacement sensors was developed.

- An algorithm for monitoring of soft tissue mechanical properties over a period of time using new wearable ultrasonic stiffness sensor was developed.
- The performance of PVDF ultrasonic sensor for soft tissue displacement measurement using some soft-tissue mimicking phantoms was evaluated.
- The signal-to-noise ratio of the PVDF ultrasonic sensor was estimated.
- Four different ultrasonic digital signal processing methods for extracting tissue displacement information were compared and accuracy and repeatability of PVDF transducer was discussed for each method.
- The hysteresis of PVDF transducer was examined through cross-correlation technique.
- The effect of uneven load on measuring system was evaluated and a method for track and remove outliers in continuous tissue displacement measurement was proposed.
- In-vivo measurement of plantar soft tissue mechanical properties at heel region was performed and pressure-displacement curve for one load-unload cycle was extracted.

1.6 Thesis Organization

Chapter 1 presents the topic discussed in this thesis.

Chapter 2 provides an overview of foot structure and diabetic foot ulceration along with the main causes of diabetic ulcer formation. This chapter provides general technical background on ultrasound principle and different ultrasonic methods for tissue

displacement measurement.

Chapter 3 describes stiffness measurement system. In this chapter the calibration of force sensor and important parameters that should be considered in stress examination are discussed. Besides the displacement sensor is also introduced.

Chapter 4 evaluates the performance of stiffness measurement system using silicone rubber phantom and pork sirloin.

Chapter 5 pertains to *in-vivo* experiments to develop a method for continuous monitoring of plantar soft tissue mechanical properties over a period of time. It describes experimental method and results along with required signal processing for continuous monitoring of applied force to the plantar soft tissue and its resulting displacement.

Chapter 6 concludes this thesis by summarizing obtained results. It includes a list of recommendations for future research.

Chapter 2: Technical Background Review

In this chapter, an introduction into the foot structure is provided. The mechanical properties of material and different methods for tissue stiffness estimation are described as well. Afterward the diabetic foot ulcer and its main causes along with current methods and researches for plantar fascia mechanical properties examination are discussed. Finally the theories of ultrasound and ultrasonic techniques for tissue displacement measurement are explained briefly.

2.1 Foot Structure

The human foot is a complex structure that is made up of bones, muscles, tendons, ligaments, skin, nerves and blood vessels. This flexible structure let human walk, run, jump and stand upright during normal daily activities.

2.1.1 Foot Muscles, Tendons and Ligaments [11]

In human bodies, a network of muscles, tendons and ligaments support the bones. There are 20 muscles that hold the bones and give shape to the foot. The main muscles of foot are: anterior tibial, posterior tibial, peroneal tibial, extensors and flexors.

Tendons, which are elastic tissue, connect muscles to the bones. The largest and strongest tendon of foot is the Achilles tendon.

Ligaments hold the tendons in place. The longest ligament of the foot is plantar fascia, which will be described in detail in the section 2.1.3.

Skin, nerves and blood vessels of the foot provide cell regeneration, nourish the muscles and control the movement.

2.1.2 Foot Bone Anatomy

About 26 bones support this organ and help it to keep its shape and gesture. These bones are grouped into three parts:

The tarsal bones (7)

The metatarsal bones (5)

The phalanges (14)

The foot itself is divided into three parts: forefoot, mid-foot, and hind-foot. The forefoot is composed of the metatarsals and the phalanges. The mid-foot includes the rest of the tarsal bones; and the hind-foot contains 2 of the 7 tarsal bones, the talus, and the calcaneus as shown in Fig. 2.1 [12-13].

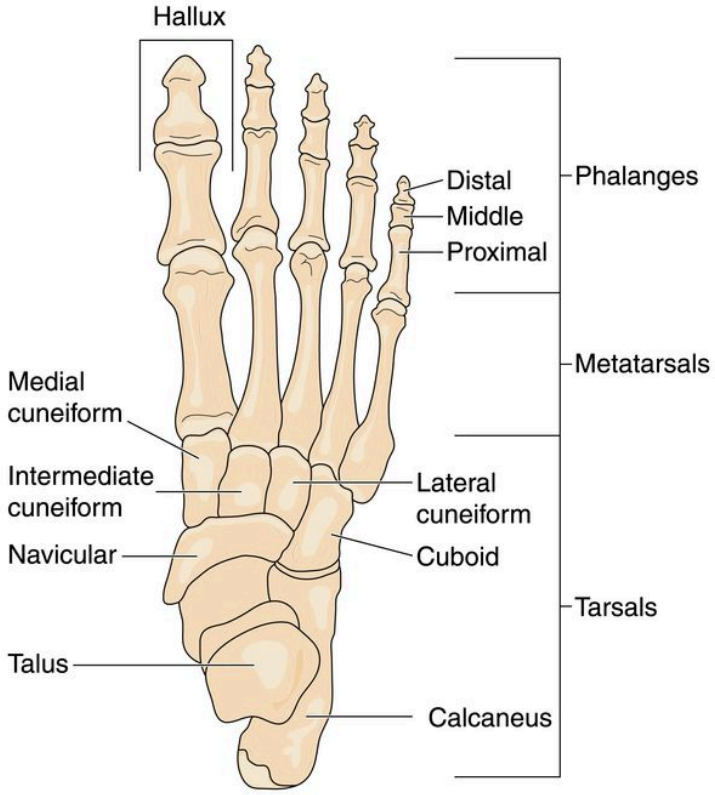

Figure 2.1 Foot bone anatomy [14]

2.1.3 Plantar Fascia

The plantar fascia is a thick connective tissue that runs from the bottom of calcaneus (heel bone) forward to the heads of the metatarsal bones (the bone between each toe and the bones of the mid-foot) as shown in Figs. 2.2 and 2.3 and its main function is to support the plantar side of the foot where it undergoes tension when the foot bears weight [15]. It is estimated that plantar fascia carries as much as 14% of the total load of the foot [16]. Extension of the toes and depression of the foot arch both cause tension in plantar fascia. Plantar fascia bears a lot of stress but it is not invincible and too much load causes irritation on it [17].

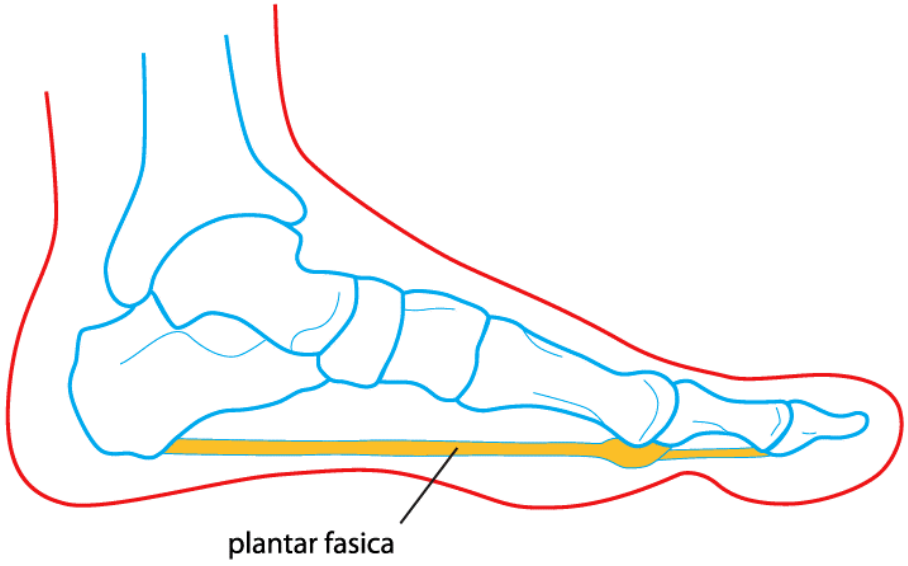

Figure 2.2 Plantar fascia [18]

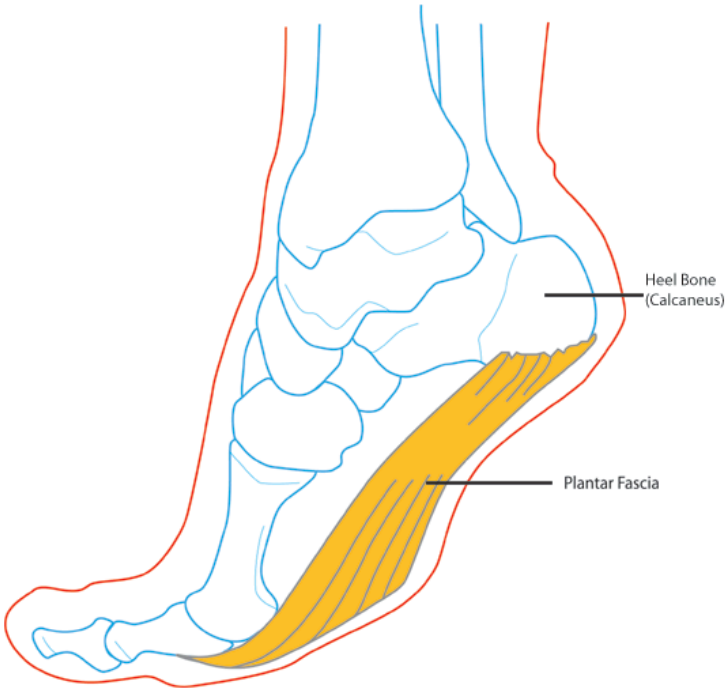

Figure 2.3 Plantar fascia, a thick connective tissue that runs from the bottom of calcaneus to the heads of the metatarsal bones [19]

Characterizing the mechanical properties of plantar fascia is important in pathology. For example, the inflammation of fascia is common in runners and in diabetes patient the stiffness of plantar fascia changes over time [20].

2.2 Mechanical Properties of Materials

The material's response to unidirectional stress provides an overview of mechanical properties. The most common properties considered are stiffness and Young's modulus. Hardness, compressibility or stiffness is the degree, to which an object resists against deformation in response to an applied force [21], [22]. Stiffness, K, has the units of force per unit length with the SI unit of Newton per meter ($N.m^{-1}$) and is defined as below:

$$K = F / \Delta l \qquad (2.1)$$

Where F is force and Δl is displacement.

Young's modulus, E, or elastic modulus is a mechanical property of linear elastic solid material. Young's modulus is defined as follows and its SI unit is Pascal (Pa):

$$E = \varepsilon / \sigma \qquad (2.2)$$

where ε and σ are stress and strain respectively. ε is obtained by dividing force by the measurement area, A, and σ is defined as ratio of displacement and initial thickness, l_0, as seen in Eqs. 2.3 and 2.4.

$$\varepsilon = F / A \qquad (2.3)$$

$$\sigma = \Delta l / l_0 \qquad (2.4)$$

The SI unit of stress is newton per square meter ($N.m^{-2}$).

Thus, to quantify mechanical properties of soft tissue, force and displacement must be measured as they are fundamental parameters and other parameters such as stiffness, strain, stress and Young's modulus could be computed using them.

2.2.1 Methods to Characterize Tissue Stiffness

Often soft tissues become stiffer in disease condition and physicians have used palpation for stiffness examination. As an example for abnormal tissue, the elastic moduli of breast tumors may differ 90-fold from its surrounding tissues [1], [2]. So it is useful to develop precise and accurate method for measuring the stiffness of tissue quantitatively in human bodies. Nowadays there are several methods for estimating tissue hardness. Some of them measure physical parameters such as stiffness and Young's modulus and others use image to obtain soft tissue stiffness. They apply internal or external stress to tissue and detect the resulting strain to examine mechanical properties of tissue.

Tissue excitation, which is performed to create displacement in the tissue, can be internal or external. In external methods force is applied to the desired area from the top of skin

while in internal methods excitation is applied internally within the desired tissue [21]. For example ultrasound can be used as a tool for radiation force generation inside the tissue [23]. Excitation methods can be also classified based on their temporal characteristics into quasi-static and continuous. In quasi-static methods a constant force is applied to the tissue and the resulting displacement is measured while in continuous methods the value of applied force changes with time. These methods are explained in details in appendix B. In this thesis continuous method is used to characterize the mechanical properties of plantar soft tissue.

There are several methods for strain detection. Ultrasound, acoustic, and MRI are the main techniques among them. In ultrasound the strain is estimated using either Doppler or pulse-echo techniques [21]. Acoustic methods examine the sound resulting from tissue vibration. In this method a vibration is created inside the object using ultrasound-stimulation and a sensitive microphone detects the acoustic field resulting from object vibration to form an image [24]. In MR technique displacement distribution in tissue is detected using a phase-sensitive MR machine [25].

Elasticity imaging methods are classified based on their excitation and detection approaches.

External excitation for ultrasound strain images was developed in 1991 by Ophir *et al*. and called elastography [26]. Dickinson et.al [27] and Wilson et.al [28] used ultrasound for examining displacement and deformation near blood vessels for the first time. They did the measurement by tracking the echo movement that resulted from cardiac contraction and pulsatile blood flow. In this method the elastic properties of tissue was acquired under the quasi-static condition. Nowadays improved two-dimensional (2-D)

analyses are substituted A-scan and M-mode analyses of endogenous tissue motion for strain imaging in measuring vascular elasticity locally and non-invasively [29]. MRI-based methods for strain detection in elastography called MR Elastography (MRE). Kevin J. Glaser *et al*. summarized some of the recent application of MRE [30].

Some medical applications of elastography in the literature include tumor detection [31], characterization of vascular plaques [32], assessment of vascular health [33], study of skeletal muscle contraction [34], assessment of fetal lung maturity [35], renal transplant rejection [36], assessment of liver fibrosis [37, 38], musculoskeletal pathology [39-40], breast diseases [41].

This thesis is based on the elastography technique. Its difference with elastography is that in this study we do not take a 2-D B-mode image. Instead we take M-mode image with an ultrasonic sensor having a single ultrasonic transducer. We observe tissue displacement at a chosen tissue area of interest continuously while the force is applied. Proper signal processing is done for plantar tissue stiffness measurement at heel region in continuous mode. For taking B-mode image we need an ultrasonic transducer array sensor, which is beyond the scope of this thesis research. Ultrasound elastography techniques are summarized in details in Appendix B.

2.3 Diabetic Foot Ulceration

Diabetic foot ulceration is the development of foot sores in diabetic patients. It is an open sore where the skin of the foot has broken down and the underlying tissues are visible. Foot ulceration in diabetes is common and disabling and often leads to the leg amputation.

2.3.1 Main Causes of Diabetic Foot Ulcer Formation

Anyone who has diabetes may develop a foot ulcer during his/her lifetime. Skin breakdown originates in microvascular disease and forms due to a combination of factors such as irritation (such as pressure or pressure in combination with shear and/or friction), peripheral neuropathy, circulatory problem and foot deformities [10].

Irritation

Nowadays it is known that prolonged pressure on the plantar soft tissue is one of the factors that cause foot ulcers. Then certain electronic pressure monitoring systems are developed that could be placed in the shoes to monitor the pressure of plantar soft tissue in some parts to provide evidence on ulcer formation [42-43].

Susan Stacpoole-Shea *et al*. evaluated pressure-time parameters on the sole of the foot to predict sites of pathology in diabetics. In this study a preliminary model from peak pressure and pressure-time integral of plantar foot measurement in diabetic patient with sever neuropathy and forefoot ulceration was introduced, which discriminate accurately between known ulcer locations in 72.7% of subjects [44]. Also the plantar pressure distribution in normal and diabetic subjects, with and without neuropathy, was evaluated by measuring certain pedobarographic parameters such as the total plantar force, total contact area and peak pressures during normal walking and it was found that pressure distribution measurement techniques are useful for analyzing the mechanical behavior of the human foot [45]. Certain researches were done to examine the pressure of plantar soft tissue at special places such as heel, big toe and metatarsophalangeal joint [46-47].

Peripheral Neuropathy

In this case the nerves of the feet are damaged and cannot sense the pain or pressure that exists in the feet. Pain may rise from tight-fitting shoes, stepping on sharp things or existing an irritating pebble in the shoes. Since patients cannot feel the pain in their feet, it is possible that they injure their feet without their knowledge. The only way to prevent the development of injuries and ulcer formation is through a routine examination and observation, which is impossible for individuals with visual impairments.

Circulatory Problems

Poor circulation in the feet not only causes the skin to be more vulnerable to injuries due to less transport of oxygen in cells, but also decreases the wound healing procedure.

Foot Deformities (Abnormalities in the Bones of the Feet)

Some conditions such as tight-fitting shoes may result in foot's bone deformation, which leads to the foot ulcers.

2.3.2 Current Diagnosis Methods and Researches

Since neuropathy is one of the reasons of ulcer formation in diabetic patients and occurs in 58% of patients with longstanding disease [48], to examine the potential of ulcer formation, the risk of neuropathy is investigated through some screening methods. These methods screen the presence or absence of neuropathy.

One rapid method is nylon monofilament test. In this test a monofilament pressed against the foot to the extent that bends the filament as shown in Fig. 2.4. If patient cannot sense the monofilament when it is pressed, there is a risk of ulcer formation.

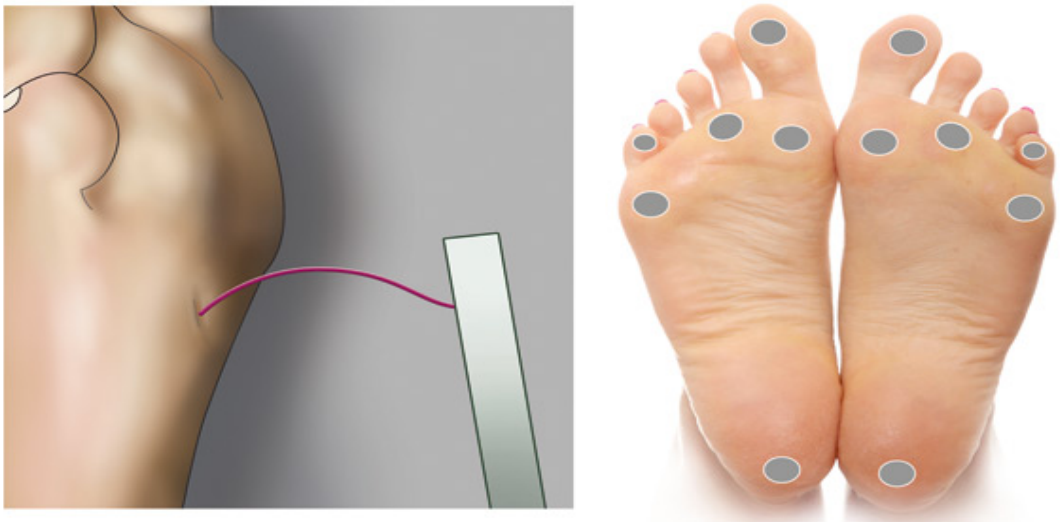

Figure 2.4 Nylon Monofilament Test [49]

Another neuropathy screening method is vibration sensory exam that is performed using vibration tuning fork as seen in Fig. 2.5. In this method a vibration is created on top of the foot's skin using tuning fork and if patient cannot understand the vibration with closed eyes, there is a potential of neuropathy and ulcer formation as well.

Figure 2.5 Vibration tuning fork used to evaluate neuropathy in diabetic patients [50].

These methods are currently conducted by health professionals in clinics and hospitals. There are some other methods, which are in research stages and have not been placed in the market yet. Those techniques that are explained briefly in the following, investigate the potential of ulcer formation directly by studying the mechanical behavior of soft tissue.

Research works indicate that compressive and shear mechanical properties of the plantar soft tissue with diabetes change and mostly this disease condition makes plantar tissue stiffer, which may increase ulceration risk [6]. Therefore, it is important to estimate stiffness of plantar soft tissue in diabetic individuals. Several investigations have been conducted to develop methods for such measurements. In those investigations MRI [51] and ultrasound are used to quantify the mechanical properties of soft tissue. In the section 2.3.3, the results of some research works where ultrasound was used as a tool for displacement estimation are summarized.

2.3.3 Ultrasound Diagnostic Method

Y.P. Zheng *et al*. have developed a foot scanner incorporating a tissue ultrasound palpation (indentation) system (TUPS) to assess the mechanical properties of plantar soft tissues under different body-weight loading in real time manner. In this foot scanner, TUPS was a 25-N load cell with a 5 MHz ultrasound transducer in series that was applied to indent soft tissue and to measure tissue initial thickness and deformation respectively. The results of *in-vivo* experiment on ten normal subjects at heel region show that the thickness decreased by 12.0% (from 13.83 ± 2.52 mm to 12.10 ± 1.95 mm) while the stiffness (in terms of Young's modulus) increased by 83.4% (from 40.0 ± 20.7 kPa to 69.0 ± 26.0 kPa) when the loading increased from 0% to 80% of the bodyweight (both p

< 0.001) [52].

D. Parker *et al*. developed a soft tissue imaging device to apply a vertical compression to the plantar soft tissue and measure its mechanical response via a combined load cell and ultrasound imaging arrangement. The results indicate that the device is reliable for implementing complex loading patterns similar to gait, and for capturing the compressive response of the plantar soft tissue for a range of loading conditions *in-vivo* [53]. In other research works the compressive mechanical properties [54] and elastic and viscoelastic shear behaviour [55], [56] of plantar soft tissue in both diabetic and non-diabetic specimens from six relevant locations beneath the foot at hallux, first, third, and fifth metatarsal heads, lateral mid-foot, and calcaneus were determined.

In addition it has been shown that aging affects stiffness of plantar soft tissue at some region such as second metatarsal head [57-58].

2.4 Theory of Ultrasound

Ultrasound is a high frequency sound wave above 20,000 Hz that cannot be heard by human being. Medical ultrasound systems operate at frequencies between 1 and 10 MHz. Ultrasound propagates by expansion and compression of the material through which it moves. Speed of ultrasound propagation in solids depends on the medium it is moving through. Ultrasound waves are reflected or refracted at plane interfaces [59].

2.4.1 Pulse Echo Technique

In this technique an ultrasonic RF pulse is transmitted into the object and received echoes reflected from boundaries are studied. The time delay between transmitted pulse and the received echoes indicates the depth of reflective structures. Ultrasonic pulse-echo technique is used for tissue characterization. Object's thickness can be determined by:

$$d = \frac{c.\Delta t}{2} \qquad (2.5)$$

Where d is the depth of material, c is sound velocity and Δt is time delay between transmitted pulse and received echoes. In this formula t is the required time for round trip as shown in diagram Fig. 2.6.

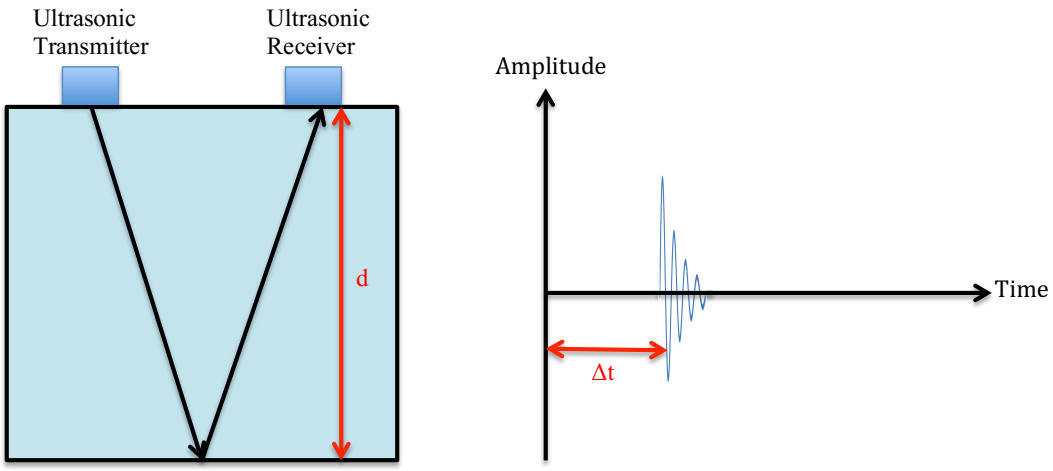

Figure 2.6 Ultrasound pulse-echo technique

2.4.2 Ultrasound Velocity

Velocity, c, of ultrasound waves depends on the density, ϱ, and stiffness of the material through which the ultrasound propagates [60-61].

$$c = \sqrt{\frac{K}{\rho}} \qquad (2.6)$$

For example the average of ultrasound velocity in bone and fat is 4080 $m.s^{-1}$ and 1450 $m.s^{-1}$ respectively [59].

2.4.3 Reflection Coefficient at Plane Interfaces

The acoustic impedance, Z, of a material is defined as the product of its density and sound velocity [59].

$$Z = \varrho c \qquad (2.7)$$

When an ultrasonic wave hits boundary of an object, some part of it gets transmitted and the rest part gets reflected as seen in Fig. 2.7. The coefficient of transmission, T, and reflection, R, of object depend on the acoustic impedance and determine as below respectively [59]:

$$T = 2Z2 / (Z1+Z2) \qquad (2.8)$$

$$R= (Z2-Z1) / (Z2+Z1) \qquad (2.9)$$

where Z1 and Z2 are acoustic impedance of the left and right objects in Fig. 2.7 respectively.

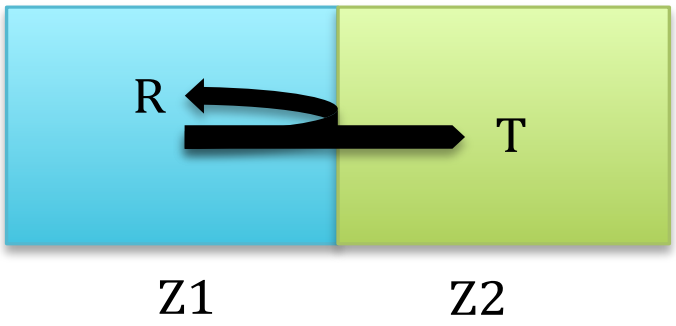

Figure 2.7 Transmission and reflection of an ultrasonic wave at plane interface

The acoustic impedance of body tissue is much bigger than that of the air. Then there is a large reflectivity at the body skin/air interface and only a small fraction of acoustic energy would enter into the body. An acoustic gel will remove the air and help to match the impedances of skin and ultrasonic transducer and transmit the pulse to the tissues.

2.4.4 Ultrasound Imaging Basics

Ultrasound is a non-invasive technique for imaging internal organs. Imaging helps to determine structures, composition, elasticity and density of tissues. Ultrasound systems

contain a piezoelectric transducer, which converts electrical signal to acoustic signals and vice versa. Piezoelectricity is a property of some materials that deform mechanically in the presence of an electrical field to generate ultrasound pulses and conversely, create electrical signal when deformed mechanically to detect a received echo. Examples of certain piezoelectric materials are quartz, lead zirconate titanate (PZT) and PVDF. When ultrasound waves hit organ boundaries, an echo is produced that return back to the transducer. By processing the received echoes some properties of tissues and organs are revealed [59].

From ultrasound wave velocity and time delay between transmitted and received echoes, the distance from ultrasound probe to reflection source can be determined. The ultrasound image is generated based on this distance information alongside the amplitude of received echoes [62].

The simplest type of ultrasound imaging is amplitude-mode or A-mode, where a single transducer scans a line through the body and echoes are plotted, as a function of depth. One application of this method is ophthalmology studies where the optic nerves and eye disorders are investigated.

B-mode or brightness mode is a two-dimensional ultrasound image where a linear array of transducers simultaneously scans a plane through the body. In other words, B-mode image is constructed from a series of A-mode signals. The brightness of each point in B-mode image is proportional to the returned ultrasonic echo amplitude. Multiple images give a realistic illusion of motion. The B-mode can be used for cardiac chamber dimensions measurement, lesion identification and anatomical structures visualization and quantification.

In M-mode or motion mode ultrasound RF signals are transmitted in quick succession and an A-mode or B-mode image is taken. In this mode the ultrasound beam is fixed and no scan is performed. M-mode is used for evaluation of rapidly moving structures such as cardiac valves and chamber walls.

2.5 Ultrasound Stiffness Measurement Principle

As described in section 2.2, stiffness is defined as force over displacement. As diagram of Fig. 2.8 shows when a vertical force is applied to a soft object, it deforms and its thickness changes. Then to find stiffness it is essential to measure the applied force and its resulting displacement.

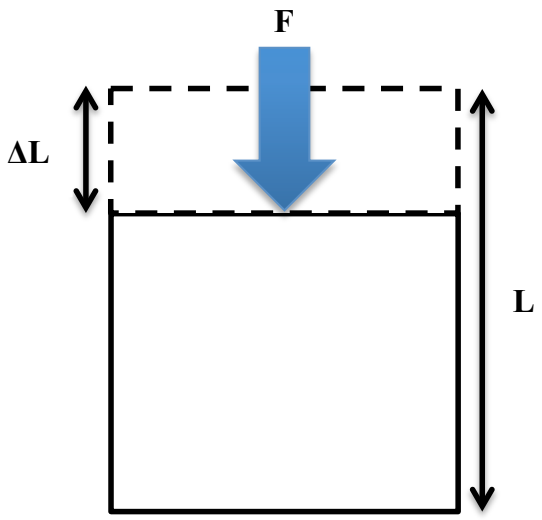

Figure 2.8 Schematic diagram of stiffness measurement

There are several tools for measuring displacement. In this study an ultrasonic method was used for displacement estimation through a pulse-echo technique.

Ultrasonic pulse-echo technique measures tissue thickness using time delay of ultrasonic RF signal reflected from desired tissue boundary. In this thesis a time-varying load is

applied to the plantar tissue. Then we measure the thickness changes of tissue over a period of time during the tissue compression-release cycle.

2.5.1 Tissue Displacement Measurement Using Ultrasound

Vertical displacement in tissues can be estimated using ultrasound, based on the change in measured time-of-flight of a target echo. Displacement can be estimated from different imaging modalities such as A-mode, B-mode or M-mode. In this thesis all displacement measurements are obtained in A-mode and M-mode. Four different techniques of estimating displacement from A-mode measurements are used in this thesis: position of positive peak of the echo, position of peak in absolute value of signal, position of the largest peak in envelope and cross-correlation. All techniques estimate vertical displacement directly from received ultrasound signals in time domain.

2.5.1.1 Position of Positive Peak of the Echo

In this technique location of positive peak in RF ultrasound signal indicates the depth of tissue where transmitted echo hits the boundary of tissue and bone. This method is simple but as will be shown it is not accurate enough for soft tissue displacement estimation.

2.5.1.2 Position of Peak in Absolute Value of Signal

Amplitude of returned echo from interfaces may be positive or negative, which depends on the acoustic impedance of mediums that echo moves through. If acoustic impedance of second medium is bigger than acoustic impedance of first medium reflection coefficient will be negative, which means reflected echo has 180° phase shift.

In this case received echo may have negative amplitude, depending on the phase of the transmitted signal, and looking at positive peak creates an error in displacement

measurement. In position of peak in absolute value technique, first the absolute value of ultrasound RF signal is calculated and the place of largest peak is considered for subsequent process.

2.5.1.3 Position of the Largest Peak in Envelope

The envelope of ultrasound signal is in fact the outlines of signal and envelope detector connects the peak points of signal. Envelope detection can be implemented through Hilbert transform.

In this method the imaginary part of signal is obtained using Hilbert transform. Mathematically the envelope of signal is defined as below:

$$E(t) = \sqrt{(y(t)^2 + \hat{y}(t)^2)} \qquad (2.10)$$

Where E(t) is the envelope of signal and $\hat{y}(t)$ is the Hilbert transform of signal, y(t). Hilbert transform is implemented on the absolute value of ultrasound signal [63].

2.5.1.4 Cross-Correlation

Cross-correlation measures the similarity between two signals as a function of lag. One of its applications in signal processing is for determining the time delay between two signals. In this method, the maximum of cross-correlation function occurs at the lag that is equal to delay between signals.

Reza Zahiri-Azar *et al*. have indicated that time-domain cross-correlation with prior estimation speed up the computation and enable us to evaluate strain measurement over a large range of displacement in real time monitoring [64].

In probing nonlinear elasticity at an interface prosthesis/bone as a promising method to monitor the osseointegration/sealing of prosthesis, cross-correlation-based methods are

more sensitive than those based on subtraction/addition such like pulse inversion method. [65]. Pulse inversion technique is an ultrasonic nonlinear imaging technique that produces a better image contrast [66]. Also it has been shown that for tracking longitudinal sciatic nerve excursion applying frame-by-frame cross-correlation is a highly repeatable method [67].

Chapter 3: Development of Stiffness Measurement System Using Wearable Sensors

3.1 Measurement Method and Configuration

The main goal of this study is to develop a stiffness sensor for monitoring the mechanical properties of soft tissue. As explained in the section 2.2, stiffness is defined as force over displacement. So it is essential to measure force and its resulting displacement simultaneously to be able to examine stiffness at a desired location. Since in this research our focus is on diabetic patients we characterize mechanical properties of plantar soft tissue at heel area. The measurement system is supposed to be placed beneath the heel to examine applied force and the resulting tissue displacement simultaneously as shown in Fig. 3.1.

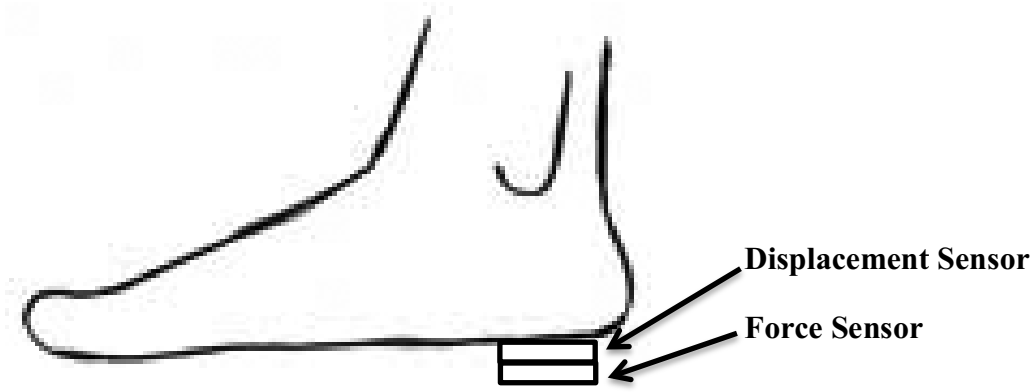

Figure 3.1 Measurement system configuration for simultaneous measurement of applied force and tissue displacement at heel.

A thin and flexible force and displacement sensors are used to measure applied load and its resulting displacement respectively. Force sensor resistance varies with the change in applied force on its active sensing area and by measuring change in resistance we are able to measure applied force. So first an electrical circuit was used to drive the force sensor

and convert the resistance to voltage. Then force sensor was calibrated for measuring unknown loads. Displacement sensor is an ultrasonic transducer that measures the thickness of soft tissue. By measuring the thickness of tissue over a period of time while a time-varying load is applied to it, the tissue displacement will be computable. The force and thickness measurements are conducted simultaneously and in continuous way and data are sampled with the frequency of 125 MHz. Software designed and developed in Matlab environment to obtain pressure-displacement curve of plantar soft tissue for one load-unload cycle where certain mechanical properties such as stiffness and Young's modulus are computable. In this research data are recorded over a certain period of time and analyzed later to quantify mechanical properties of soft tissue. The block diagram of Fig. 3.2 illustrates the measurement system.

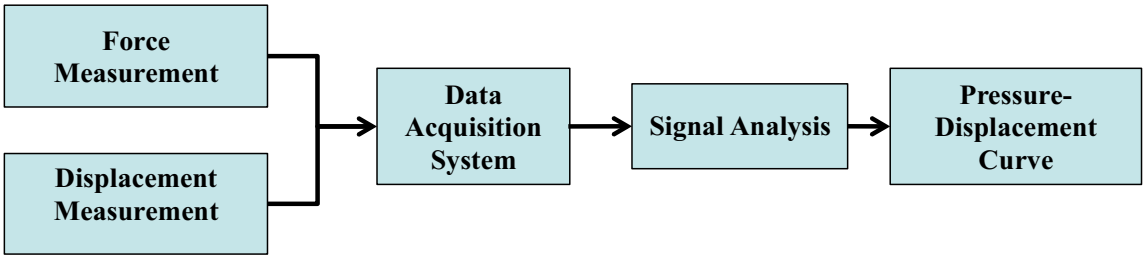

Figure 3.2 Block diagram of tissue mechanical properties measurement system.

3.2 Force Sensor

To measure the pressure under the foot during walking we need to measure the force, as pressure equals force divided by area. Since a wearable force sensor would be placed within a diabetic shoe and beneath the heel, it is required to use a thin and flexible sensor to prevent a subject's discomfort; because as explained in section 2.3.1 prolonged pressure on the plantar soft tissue may cause foot ulcers. Thus FlexiForce sensor (Model A401, TekScan, South Boston, USA) was chosen [68]. This sensor is thin (0.203-mm

thick) and flexible, and measures forces up to 445 N, which is suitable for the proposed method and application.

This is a piezoresistive force sensor and applying mechanical strain on it will change its electrical resistivity. This sensor is made up of two polyester film layers that are laminated together using an adhesive. On each substrate, there is a conductive material (silver), which is followed by a layer of pressure ink. The active sensing area is a circle at the end of the sensor and resistance changes only when pressure is applied to the active sensing area of the sensor. This sensor exhibits a decrease in resistance with an increase in the applied force. The relationship could be linear or nonlinear depending on the electrical drive circuit configuration as will be discussed in sections 3.2.2.1 and 3.2.2.2.

In this study we examine three different kinds of FlexiForce sensors: A201 (measuring force range: 111N), A201 (measuring force range: 445N) and A401 (measuring force range: 111N) in order to select the best option for our application. The diameter of active sensing area of sensor type A201 and A401 is 9.53 mm (0.375 in.) and 25.4 mm (1 in.) respectively [68]. Figs. 3.3 and 3.4 illustrate these sensors.

Figure 3.3 FlexiForce A201 [68]

Figure 3.4 FlexiForce A401 [68]

The FlexiForce sensor is integrated to this application through an electrical drive circuit. This circuit produces an analog output voltage based on the sensor's resistance, which is in turn proportional to the applied load on the active sensing area of force sensor. Related equations are shown in the sections 3.2.2.1 and 3.2.2.2. Different circuits were verified to get the best results in terms of required hardware and process time, full range adjustment, linearity and sensitivity in force to voltage conversion.

In this study LabPro (Vernier, Beaverton, USA) was used for collecting data contains applied force to the force sensor and its output voltage. LabPro is an interface with four analog and two digital input channels that was used for continuous measuring of voltage and force. It also has a connector that connects to the computer for transferring data. Once the Logger Pro software run on the computer, the connected sensor is detected by software immediately and the data is plotted. In addition it is possible to store numeric data and process them later [69].

A force plate (Vernier, Beaverton, USA) was used for measuring applied force during sensor calibration procedure. This plate is designed to measure forces during stepping, jumping, and other human-scale actions and its measurement range is –850 to +3500 N or –200 to +850 N depending on the position of a range selection switch, which is embedded beside the plate.

A voltage probe (Vernier, Beaverton, USA) was applied for examining the output voltage of force sensor. This probe is a bipolar sensor with the measuring range of ±10V that reports the potential difference between the measuring point and ground.

Vernier force plate was calibrated before use according to the manufacturer's user manual [70]. In each experiment the zeroing of both force and voltage reference probes were done via Logger Pro software.

3.2.1 Conditioning of Force Sensor

According to the manufacturer's documents, the new sensors must be conditioned before use to reduce the effects of drift and hysteresis. To do conditioning, 110% of the maximum test load was placed on the active sensing area of the sensor for approximately 3 seconds, 4-5 times. This process will "break in" the sensor and according to the manufacturer's recommendation should be done before calibration and use for best results.

3.2.2 Calibration of Force Sensor

Force monitoring was implemented using force sensor through a force-to-voltage circuit that produces an analog output voltage with respect to the applied load to the sensor. The force sensor calibration procedure consisted of applying known forces to the sensor while measuring the output voltage. An equation that represents the relationship between the output voltage and applied force is extracted by the means of curve fitting. In other words the behavior of force sensor can be modeled by a mathematical function. Sensor calibration was performed using a Vernier force plate. Some factors must be considered in calibration procedure, which will be explained below.

When the footprint of applied load is larger than active sensing area of sensor, it may be necessary to use a "puck". Puck is a rigid plastic material for adjusting the applied force surface with the active sensing area of the sensor to make sure that the entire load path goes through this area. The area of puck must be smaller than sensing area of sensor otherwise some erroneous reading would happen. In this research a puck with area smaller than active sensing area of sensor was used in both conditioning and calibration tests.

An important consideration for force sensor calibration is that, if the sensor is used in dynamic conditions, this condition must be accounted for in the calibration process [71]. Force sensor response time is less than 5μs and manufacturer recommends that for applications involving quick impact, sensor must be calibrated dynamically against a load cell with a quicker rise time [68]. Since our application does not involve quick impact forces, load cell is not needed for calibration and Vernier force plate will be appropriate for the proposed dynamic calibration method.

In addition, the force sensor output changes with temperature, presenting a drift of 0.36%/°C [68]. Thus, if the sensor is being used at different temperatures, it should be calibrated at each temperature and appropriate equation must be used in each case. Herbert-Copley *et al*. [72] analyzed changes of in-shoe plantar temperature over time. They found that the temperature of F-scan (Model 3000E, Tekscan, South Boston, USA) was increased during the first hour and then leveled off. Since the in-shoe measurements including preparation took a short time in this study (section 5.4), less than 5 minutes, temperature was considered constant and temperature change effects was not accounted.

3.2.2.1 Drive Circuit with Resistance Bridge

Force sensor is made up of piezoresistive material. Applying electrical current to this sensor will create voltage. The FlexiForce sensor is integrated to this application through an electrical drive circuit. This circuit produces an analog output voltage based on the sensor's resistance, which is in turn proportional to the applied load on the active sensing area of force sensor. Based on the datasheet of FlexiForce sensor the maximum current that can pass through sensor is 2.5 mA. Drive circuit must be designed in such a way that does not damage the sensor while provides the maximum of sensitivity and linearity.

A force to voltage circuit can be made by a simple voltage divider however the bridge circuit was used because of its more sensitivity and precision as shown in Fig. 3.5. In this circuit I is the current that pass through the force sensor, R_S is the force sensor resistance and R_1, R_2 and R_3 are bridge resistors. The output voltage of force sensor is obtained through the following equation:

$$V_{out} = \frac{Vin}{1+(R3/Rs)} \qquad (3.1)$$

Where V_{in} was set to 9 V. To choose the appropriate resistors for bridge circuit, first it is essential to limit the maximum current of force sensor to 2.5 mA. The FlexiForce is a piezoresistive sensor and the greater force results in lower sensor's resistance. The resistance decreases from 5 MΩ to ~300KΩ with the increasing force. Thus the minimum of R_S is approximately 300 KΩ. Since a 9 volt battery was used as an voltage source for this circuit, the current of force sensor, I, never exceed 2.5 mA no matter how much is R_3 as can be seen from the below circuit analysis.

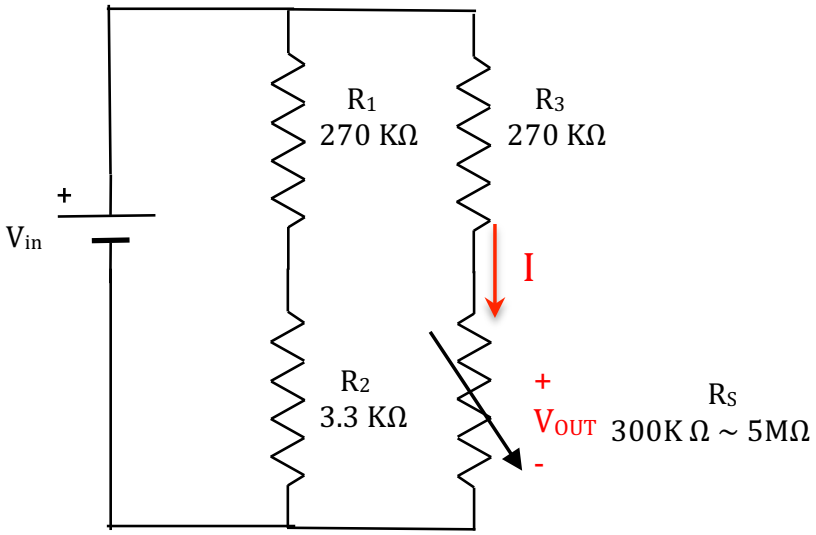

Figure 3.5 Diagram of force sensor's drive circuit with resistance bridge

$$I = \frac{9}{Rs+R3} < 2.5\ mA \qquad (3.2)$$

For I to be the maximum, the summation of R_3 and R_S must be the minimum. The minimum amount of R_S is 300 kΩ, therefore by substituting this value in the Eq. 3.2 we have:

$$300\ k\Omega + R_3 > 3.6\ k\Omega \qquad (3.3)$$

Since R_3 is a positive value, Eq. 3.3 is always true and is independent from R_3 value.

In order to select R_1, R_2 and R_3 some experiments were conducted where increasing loads were applied on the sensor through the puck as shown in Fig. 3.6. R_2 was fixed on the 3.3 kΩ arbitrarily and the same value for resistors R_1 and R_3 in the range of 10 kΩ to 400 kΩ was examined and output voltage of force sensor was plotted versus applied force in each trial. It was found that resistors R_1 and R_3 between the range of 220 kΩ and 330 kΩ are ideal for drive bridge circuit because in this range of resistance the circuit showing the steady linear decline in voltage as the applied force to the sensor was increased. Since the final goal of in this study is continuous monitoring of applied pressure to the plantar soft

tissue in real time manner and in embedded environment, the volume of computation is crucial and linear relationship between applied force and output voltage of sensor is desired. The linearity of drive circuit with resistance bridge will be discussed in detail at the end of this section.

For calibrating force sensor an experiment was done using FlexiForce A201 (445 N) dynamically. This sensor was chosen arbitrarily to find a proper drive circuit for force to voltage conversion. In the section 3.2.3 it will be explained in detail that how the right size and range for force sensor was selected for this application. In this experiment load was increased and decreased by pushing and releasing finger, which was placed on top of the puck. Fig. 3.6 illustrates the diagram of test layout.

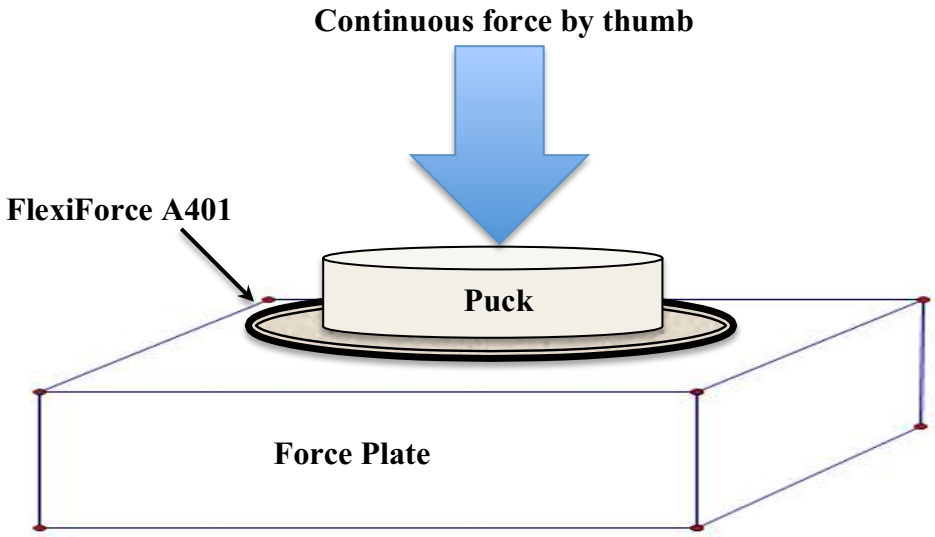

Figure 3.6 Experimental setup for dynamic calibration of force sensor

Vernier data acquisition interface was used for recording output voltage and applied force and voltage-to-force graph was plotted in Matlab environment using curve fitting tool as shown in Fig. 3.7.

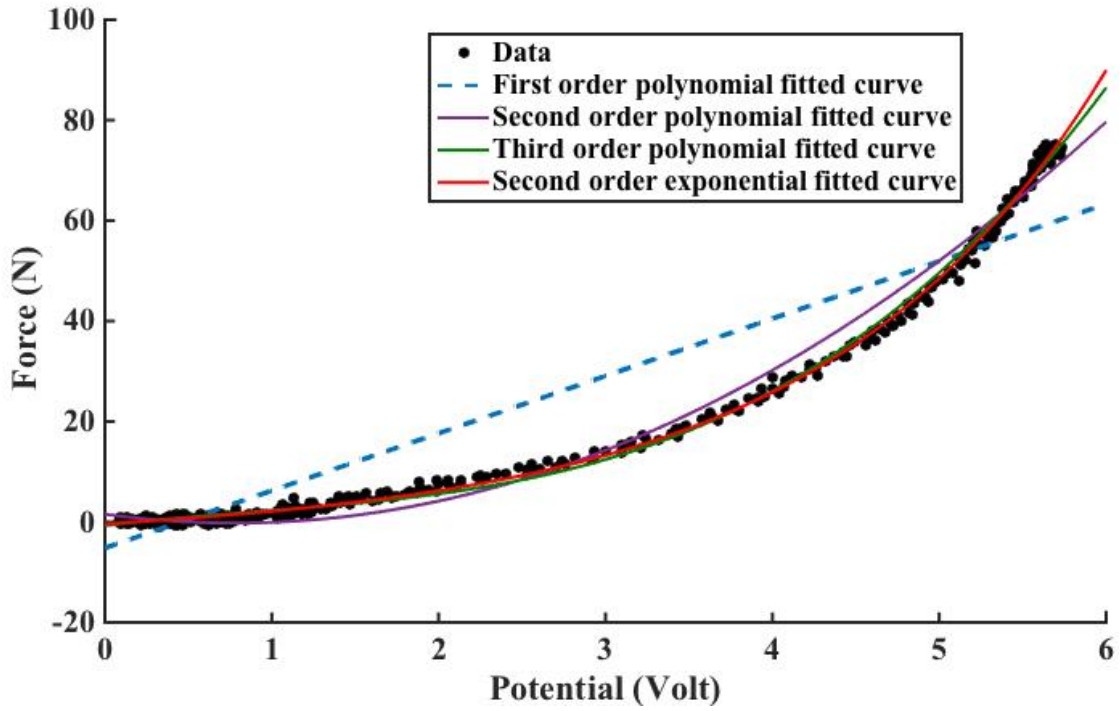

Figure 3.7 Voltage-to-force graph and four different models of fitted curves

The voltage to force graph was modeled with different functions. Table 3-1 represents the results.

Table 3-1 Relationship of force and output voltage of force sensor that obtained using drive circuit with resistance bridge and modeled with different functions

Model Function	Voltage-to-Force equation	R-Square
First Order Polynomial	$F = 11.42\ V_{out} - 5.18$	0.9135
Second Order Polynomial	$F = 2.93\ V^2_{out} - 4.56\ V_{out} + 1.56$	0.9917
Third Order Polynomial	$F = 0.54\ V^3_{out} - 1.47\ V^2_{out} + 3.96\ V_{out} - 0.72$	0.9978
Exponential Function	$F = 2.34\ exp\ (0.61\ V_{out}) - 2.76\ exp\ (-0.22\ V_{out})$	0.9986

As can be seen from table 3-1, second and third order polynomials and second order exponential function fit data with R-square more than 99%. Bridge circuit does not require too much electrical components and can be implemented with a battery and some resistors but the voltage to force equation is not linear.

If we consider the second order polynomial function from table 3.1 that defines the relationship between applied force and output voltage of force sensor and substitute V_{out} from Eq. 3.1, where R_3 is 270 KΩ, we will have Eq. 3.4 that represents the relationship between applied force and force sensor's resistance.

$$F = \frac{273.33}{(1+(270/Rs))^2} + \frac{41.04}{1+(270/Rs)} + 1.56 \qquad (3.4)$$

As can be seen from this equation, applied force and sensor resistance does not have a linear relationship. This is true for other cases where third order polynomial or exponential function is chosen for voltage-to-force conversion. Therefore to have a more linear system, a drive circuit with a linear op-amp was examined as will be explained in the next section.

3.2.2.2 Drive Circuit with Linear Operational Amplifier

In this circuit a linear op-amp MC6004 was used to drive the force sensor. Microchip MC6004 is an inverting operational amplifier, which is designed for general-purpose applications. This microchip has a 1 MHz Gain Bandwidth Product (GBWP) and operates from a single supply voltage as low as 1.8V to 6V [73]. Based on the sensor user manual, the supplied voltage should remain constant and R_F must be between 1 KΩ and 100 KΩ. In this study positive supply voltage of op-amp (V_{DD}), feedback resistance (R_F) and drive voltage of force sensor (V_T) were set to +5V, 79.8 KΩ and -1V respectively. The reason of choosing those values will be explained in the section 3.1.5. The output voltage of

force sensor in this circuit is obtained through the Eq. 3.5. As seen from this equation V_{out} has a linear relationship with the inverse of R_S.

$$V_{out} = -V_T * (R_F/R_S) \qquad (3.5)$$

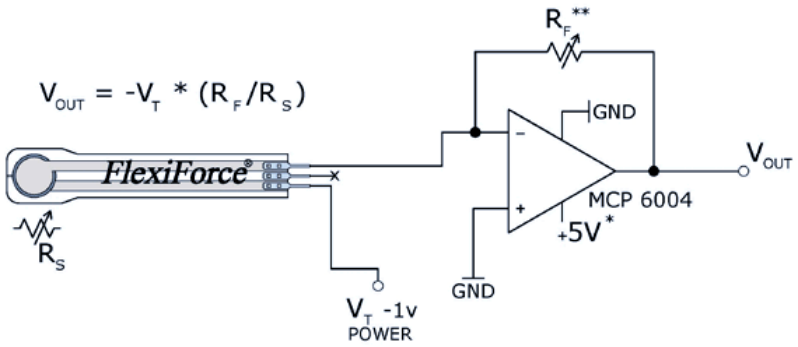

Figure 3.8 Diagram of force sensor's drive circuit with linear operational amplifier

The same experiment was run where applied force to the sensor was increased and decreased by pushing and releasing finger on top of it (Fig. 3.6) to examine the relationship between applied force and sensor's output voltage. Acquired data was processed in Matlab environment. Fig. 3.9 represents voltage to force graph, which has been fitted to different functions.

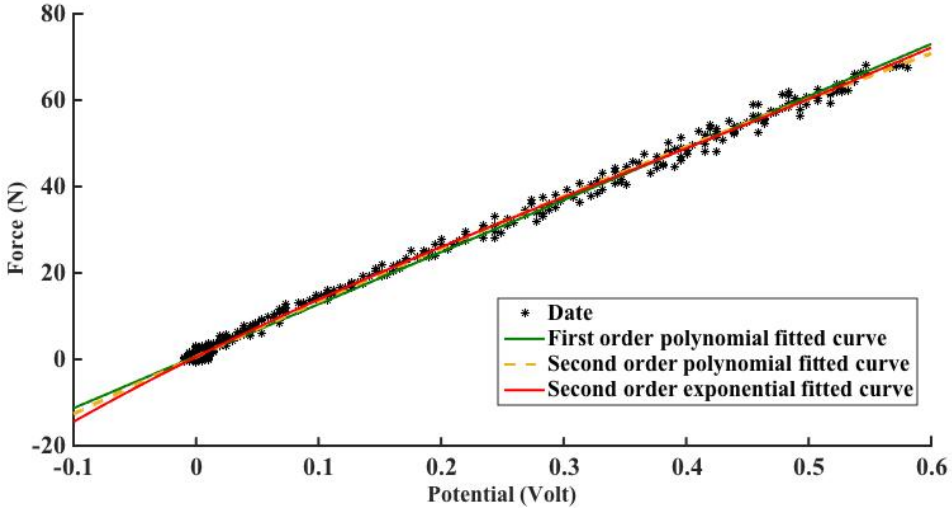

Figure 3.9 Voltage-to-force graph and four different models of fitted curves

Table 3-2 represents the relationship of applied force to the sensor and its output voltage that has been modeled with different functions.

Table 3-2 Relationship of force and output voltage of force sensor that obtained using drive circuit with operational amplifier and modeled with different functions

Model Function	Voltage-to-Force equation	R-Square
First Order Polynomial	$F = 120.4\ V_{out} + 0.73$	0.997
Second Order Polynomial	$F = -22.15\ V^2_{out} + 130.3\ V_{out} + 0.6$	0.9975
Exponential Function	$F = -37.37\ exp\ (-2.5\ V_{out}) + 37.92\ exp\ (-1.26\ V_{out})$	0.9975

All results confirm that the voltage to force relationship is linear relatively and even a first order polynomial fits data with R-square more than 99%. By considering first order polynomial from table 3.2 and substituting V_{out} from Eq. 3.5, where R_F is 100 KΩ, the relationship between applied force and force sensor's resistance will be obtained as follow:

$$F = -12000 * (V_T/R_S) + 0.73 \qquad (3.6)$$

As seen from this equation applied force to the sensor has a linear relationship with the inverse of R_S. In this application drive circuit with op-amp was used because of the linearity that it offers.

3.2.3 Choose the Force Sensor with Right Range and Size

The final goal of this research is to examine mechanical properties of plantar soft tissue under the foot at heel region, where is at most risk in terms of ulcer formation. Some experiments were conducted to choose the force sensor with the right size and range, as FlexiForce is available in different force ranges.

Force peak was measured under the foot at heel region, while the participant (female, 57 Kg, 559.3N) was standing. In this test, force sensor was placed on the flat plate and the puck was fixed on its active sensing area. Measured force peak at heel was 78 N. Same measurements was done by Sareh *et al*. [74] during normal walking of a participant (male, 90 Kg, 882 N) and the force peak was 93.8 N. As can be seen from the results force peak does not exceed 100 N and it might be better to use a sensor with force range of 25lbs (111 N) instead of 100lbs (445 N), since this sensor covers the desired measurement scope in this application and works more precisely in low force ranges.

Force sensor 25lbs are available in two different sizes, FlexiForce A201 and FlexiForce A401 with active sensing diameter of 0.953cm and 2.54cm respectively. A trade off in the sensor size must be considered, since smaller sensors underestimate the total force and may not be placed well to get the peak force. On the other hand, larger sensors are more likely to get the peak pressure but the measurement may underestimate the peak pressure value [74]. FlexiForce sensor was used in other research works where trade off in the number, size and location of pressure sensors in designing pressure-sensing insole was discussed [74] and continuous plantar pressure image was reconstructed from small number of pressure sensors [75].

One of the desired parameters to be measured in this research is heel stiffness. Therefore it is important to get the peak force at heel section and estimate plantar soft tissue displacement. Using FlexiForce A401 increases the possibility of getting the peak force while it covers required force range with acceptable precision. Furthermore, since it is desired to use the same size of force and displacement sensors, larger area of ultrasonic sensor increases the probability of getting received echo. There should be a tradeoff in ultrasonic sensor size. With larger ultrasonic transducers, the number of scattering echoes increased where the interface is larger than beam size. In other words larger ultrasonic transducer is more likely to receive echoes from adjacent tissues, which makes it difficult to discriminate between desired echo from bone and scattering ones.

3.2.4 Adjust Full Range and the Highest Sensitivity of Force sensor

The force sensor (A4101) with the right size and range were chosen, and a proper drive circuit was designed for measurement system. Since there are different possible combinations for V_T and R_F for drive circuit, an experiment was conducted in order to choose the best configuration for drive circuit to cover its full range and have the highest possible sensitivity.

The final goal for this project is real time monitoring in embedded environment, so it is desired to keep system's energy consumption at the minimum level. To fulfill this goal the minimum possible amount for V_T, which is -1 volt, was chosen. The amplifier used in this study is an inverted op-amp. So to avoid negative voltage in output the negative value was chosen for V_T. By substituting V_T in Eq. 3.5 we have:

$$V_{out} = R_F / R_S \qquad (3.7)$$

To select the proper value for R_F some trials were done using different R_F where the maximum anticipated load (102 N) was applied on top of the sensor through a puck and Plexiglas plate as an available flat plate in our lab as illustrated in Fig. 3.10 to investigate the sensitivity and full range of force sensor.

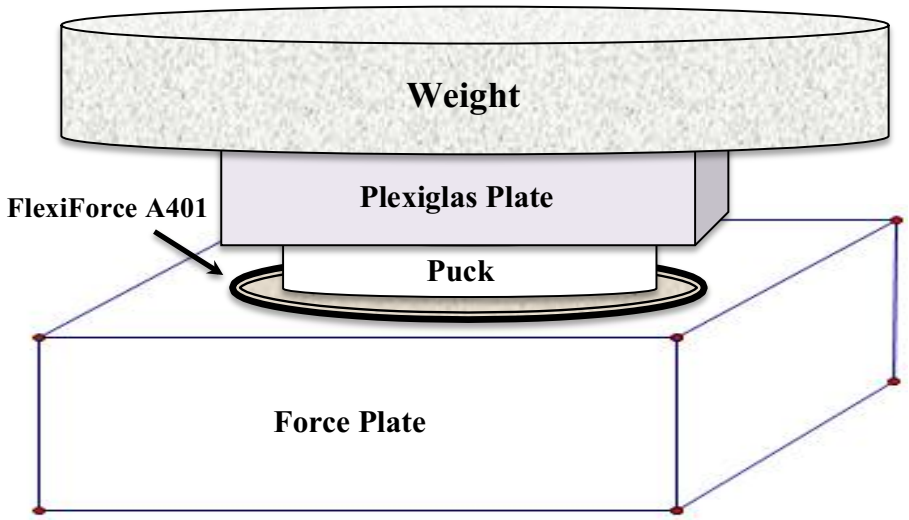

Figure 3.10 Experimental setup for full range and highest sensitivity of FlexiForce A401 adjustment

All experiments were done using Vernier force plate and voltage probe. The mean value of force and output voltage was calculated in each trial and all results were plotted together for comparison purpose as seen in Fig. 3.11. This graph represents the results of different trials with V_T = -1v and varying R_F to adjust the full range of sensor with the maximum sensitivity. Here sensitivity is the minimum of applied force that is required to produce detectable change in force sensor's output voltage and is calculated by measuring the slope of force-voltage curve in the following figure.

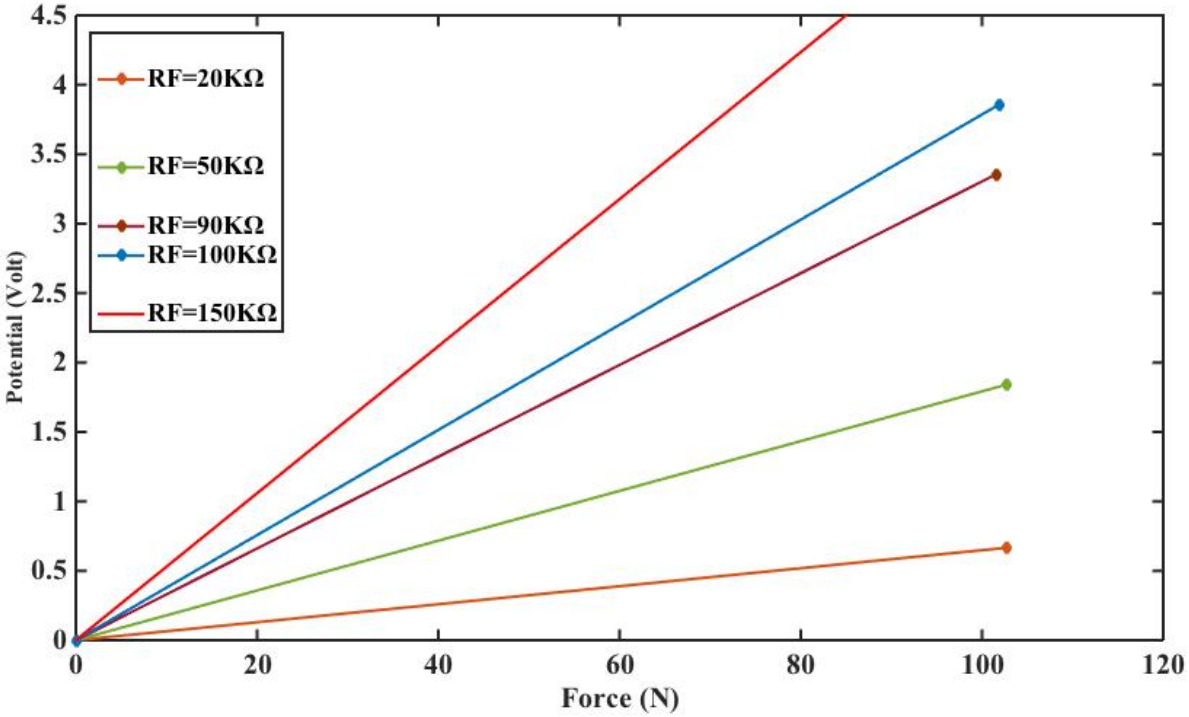

Figure 3.11 Force-to-voltage of FlexiForce A401 graph with varying feedback resistor (R_F) and V_T fixed at -1 V.

Sensitivity and full range was calculated in each test and the results are summarized in table 3-3.

Table 3-3 Covered full range and sensitivity of force sensor's drive circuit with different resistance feedback (R_F) and fixed V_T at -1v.

Resistance Feedback Value (KΩ)	Maximum of Covered Force Range (N)	Sensitivity (%)
20	102	0.648
50	102	1.79
90	101	3.30
100	101	3.78
150	85	5.29

As results revealed by R_F greater than 100 KΩ, the full range of force sensor, which is 102 N is not covered and the force measurement system is saturated. It seems that R_F between 90KΩ to 100 KΩ is suitable for this application because with these resistances the full range of force sensor is achievable and we have a better sensitivity.

In these experiments a puck with smaller area than active sensing area of force sensor was used. Using puck helps to transfer the maximum of applied force to the active sensing area of sensor. In actual condition puck cannot be applied because it creates discomfort in the shoe, which may cause ulcer formation in turn. Since in this research the main goal is extraction of pressure - displacement curve of plantar soft tissue during walking, the relative measurement of force is desired and lack of puck does not affect the accuracy of final results.

3.2.5 Calibration of FlexiForce A401

Based on the results from the previous experiments, FlexiForce A401 was chosen for next tests. This sensor was driven via op-amp circuit shown in Fig. 3.8 where R_F was 100 KΩ. As a next step, the sensor was calibrated dynamically. An experiment was conducted where applied load increased and decreased three times by pushing and releasing finger on top of the force sensor through a puck. Fig. 3.12 and 3.13 indicate applied force and output voltage of force sensor and their related force-voltage plot respectively.

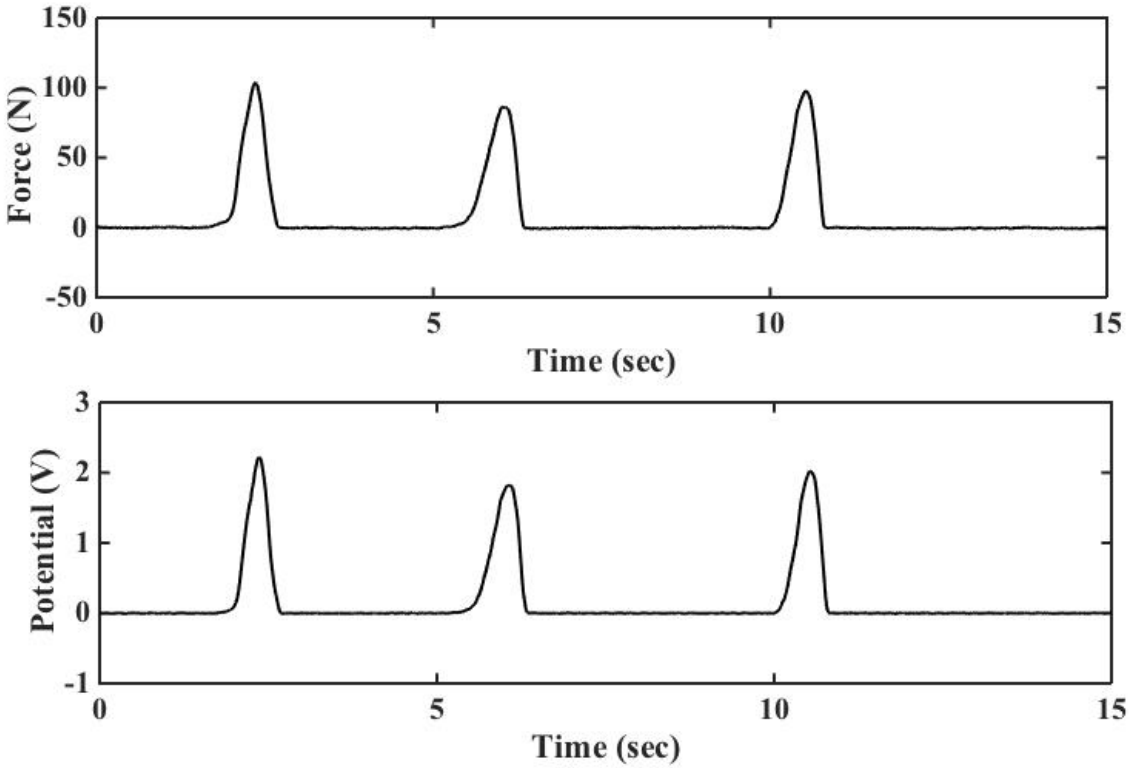

Figure 3.12 Measured applied force and output potential during three compression-release cycles

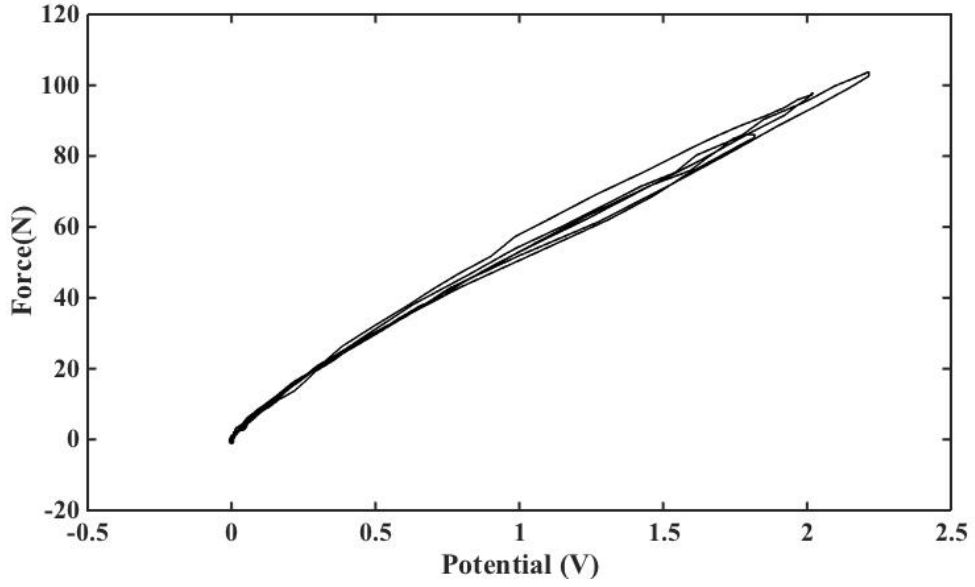

Figure 3.13 Voltage-to-force curve of FlexiForce A401 calibration test

To reduce measurement error this test was repeated two times and voltage to force relation was modeled with different functions as shown in the following table.

Table 3-4 Voltage –to-force equations in force sensor calibration trials modeled with different equations.

Measurement Number	Model Function	Voltage-to-Force equation	R-Square	Average of Equations
1	First Order Polynomial	$F = 49.12\ V_{out} + 0.1192$	0.994	$F = 49.85\ V_{out} + 0.2168$
2	First Order Polynomial	$F = 50.59\ V_{out} + 0.3145$	0.9912	
1	Second Order Polynomial	$F = -7.239\ V_{out}^2 + 61.49\ V_{out} - 0.1213$	0.9978	$F = -9.17\ V_{out}^2 + 63.45\ V_{out} - 0.078$
2	Second Order Polynomial	$F = -11.11\ V_{out}^2 + 65.41\ V_{out} - 0.0356$	0.9971	
1	Exponential Function	$F = 41.55\ exp(0.4254\ V_{out}) - 41.76\ exp(-1.445\ V_{out})$	0.9987	$F = 41.48\ exp(0.4236\ V_{out}) - 41.63\ exp(-1.439\ V_{out})$
2	Exponential Function	$F = 41.41\ exp(0.4218\ V_{out}) - 41.51\ exp(-1.433\ V_{out})$	0.9976	

Since R-square is more than 99% for all equations, the results were modeled through the first order polynomial and the following equation was used for next tests where the resistance feedback set to 100 KΩ due to simpler computations.

$$F = 49.85\ V_{out} + 0.2168 \qquad (3.8)$$

From Eqs. 3.7 and 3.8 the relationship between force and sensor resistance is obtained as below where R_F is set to 100 KΩ:

$$F = 4985\ R_S + 0.2168 \qquad (3.9)$$

A microcontroller-based board was used to display applied force in real time manner. The detail of used hardware and source codes of developed software could be found in appendix A.

3.3 Ultrasonic Sensor for Displacement Measurement

In this study ultrasonic sensor was used for tissue displacement measurement. Since displacement sensor is supposed to be placed in the shoe, desirable sensor must be thin and flexible and should tolerate body weight. A polyvinylidene fluoride (PVDF) piezoelectric polymer film ultrasonic sensor [8] was used to estimate plantar tissue displacement due to an applied force by means of an ultrasonic pulse echo method as shown in Fig. 3.14. Tissue displacement was obtained from a time delay change of ultrasonic RF signals reflected from a desired tissue boundary.

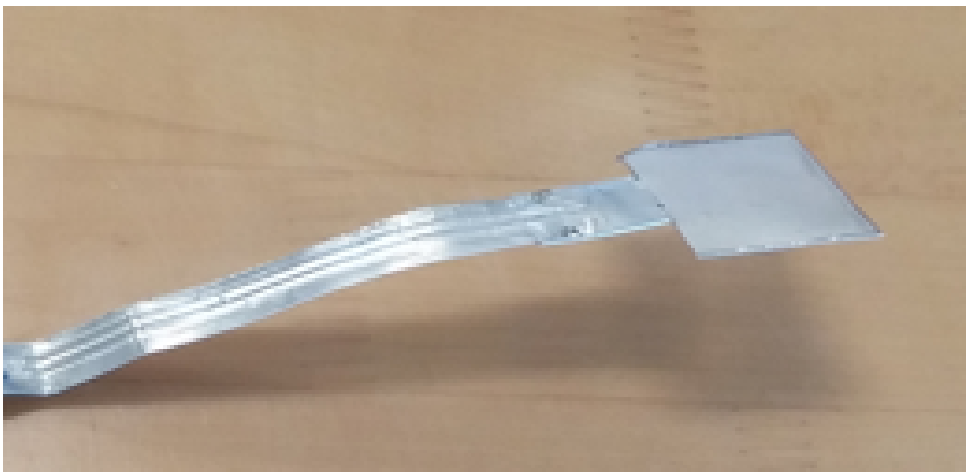

Figure 3.14 Thin and flexible PVDF ultrasonic transducer

PVDF film is light and thin and has a good acoustic impedance matching to biological soft tissue and broadband ultrasonic performance [76-78], thus non-invasive continuous monitoring of plantar soft tissue thickness is possible, which is difficult using a conventional ultrasonic probe [8]. This sensor is constructed without any matching layer

or backing material and can be cut into desired size and shape. This sensor is used in combination with force sensor to measure strain and stress respectively.

Ultrasonic sensor was driven by an ultrasonic pulser/receiver (Model: 5900, Panametrics-NDT, Waltham, MA, USA) and signals were acquired by a PCIe digitizer (Model: ATS1440, AlazarTech, Montreal, QC, Canada) with sampling rate of 125 MS/s and 14-bit resolution as presented in block diagram Fig. 3.15.

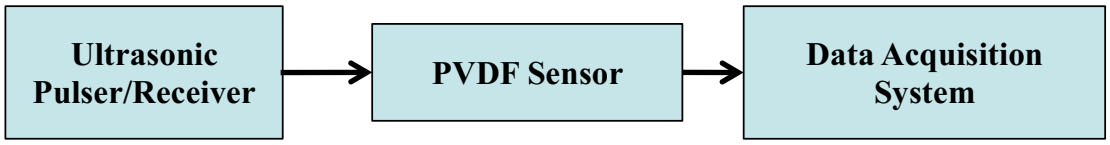

Figure 3.15 Block diagram of displacement measurement system

Performance of this transducer is evaluated using tissue-mimicking phantoms that will be explained in detail in the next chapter.

Chapter 4: Performance Evaluation Using Tissue-mimicking Phantoms

In the following chapter the performance of stiffness measurement system is evaluated by determining accuracy, reparability and hysteresis of force and displacement sensors while measurements are done on tissue mimicking phantoms. Signal to noise ratio (SNR) of both commercial and PVDF transducers are measured as well.

4.1 Test Principle

The stiffness measurement system includes force and displacement sensors, so to evaluate the performance of stiffness sensor we need to examine the performance of its force and displacement sensors in simultaneous measurement. An experiment was conducted where a known displacement was created in phantoms using a positioning device. Applied force and distances was measured simultaneously using FlexiForce A401 and PVDF sensor respectively. Because of the limitations that existed in our laboratory for measuring the absolute value of force, accuracy of the FlexiForce A401 force sensor could not be examined and only its repeatability was estimated. Displacement information was extracted through four different ultrasonic DSP methods and compared with the reference displacement value. The accuracy and precision of PVDF transducer were discussed for each method. Used phantoms in this experiment were silicone rubber and pork sirloin.

The rubber phantom was made of silicone with graphite powder for scattering. The silicone rubber phantom had a flat cone shape (Diameter of small circle: 5.8 cm, Diameter of big circle: 6.8 cm and Height: 8.63 cm) as seen in Fig. 4.1. The reason for choosing rubber phantom is that in the following tests applied force is increased gradually as consequence of positioning device movement. Other material such as agar cannot

tolerate applied load and would break. In addition silicone rubber is homogenous creating less ultrasonic noise and making the position of desired echo easer to be observed.

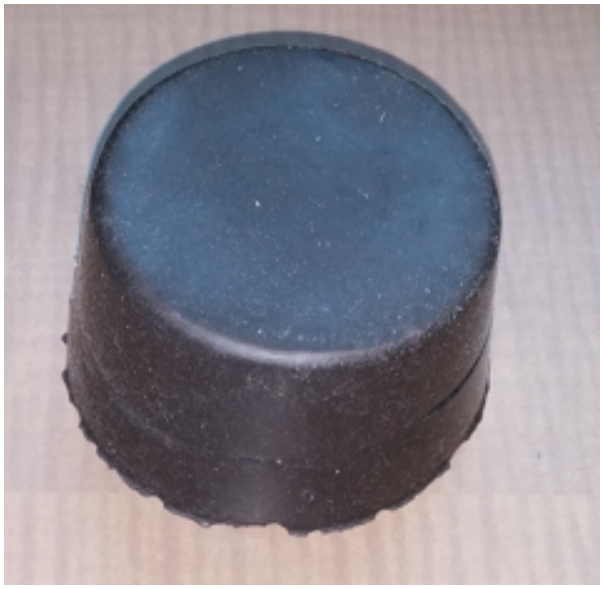

Figure 4.1 Silicone rubber phantom used for performance evaluation tests

The pork sirloin used had a semi cylindrical shape with the approximate size of l=15 * w=12 * h=8 cm. Pork sirloin simulates human body tissue properties well. In literature sound velocity in pork ranges from 1617±6 to 1622±5 m.s−1 [79], which is close to the sound speed in human muscles (1570 m.s−1) [59]. In our study the average of sound speed in pork sirloin was 1769 ± 199.7 m.s−1, measured using commercial ultrasound transducer. The difference of sound speed values may be explained with differences in temperature, muscle fiber orientation and investigated specimen.

4.2 Test Method

In this test phantoms were placed on the flat Plexiglas plate while the force sensor and the PVDF ultrasound transducer were located under the phantom, between plate and phantom. The commercial transducer was placed on top of the rubber phantom with another Plexiglas plate. This plate acted as a stand for commercial sensor to avoid any

movement. In addition it created an equal distribution of the load on the surface of phantom. The diagram of test setup is shown in Fig. 4.2.

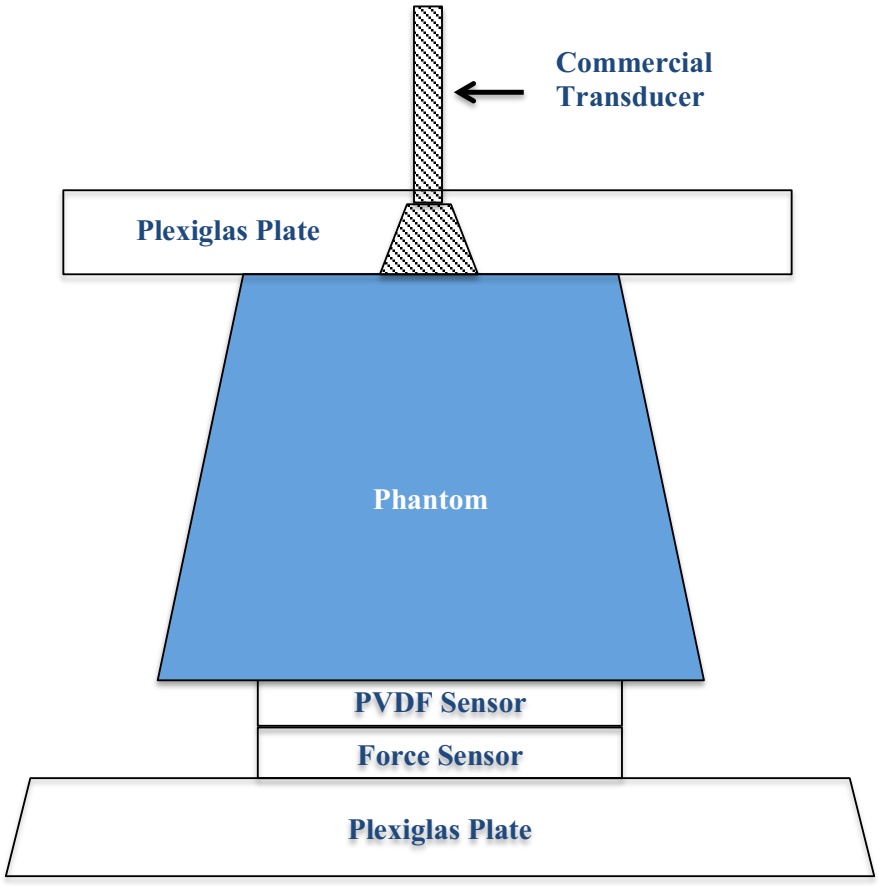

Figure 4.2 Experimental setup and sensor configuration for performance evaluation test with phantoms.

An acoustic gel was applied between phantom and both ultrasound transducers to make sure that there is not air between test objects and transducers. In this test the PVDF sensor transmitted and received the echoes (pulser/receiver mode) while the commercial one only detected the received echoes. The following pictures show test configuration with silicone rubber phantom and pork sirloin respectively.

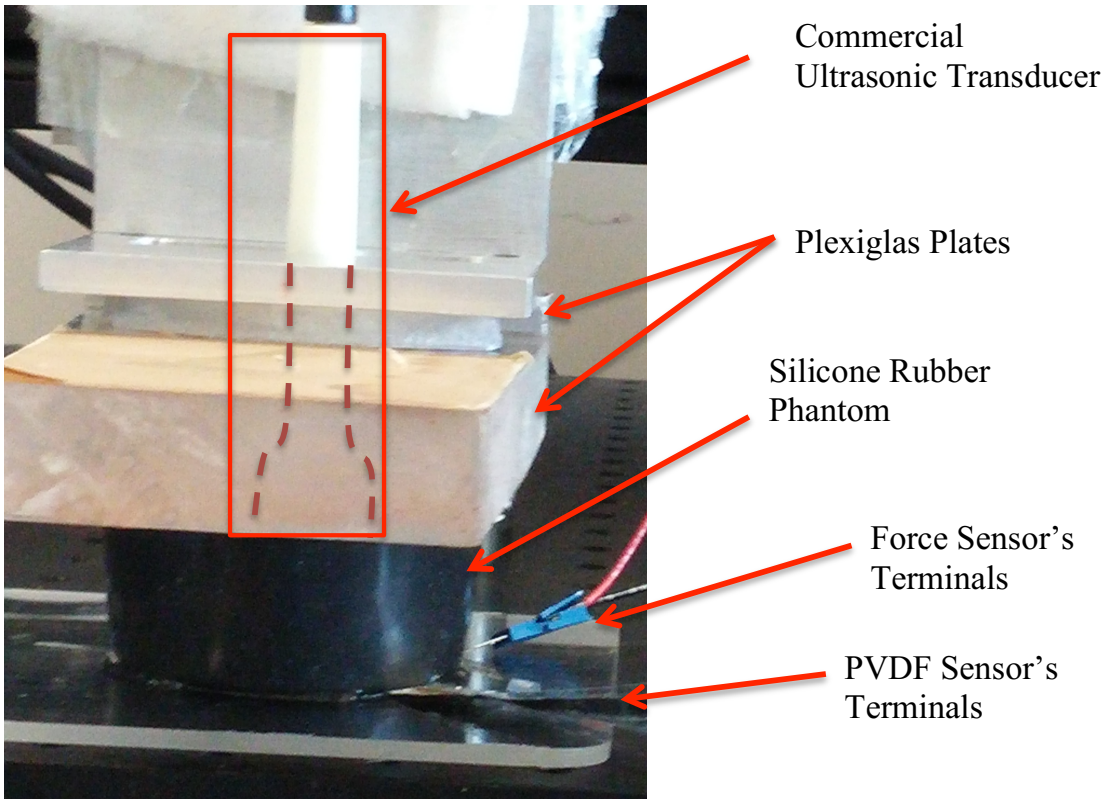

Figure 4.3 Experimental setup for performance evaluation test with silicone rubber phantom.

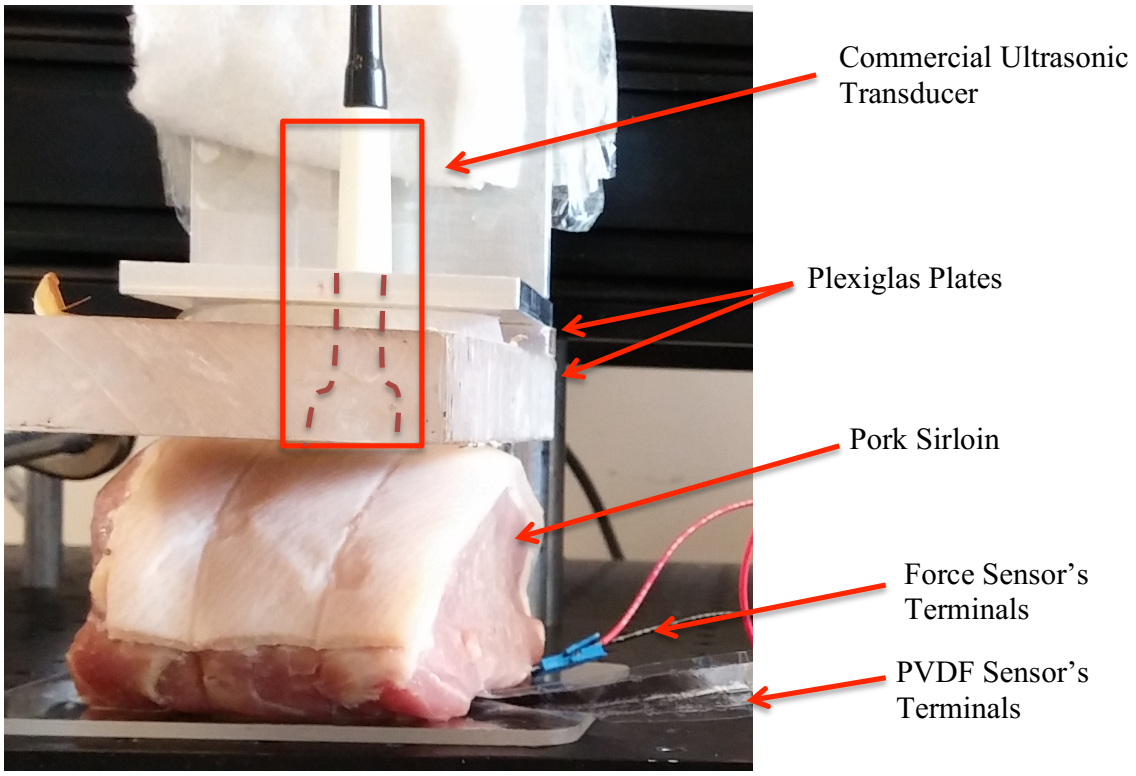

Figure 4.4 Experimental setup for performance evaluation test with pork sirloin.

The Plexiglas plate with the commercial transducer was attached to a Z-stage that is a positioning device. The Z-stage offers a resolution of 0.2500 mils (i.e. 6.350 μm) with a repeatability of 0.2 mils (5.080 μm) [80]. The positioning precision of Z-stage was used as a reference for displacement estimation in these tests. Z-stage is programmed to make a displacement in 6 steps equal to 0.6096 mm each (Δd of Fig. 4.5) to reach the overall displacement of 3.6576 mm. The displacement pattern that is shown in Fig. 4.5 was considered as a one measurement cycle. This measurement cycle was repeated 7 times to reduce the measurement errors.

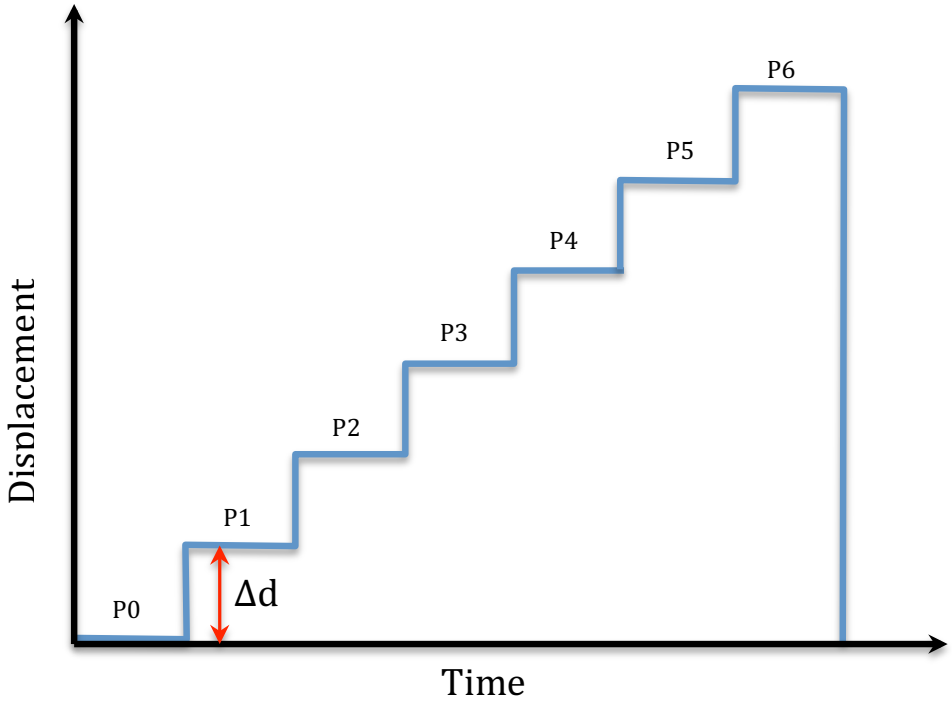

Figure 4.5 Movement pattern of positioning device for one measurement cycle.

Ultrasonic sensor was driven by an ultrasonic pulser/receiver (Model: 5900, Panametrics-NDT, Waltham, MA, USA) and signals were acquired by a PCIe digitizer (Model: ATS9440, AlazarTech, Montreal, QC, Canada) with sampling rate of 125 MS/s and 14-bit resolution while the frame rate was 100 Hz. The acquired data included the RF signal from both ultrasound transducers and the output voltage of the driver circuit of the FlexiForce A401 force sensor. Data were transferred to Matlab environment for processing and measurement. FlexiForce A401 was driven using op-amp circuit with R_F and V_T equal to 100 KΩ and -1 V respectively to obtain maximum sensibility within the force range applied, as shown in the section 3.2.

4.3 Data Analysis

We used commercial ultrasonic transducer as a reference for sound speed measurement in phantoms. As will be shown in section 4.4.3 the SNR of commercial transducer is higher than that of PVDF, which supports our decision.

To measure sound speed in silicone rubber and pork sirloin phantoms both transducers were used simultaneously as shown in diagram Fig. 4.2 and the time-of-flight of the ultrasound pulse was extracted from both RF ultrasonic signals through four different DSP methods. The time delay (Δt) was calculated using the difference of the time of fly for two consecutive positions of mechanical positioning device. Sound speed of commercial transducer was determined through Eq. 4.1. In sound speed measurements, we assumed that real displacement between two consecutive positions is what was applied through Z-stage (0.6096 mm).

$$c = 0.6096 / \Delta t_{comm} \qquad (4.1)$$

Having sound speed from above equation and measuring time delay of received RF signal from PVDF transducer, the displacement of phantom will be determined.

$$\Delta d = c * \Delta t_{PVDF} \qquad (4.2)$$

When Δd is obtained between each two positions (Δd11, Δd12…), the average of displacement for each measurement cycle will be calculated through the following equation:

$$\Delta d1 = \frac{\Delta d11 + \Delta d12 + \cdots + \Delta d16}{6} \pm sd1 \qquad (4.3)$$

Where sd is the standard deviation and obtained by taking square root of average value of calculated variance for each measurement cycle. Displacement for each method is the mean of calculated Δd for seven measurement cycles.

Since different ultrasonic techniques were applied for displacement measurement, and we aimed to compare the results and discuss the performance of PVDF transducer for tissue displacement measurement with respect to the applied method, it was essential to calculate some error indexes. Absolute error, percent of relative error, percent of relative standard deviation (RSD) and percent deviation were computed through below formulas:

$$Absolute\ Error = |\Delta d - actual\ value| \qquad (4.4)$$

$$Percent\ of\ Relative\ Error = \frac{|\Delta d - actual\ value|}{actual\ value} * 100 \qquad (4.5)$$

Where actual value is 0.6096 mm.

$$Percent\ of\ RSD = \frac{sd}{\Delta d} * 100 \qquad (4.6)$$

$$Percent\ Deviation = \frac{|\Delta d - mean\ value|}{mean\ value} * 100 \qquad (4.7)$$

4.4 Estimating SNR of Ultrasonic PVDF and Commercial Transducers

Since we used commercial transducer as a reference for sound velocity measurement in phantoms, it was important to examine the SNR of both commercial and PVDF transducers to make sure that the commercial transducer has a better SNR in test with silicone rubber and pork sirloin. To this end, an ultrasonic signal was transmitted through phantoms and the received echo was recorded. This test was done for each transducer in pulse-echo mode. Therefore for each phantom, we did two tests, one with commercial

transducer and another one with PVDF sensor. Received echo was processed and SNR was computed as follow.

Signal to noise ratio is defined as a ratio of power of signal to the power of noise. If signal and noise are measured across the same medium, then SNR can be obtained by calculating the square of amplitude ratio [81]. Peak-to-peak of signal window was considered as a signal amplitude. For noise amplitude estimation, the standard deviation of noise window was calculated and multiplied by 6 to guarantee the error range of less than 0.3%. Following equation was used for SNR computation in decibel:

$$SNR_{dB} = 20log(A_{Signal}/A_{Noise}) \qquad (4.8)$$

For SNR estimation, amplitude drift value from zero was removed in received RF echo. Next it was split up to separate desired signal and noise parts as shown in Figs. 4.6 and 4.7. The signal window was chosen in such a way that returned echo from tissue boundaries be covered. The noise window was selected arbitrarily in the area between transmitted pulse and received RF ultrasonic signal when the transmitted signal was damped.

4.4.1 SNR Estimation in Test with Silicone Rubber Phantom

In this test PVDF and commercial transducers were connected to the ultrasound pulser/receiver where the energy and gain was set on 32μJ and 54.0dB for PVDF sensor and 4μJ and 54.0dB for commercial transducer respectively. By changing energy of pulser/receiver for PVDF and commercial sensors, we tried to compare the optimal settings of both sensors. As Eq. 4.8 shows, amplitude of signal and noise was considered for SNR measurements and different values of energy do not affect the results. Increasing gain amplifies the amplitude of both signal and noise by the same amount and

since in SNR calculation the amplitude of signal is divided to the amplitude of noise, using different gain keeps the ratio. Fig. 4.6 represents received RF signal from PVDF transducer.

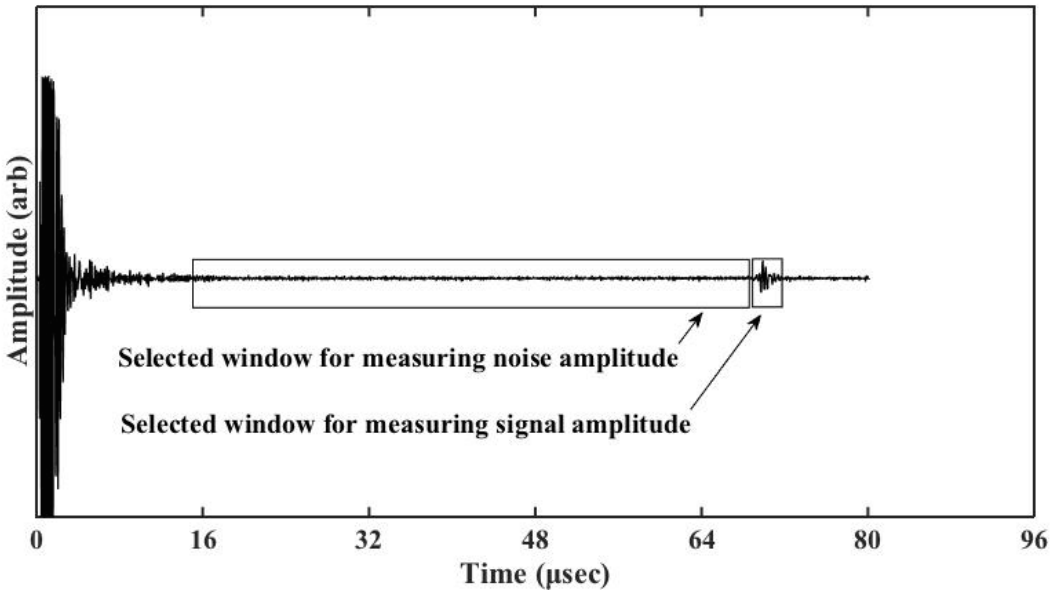

Figure 4.6 One frame of ultrasonic RF signal received from commercial transducer in test with silicone rubber phantom used for SNR measurement.

Table 4-1 represents the results of test with silicone rubber phantom that were obtained using Eq. 4.8.

Table 4-1 SNR of PVDF and commercial transducers in test with silicone rubber phantom

Test Material	SNR of PVDF Transducer (dB)	SNR of Commercial Transducer (dB)
Silicone Rubber	2.33	14.24

As results indicate the SNR of commercial transducer is greater than that of PVDF sensor in test with silicone rubber phantom. Thus in test with silicone rubber commercial transducer can be used as a reference for sound speed measurement.

4.4.2 SNR Estimation in Test with Pork Sirloin

This experiment was done using pork sirloin where the energy and gain was set on 32μJ and 54.0dB for PVDF sensor and 8μJ and 40.0dB for commercial transducer respectively. Fig. 4.7 represents a frame of received RF signal from commercial transducer that was chosen for SNR computation.

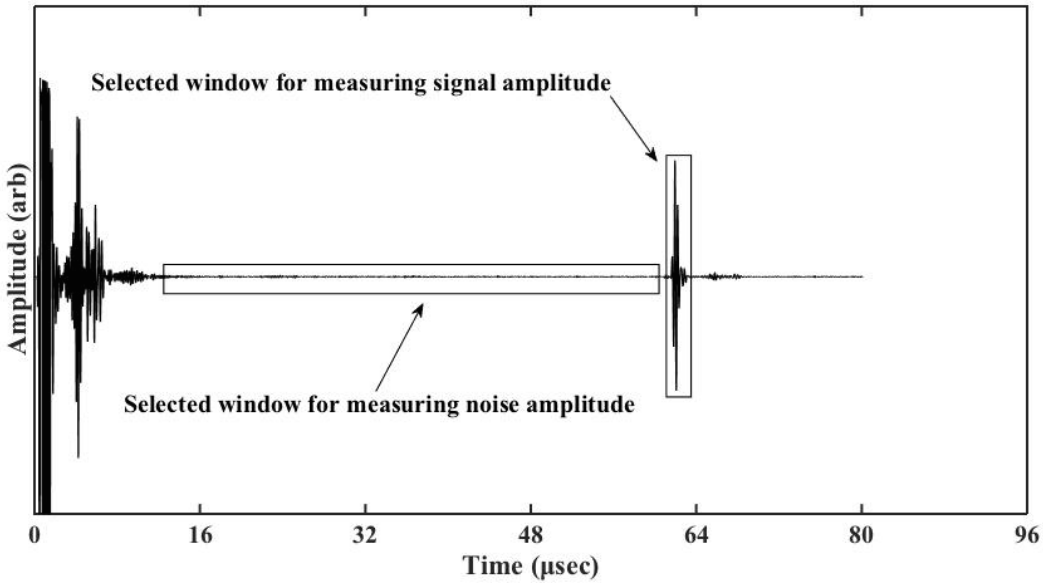

Figure 4.7 One frame of ultrasonic RF signal received from commercial transducer in test with pork sirloin used for SNR measurement.

Table 4-2 represents the results of test with silicone rubber phantom that were obtained using Eq. 4.8.

Table 4-2 SNR of PVDF and commercial transducers in test with pork sirloin.

Test Material	SNR of PVDF Transducer (dB)	SNR of Commercial Transducer (dB)
Pork Sirloin	4.38	38.46

As can be seen from the table 4-2, the commercial transducer has better SNR than PVDF sensor in test with pork sirloin.

4.4.3 Conclusion

Following graph summarizes the results:

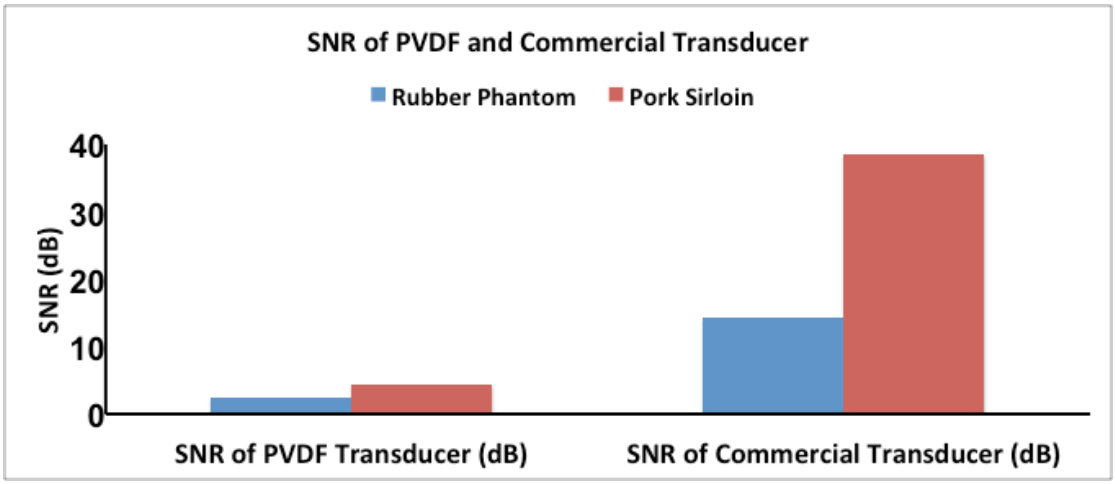

Figure 4.8 Comparison of PVDF and commercial transducers' SNR in simulation test with phantoms.

As can be seen in both cases commercial transducer has stronger SNR than PVDF sensor. Then it can be used as a reference for sound speed measurements in next experiments. Also the SNR of PVDF transducer is good enough to separate echo and noise. Therefore PVDF could be used for displacement measurement in this application.

Amplitude attenuation coefficient of silicone rubber phantom is bigger than that of the pork sirloin. Thus based on the Eq. 4.9 the amplitude of reflected echo in test with pork sirloin is bigger than that of silicone rubber phantom. Figs. 4.6 and 4.7 also confirm this matter.

$$A_z = A_0 e^{-\mu z} \qquad (4.9)$$

Comparing noise amplitude reveals that noise amplitude is independent from phantoms and it probably relates to the electronics.

4.5 Displacement Measurement Evaluation through Four Different Ultrasonic Methods

In this part the performance of PVDF transducer for tissue displacement measurement was examined via four different DSP techniques. A known displacement was created in phantoms as explained in section 4.2 and displacement and error index were calculated based on the methods described in section 4.3.

Vertical displacement in tissues can be estimated using ultrasound, based on the change in measured time-of-flight of a target echo. There are several methods for processing ultrasound RF signals and measuring time delay between transmitted and received echoes. Four different methods of extracting displacement information from A-mode measurements were used in this research: position of positive peak of the echo, position of peak in absolute value of signal, position of the largest peak in envelope and cross-correlation, which will be explained in details below. All techniques obtain vertical displacement from differences in time delays in received ultrasound RF signal. Samples of analyzed data for each method are presented in appendix C.

In this experiment a known displacement of 0.6096 mm, hereinafter referred to as actual value, was created in the phantoms in six steps to reach the overall displacement of 3.6576 mm and time delay of ultrasonic RF signal was calculated for displacement measurement in each step. Details of measurement and signal processing are explained below.

Data was taken in each measurement cycle (Fig. 4.5) and was saved in a separate file, each one containing frames including received echoes from both PVDF and commercial transducers. For each file it was important to separate frames with respect to the position they were recorded. To do so, several frames were plotted together to trace the movement of Z-stage between the positions of movement pattern (Fig. 4.5). For example in test with pork sirloin 389 frames were recorded in measurement cycle #1. We needed to determine how many of them are taken in each Z-stage position. For instance to define the number of recorded frames during the time when the Z-stage was in position P0, first 60 frames were plotted together. Positions of received echoes were the same that was indicating no movement has happened and all those frames belonged to the position P0. Then frames 59-70 were plotted together. The graph showed that a movement occurred because the position of received echo was changed as shown in Fig. 4.9. We looked to the fewer number of frames between 59 and 70 to find the exact time of Z-stage movement. By trial and error method it was found that relocation was happened when the frames 66-68 were recorded.

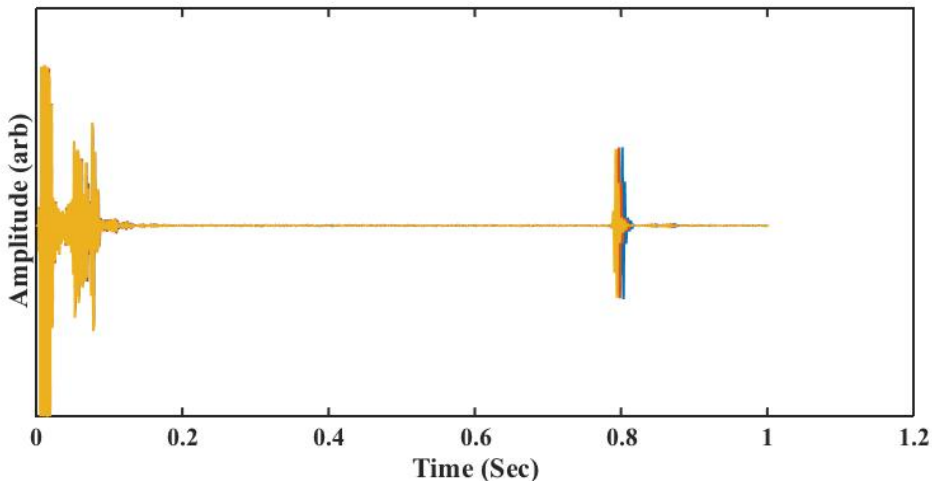

Figure 4.9 Three frames of ultrasonic RF signals recorded during the movement of positioning device between two consecutive positions.

As the same way, corresponding frames for each position were determined. Next the average of frames in each position was calculated to reduce the level of noise.

4.5.1 Position of Positive Peak of the Echo

In this method location of positive peak in the averaged RF signal from both PVDF and commercial transducers, which represents the thickness of phantom, was measured visually in each position. Then displacement of phantoms between two positions was computed by subtracting the calculated thickness of phantom for each position. Fig. 4.10 indicates one sample of average received RF signal from both transducers.

This procedure was repeated for 7 measurement cycles and displacement, percent of error and percent of RSD was calculated based on the method described in section 4.3.

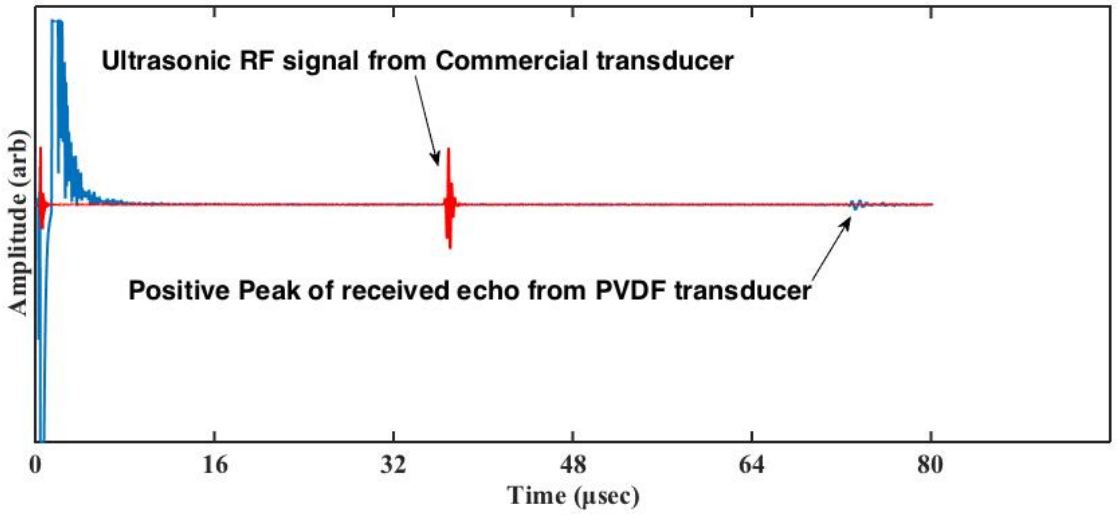

Figure 4.10 One sample of averaged ultrasonic RF signals from commercial and PVDF transducers in simulation test with silicone rubber phantom

In this test PVDF and commercial transducers measured same objects but only PVDF sensor was set on pulse-echo mode and commercial transducer acted as a receiver and was detecting the transmitted pulse. That is why the position of positive peak is different in the Fig. 4.10; while the time delay observed by the PVDF transducer represented the

"round trip" of the ultrasound in the phantom the time delay observed by the commercial transducer represented the "one way trip". As explained before, commercial sensor was used as a reference for sound speed measurement in phantoms.

Following graphs illustrate the performance of PVDF transducer for measuring the known displacement of 0.6096 mm in test with silicone rubber phantom and pork sirloin respectively.

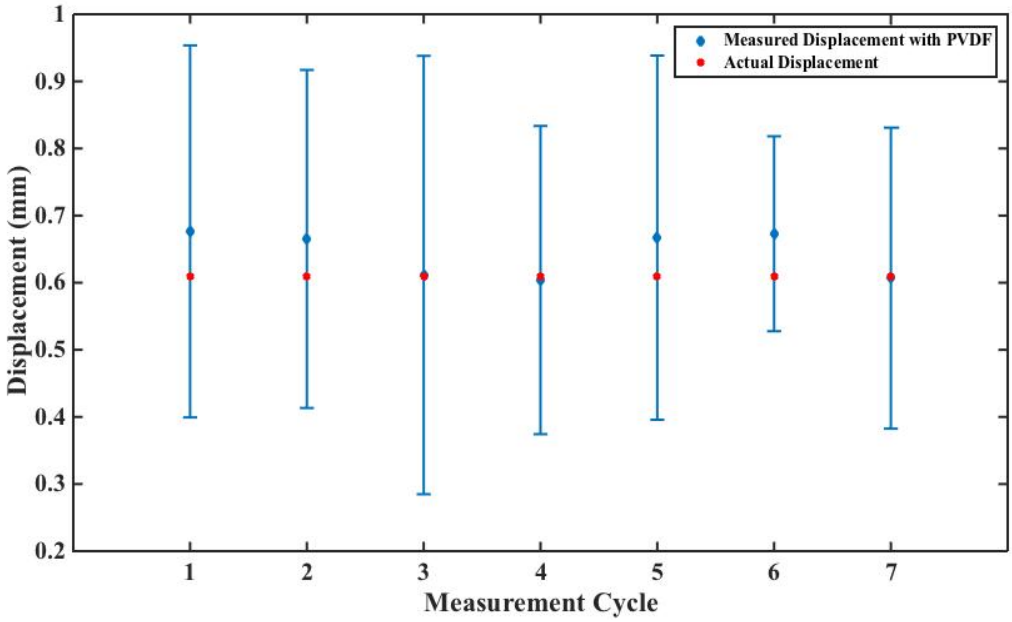

Figure 4.11 Average of measured displacement at different measurement cycles with PVDF transducer using "position of positive peak" technique in comparison with actual value in test with silicone rubber phantom.

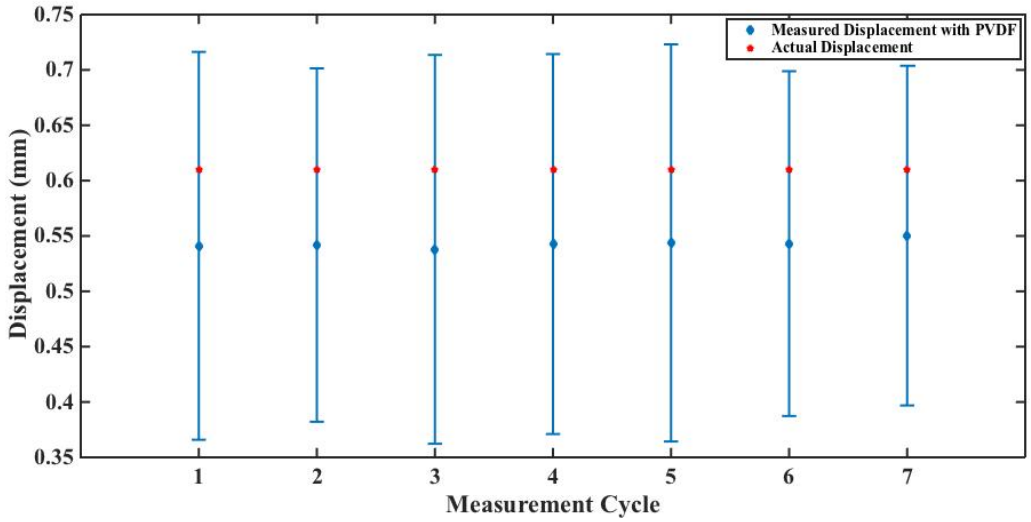

Figure 4.12 Average of measured displacement at different measurement cycles with PVDF transducer using "position of positive peak" technique in comparison with actual value in test with pork sirloin.

The average of measured displacement using PVDF in test with silicone rubber phantom and pork sirloin was 0.6434 ± 0.2520 mm and 0.5429 ± 0.1675 mm respectively.

4.5.2 Position of Peak in Absolute Value of Signal

In this method first the average of ultrasonic RF signal in each position was measured as explained in section 4.5 but the thickness of phantoms was estimated by finding the position of peak in absolute value of signal. In this technique after removing amplitude drift value from zero, absolute value of RF signal was computed to flip the negative part of RF signal. Then the position of peak in absolute value of signal was found visually. The graphs below, which are a sample of results in test with silicone rubber phantom, illustrate the procedure:

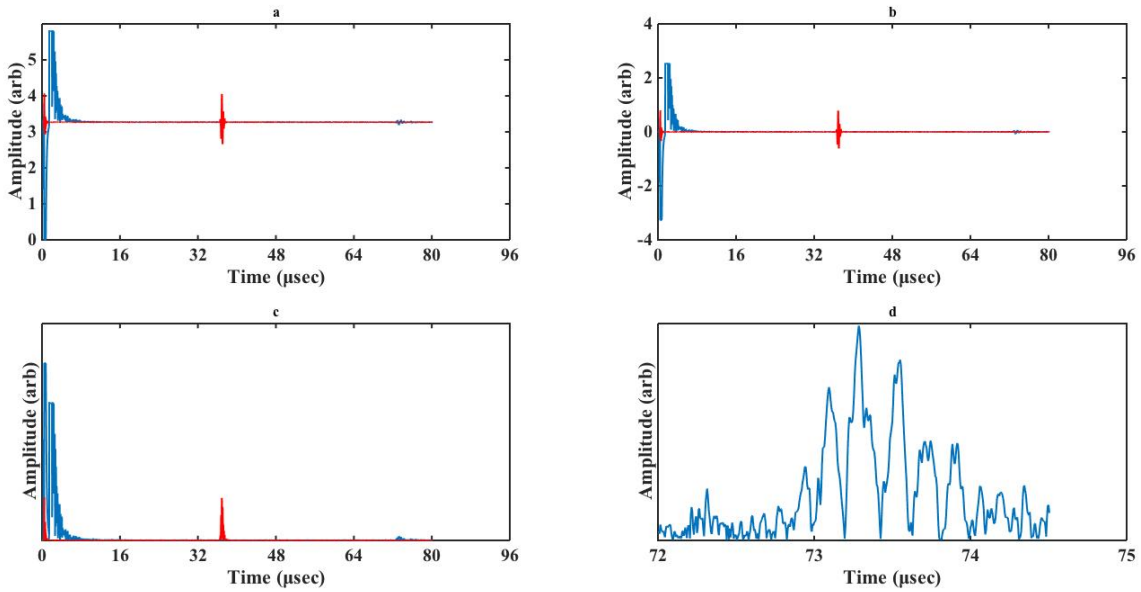

Figure 4.13 A sample of analysis procedure used for finding the position of largest peak in absolute value of ultrasonic RF signal from commercial (red line) and PVDF (blue line) transducers in test with silicone rubber phantom (a), signals after removing drift value (b), absolute value of signals (c), zoomed part of received Echo from PVDF transducer (d).

Same as previous experiment this one was repeated for 7 measurement cycles, the displacement on each position was calculated and the average of displacement was computed for each measurement cycle. Figs. 4.14 and 4.15 indicate the performance of PVDF transducer for displacement measurement in test with silicone rubber phantom and pork sirloin respectively.

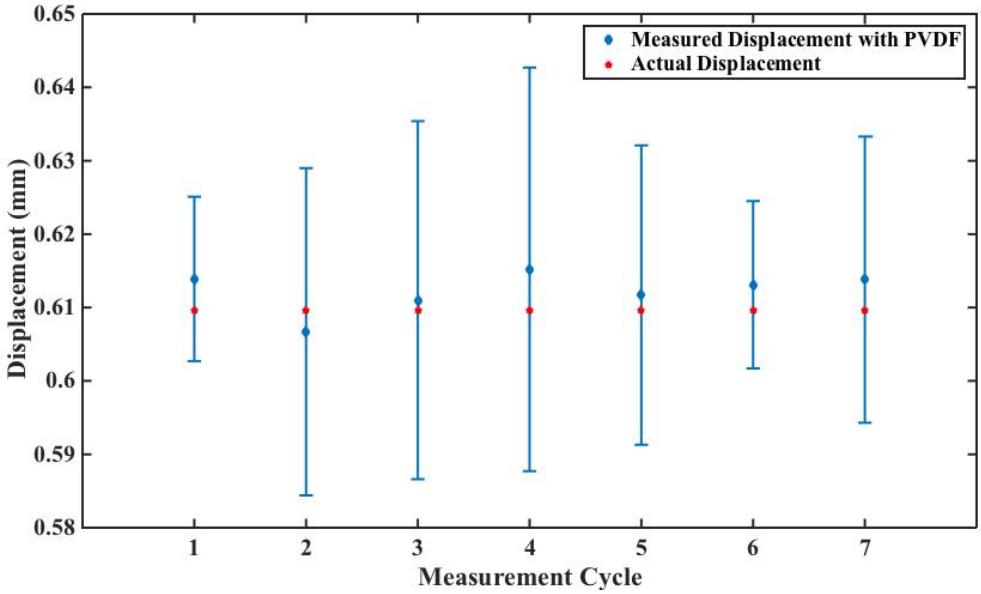

Figure 4.14 Average of measured displacement at different measurement cycles with PVDF transducer using "position of largest peak in absolute value of signal" technique in comparison with actual value in test with silicone rubber phantom.

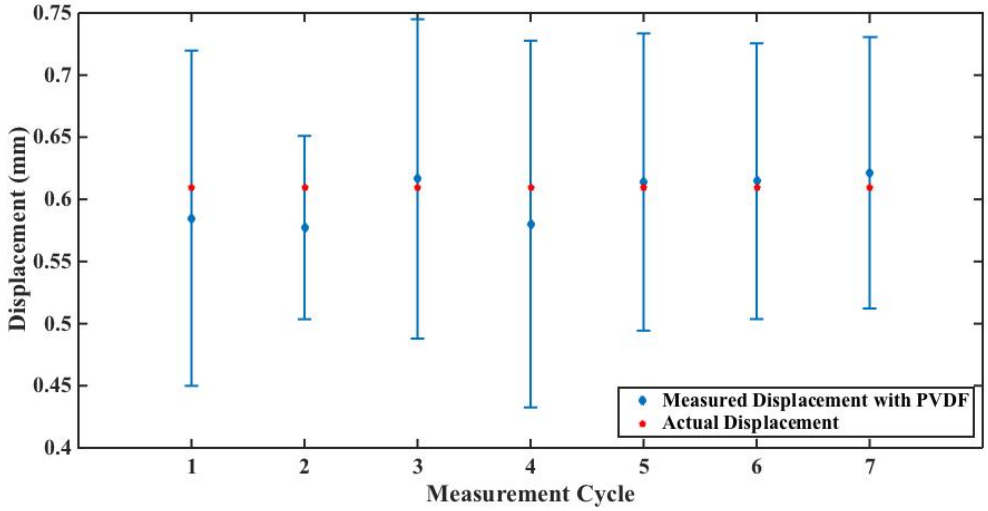

Figure 4.15 Average of measured displacement at different measurement cycles with PVDF transducer using "position of largest peak in absolute value of signal" technique in comparison with actual value in test with pork sirloin.

The average of measured displacement using PVDF test with silicone rubber phantom and pork sirloin was 0.6122 ± 0.0222 mm and 0.6012 ± 0.1198 mm respectively.

4.5.3 Position of the Largest Peak in Envelope

Here thickness of test objects was measured by finding the location of largest peak in the envelope of the averaged RF signal for each position. The Hilbert transform of the absolute value of the ultrasound RF signal was computed to take the envelope of signal. Position of peak value in envelope may better represent the position of the object that generated the echo, as the position can be between two peaks of the RF signal. The graphs below are a sample of results obtained in test with silicone rubber phantom.

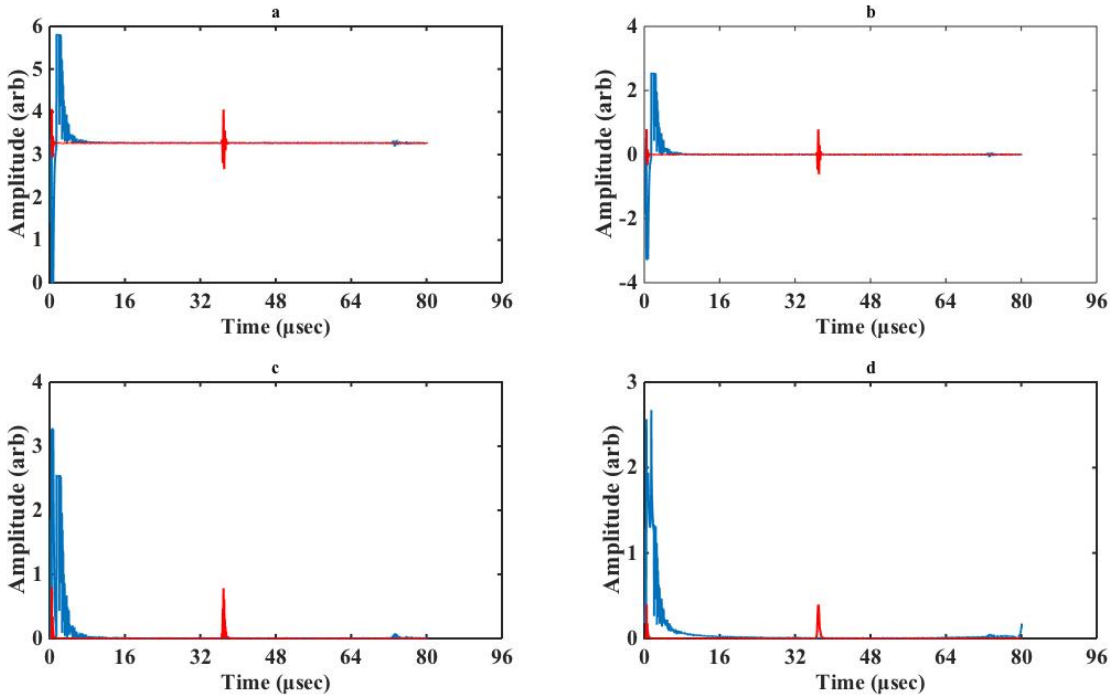

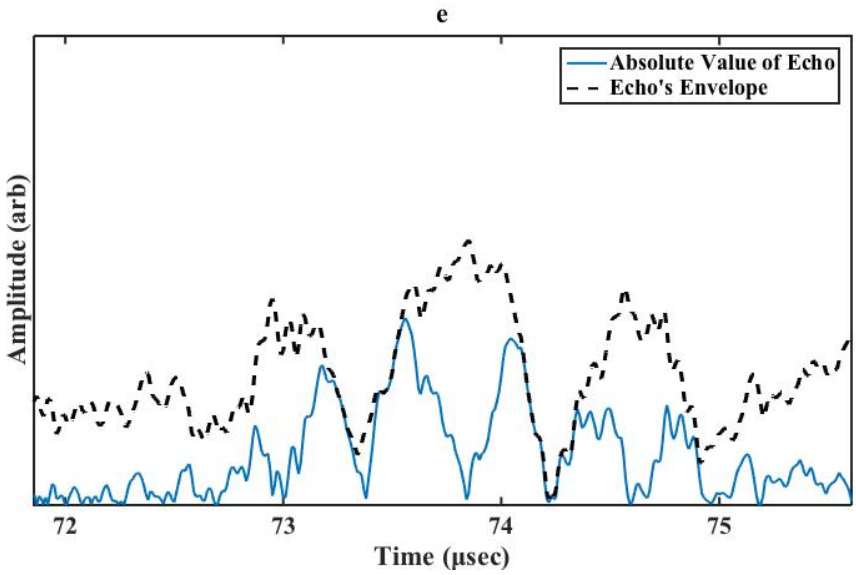

Figure 4.16 A sample of analysis procedure used for finding the position of largest peak in the envelope of ultrasonic RF signals from commercial (red line) and PVDF (blue line) transducers in test with silicone rubber phantom (a), signals after removing drift value (b), absolute value of signals (c), envelope of signals (d), zoomed part of received echo from PVDF transducer and its envelope (e).

Thickness of test objects in each position was calculated to find the displacement between them. Average value of displacement for each measurement cycle was found and plotted along with actual value in test with silicone rubber phantom and pork sirloin as shown in Figs. 4.17 and 4.18 respectively.

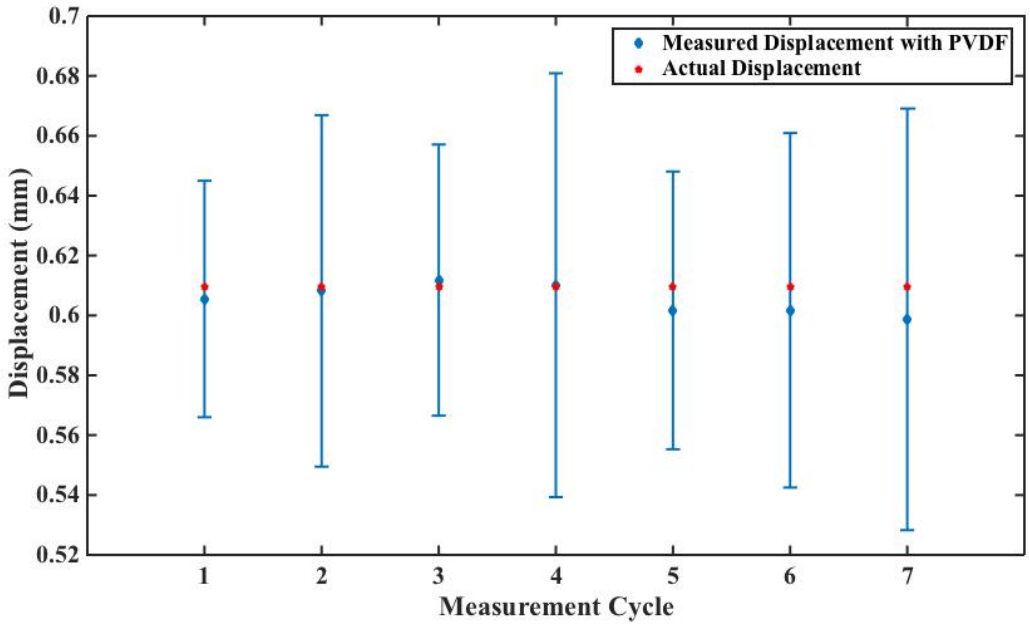

Figure 4.17 Average of measured displacement at different measurement cycles with PVDF transducer using "position of largest peak in the signal envelope" technique in comparison with actual value in test with silicone rubber phantom.

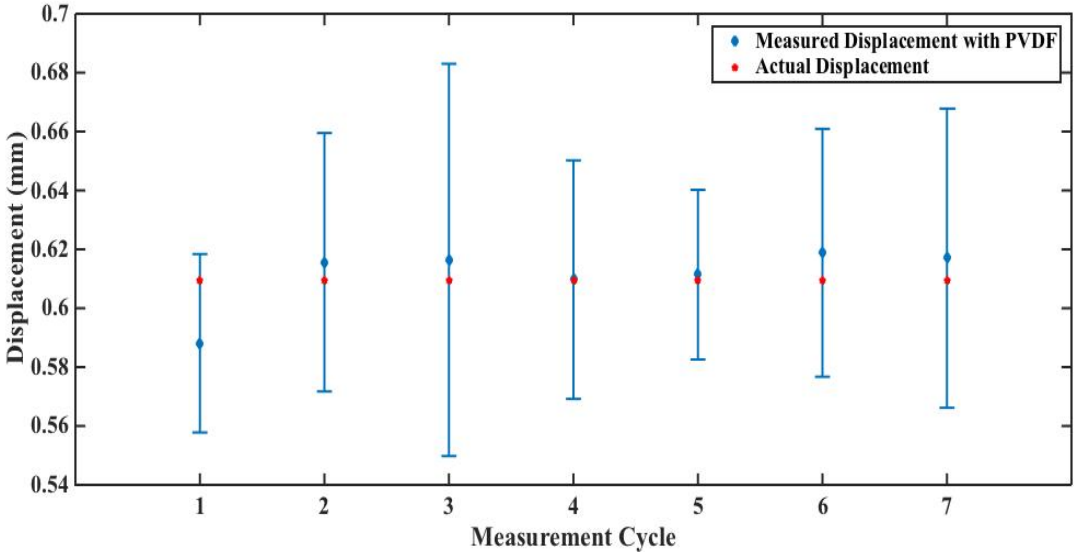

Figure 4.18 Average of measured displacement at different measurement cycles with PVDF transducer using "position of largest peak in the signal envelope" technique in comparison with actual value in test with pork sirloin.

The average of measured displacement using PVDF test with silicone rubber phantom and pork sirloin was 0.6054 ± 0.0569 mm and 0.6110 ± 0.0449 mm respectively.

4.5.4 Cross-Correlation

This technique measures the similarity between two signals at different time lag positions. One of its applications is measuring time delay between two signals. Cross-correlation of two sequences is the maximum at lag, which is equal to time delay between these sequences. In this method, first the average of ultrasound RF signal from both PVDF and commercial transducers at each position were obtained using the method was explained in section 4.5. Then the displacement between them was examined through cross-correlation. Fig. 4.19 shows the results of the cross-correlation function in test with pork sirloin in measurement cycle #1, between positions P5 and P6 (Fig. 4.5). As can be seen the peak value occurs at the lag of 32μs, which is equal to the sample delay between the two signals.

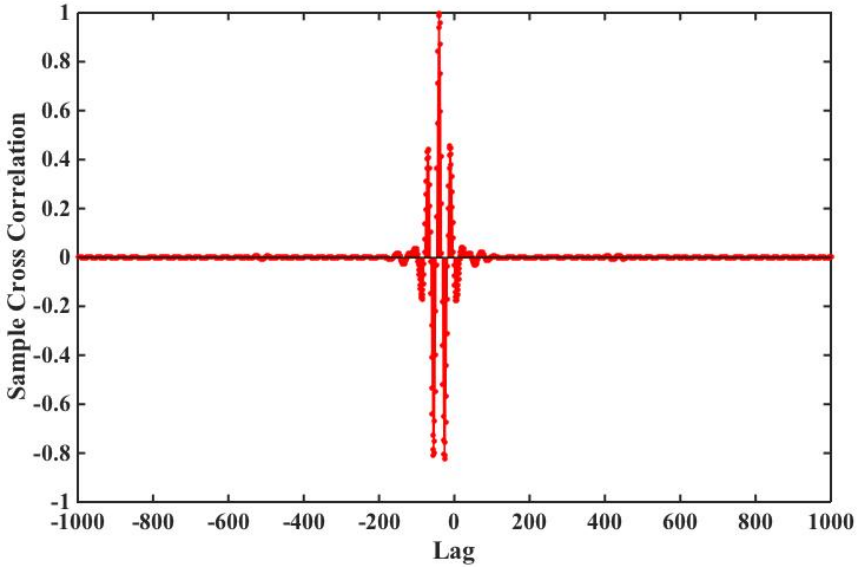

Figure 4.19 A sample of cross-correlation of two consecutive frames of ultrasonic RF signal used for finding the position of largest peak.

The average of displacement in each measurement cycle was calculated to compare with the actual value. Figs. 4.20 and 4.21 represent the performance of PVDF transducer for displacement measurement in test with silicone rubber phantom and pork sirloin respectively.

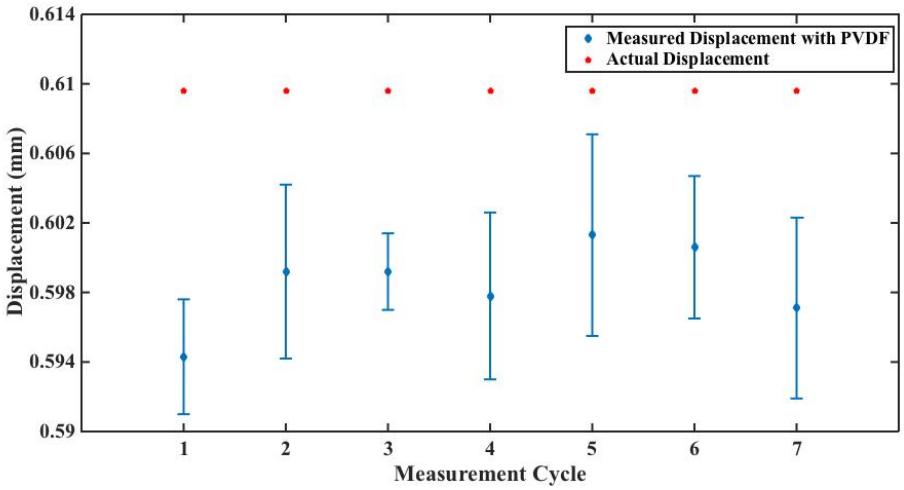

Figure 4.20 Average of measured displacement at different measurement cycles with PVDF transducer using "cross-correlation" technique in comparison with actual value in test with silicone rubber phantom.

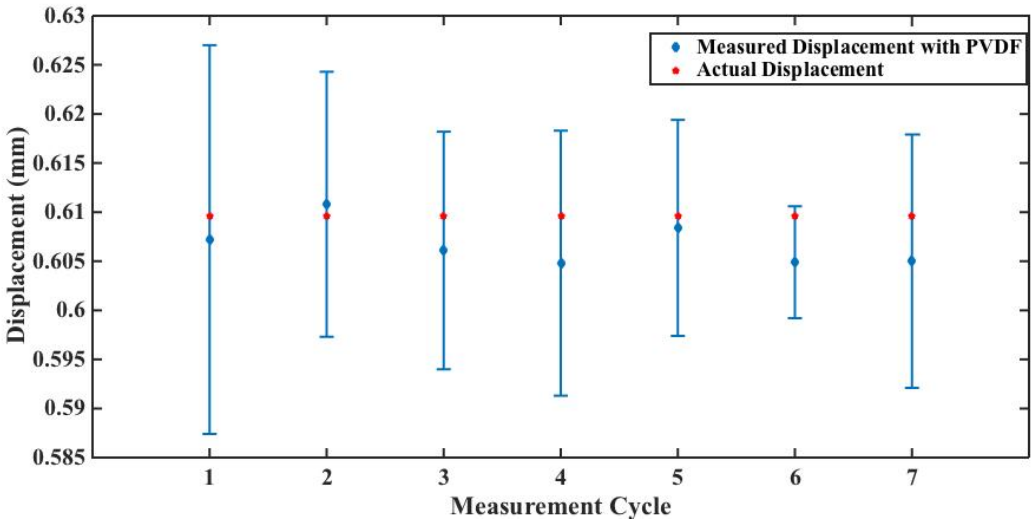

Figure 4.21 Average of measured displacement at different measurement cycles with PVDF transducer using "cross-correlation" technique in comparison with actual value in test with pork sirloin.

The average of measured displacement using PVDF test with silicone rubber phantom and pork sirloin was 0.5985 ± 0.0045 mm and 0.6068 ± 0.0132 mm respectively.

4.5.5 Results and Discussion

Tables 4-3 and 4-4 summarize obtained results of displacement measurement via the four different methods tested using PVDF transducer along with error indexes in tests with silicone rubber phantom and pork sirloin respectively.

Table 4-3 Error indexes of PVDF transducer for displacement measurement through four different ultrasonic techniques in simulation test with silicone rubber phantom.

Technique for Time Delay Measurement	Average of Measured Displacement (mm)	Standard Deviation (mm)	RSD %	Percent Deviation	Absolute Error (mm)	Relative Error %
Position of Positive Peak of the Echo	0.6434	± 0.2520	39.17	4.795	0.0338	5.54
Position of Peak in Absolute Value of Signal	0.6122	± 0.0222	3.63	0.3354	0.0026	0.43
Position of the Largest Peak in Envelope	0.6054	± 0.0569	9.40	0.6597	0.0042	0.69
Cross - Correlation	0.5985	± 0.0045	0.752	0.2983	0.0111	1.82

Table 4-4 Error indexes of PVDF transducer for displacement measurement through four different ultrasonic techniques in simulation test with pork sirloin.

Technique for Time Delay Measurement	Average of Measured Displacement (mm)	Standard Deviation (mm)	RSD %	Percent Deviation	Absolute Error (mm)	Relative Error %
Position of Positive Peak of the Echo	0.5429	± 0.1675	30.85	0.4325	0.0667	10.94
Position of Peak in Absolute Value of Signal	0.6012	± 0.1198	19.92	2.919	0.0084	1.38
Position of the Largest Peak in Envelope	0.6110	± 0.0449	7.35	1.131	0.0014	0.23
Cross - Correlation	0.6068	± 0.0132	2.17	0.291	0.0028	0.46

Table 4-5 indicates the mean values of error indexes for each method that is the average of related measured values in test with different phantoms.

Table 4-5 Average of error indexes of PVDF transducer for displacement measurement through four different ultrasonic techniques in simulation test with silicone rubber phantom and pork sirloin.

Technique for Time Delay Measurement	Absolute Error (mm)	Relative Error%	Percent Deviation	RSD %
Position of Positive Peak of the Echo	0.0502	8.24	2.614	35.01
Position of Peak in Absolute Value of Signal	0.0055	0.905	1.627	11.77
Position of the Largest Peak in Envelope	0.0028	0.46	0.8953	8.37
Cross - Correlation	0.00695	0.92	0.2946	1.46

Literature indicates that the mean difference of heel thickness between people with diabetic peripheral neuropathy and healthy subjects is 0.62 mm [3]. Thus the minimum of 0.62 mm spatial resolution is required to enable us distinguish between diabetic and healthy subject groups.

Comparing absolute errors confirms that this value in different method does not exceed 0.05 mm. Thus, all above-mentioned techniques cover the minimum required spatial resolution. We also need to consider the accuracy and precision of different techniques.

Accuracy is how close a measured value is to the actual (true) value that may be obtained by standard tools. By calculating percentage of relative error, we can determine exactly how accurate the measurements are. For measured values, the percent of relative error was calculated through Eq. 4.5. One can see in the results that the percent error in first method, position of positive peak in the echo, is more than those of others and is equal to 8.24% while percent error of displacement examined by other techniques does not exceed 1%. In other words, the measured values in other methods are approximately 1% far off from actual value while with the positive peak method the measured values are 8.24% off.

Precision defines how close the measured values are to each other. In other word precision is the percentage of repeatability or consistency of a measuring system. To evaluate sensor reproducibility, we looked at percent RSD and percent deviation, which are computed from Eqs. 4.6 and 4.7 respectively. Comparison of these parameters shows that cross-correlation has the most repeatability. Since in this research continuous measurement is desired, the precision of the measurements using the PVDF transducer is an important parameter.

In this study the motion of test objects was quasi-static and all processed data were taken while the phantoms were stable and motionless. In addition the number of scattering echoes was very low and applying averaging filter reduced the noise level. In this condition we may conclude that cross-correlation is the most consistent technique for displacement measurement. However, in the real application, monitoring the displacement of the tissue of the foot while moving, we may have different results.

4.6 Hysteresis of Measurement System

In this study we are interested in the tissue viscoelasticity, which is the area between the strain-stress curves obtained during load-unload cycle. Thus, it is essential to evaluate the measurement system hysteresis and subtract this value from whole hysteresis amount to make sure that measured value is related to the viscoelasticity of target tissue.

Measurement system contains force and ultrasonic sensors. Based on the specification of force sensor, hysteresis of FlexiForce A401 is less than 4.5% of full range that should be applied in tissue viscoelasticity calculations.

In order to examine PVDF transducer hysteresis an experiment was run using the previous setup with the exception that movement pattern was changed to the pattern is shown in the Fig. 4.22. With this pattern the z-stage increased the known displacement of 0.6096 mm in silicone rubber phantom in 6 steps to reach the overall displacement of 3.6576 mm and then decreased the displacement with the same steps to return back to the initial position. This experiment was done using silicone rubber phantom because viscosity of silicone rubber is negligible and we can assume that any drift value is due to the sensor.

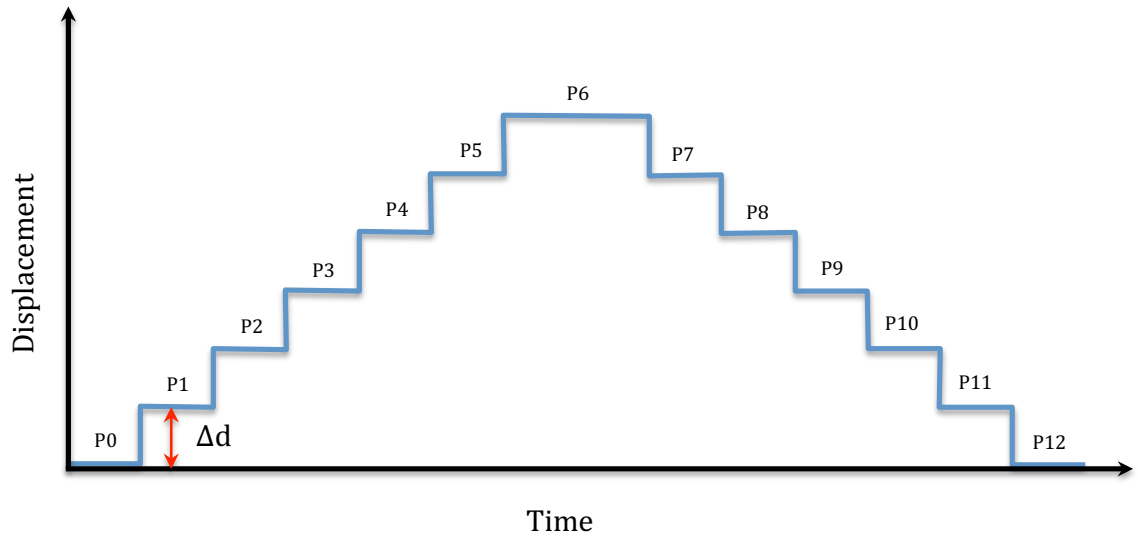

Figure 4.22 Movement pattern of positioning device in one measurement cycle for measuring the hysteresis of PVDF sensor.

The test was repeated for seven measurement cycles and the average of displacement was calculated through cross-correlation technique for each position as shown in table 4-6.

Table 4-6 The average of measured displacement using PVDF sensor in seven measurement cycles at different positions of Fig. 4.22

Position in Movement Pattern	Average of Overall Displacement (mm)	Position in Movement Pattern	Average of Overall Displacement (mm)
P0	0	P12	0.0016
P1	0.6096	P11	0.6064
P2	1.223	P10	1.221
P3	1.827	P9	1.836
P4	2.440	P8	2.440
P5	3.054	P7	3.056

The measured values were compared with the same position in the measurement cycle Fig. 4.22. For instance measured displacement in P0 was compared to the measured value in P12 and so forth and percent of hysteresis for displacement measurement was obtained through Eq. 4.10.

$$Hysteresis\ \% = \frac{|Difference\ of\ Displacement\ in\ the\ Same\ Positions|}{Actual\ Displacement} * 100 \qquad (4.10)$$

The results revealed that the maximum of hysteresis of displacement measurement system is approximately 0.52% of full measured range (3.6576 mm). This value shows the total hysteresis of z-stage, silicone rubber phantom and PVDF sensor. Since this experiment was performed under the quasi-static condition, the hysteresis of silicone rubber phantom is negligible. Positioning device displaces in steps with the repeatability of 5.080 μm. This error in comparison with the distance that is measured in this test, 0.6096 mm, is negligible as well and one can say that measured hysteresis belongs to the PVDF ultrasonic sensor. Research works indicate that hysteresis of the loading and unloading curves determines the soft tissue energy loss [82]. Measured hysteresis value is small in comparison with the percent of plantar soft tissue energy loss, which is 46.3 and 43.8 in diabetic and non-diabetic people respectively [82] however it can be considered in calculation while mechanical behavior of tissue is examined.

4.7 Repeatability of FlexiForce A401

The purpose of performing this test was to evaluate the precision of FlexiForce A401 sensor for pressure measurement in quasi-static motion. To do so, in previous experiments FlexiForce A401 was placed under the PVDF transducer as shown in Fig. 4.2 and force was calculated for each position in a measurement cycle through Eq. 3.8.

For force measurement the average of same frames that was used for displacement measurement at each position was considered.

Fig. 4.23 shows the force variations during one measurement cycle that was obtained using FlexiForce A401.

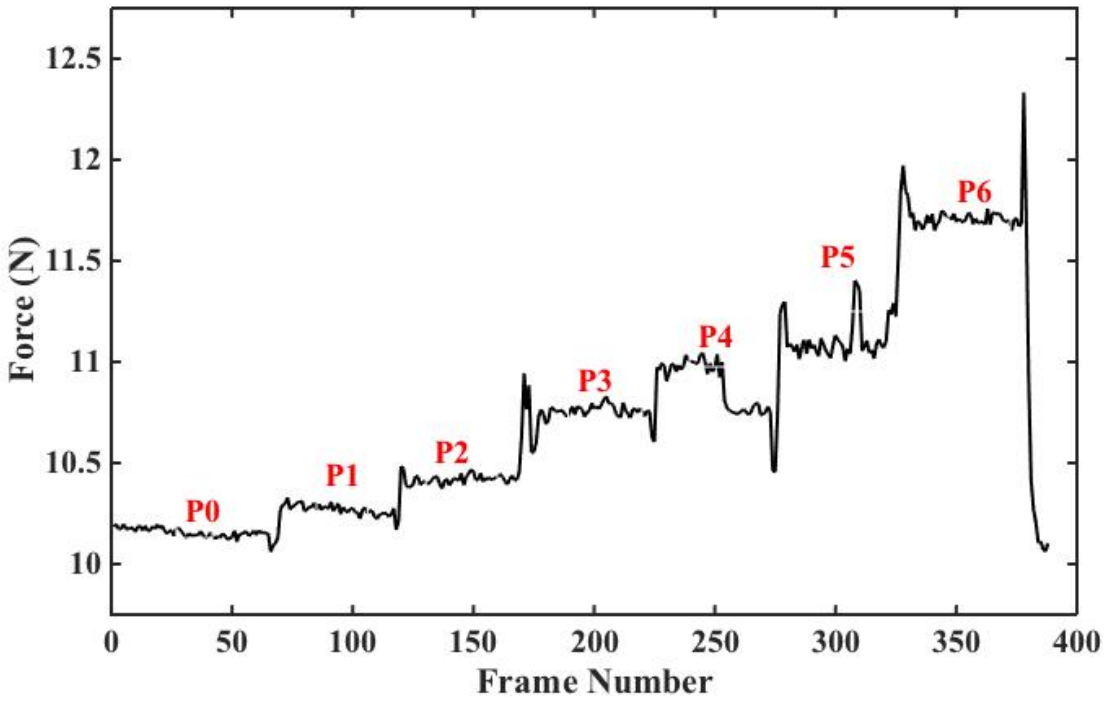

Figure 4.23 Average of measured force during one measurement cycle in simulation test with silicone rubber phantom.

Experiment was repeated 7 times and the average of force and standard deviation for position i was calculated through the following formulas:

$$F_{avg}.(i) = \frac{\Sigma(Fij)}{7} \qquad 1 \leq j \leq 7 \qquad (4.11)$$

$$\mathrm{sd}_{\mathrm{avg}}.(\mathrm{i}) = \frac{\Sigma(sdij)}{7} \qquad 1 \leq j \leq 7 \qquad (4.12)$$

Where j represents the number of measurement cycle. Fig. 4.24 illustrates the results of force measurement in test with silicone rubber phantom.

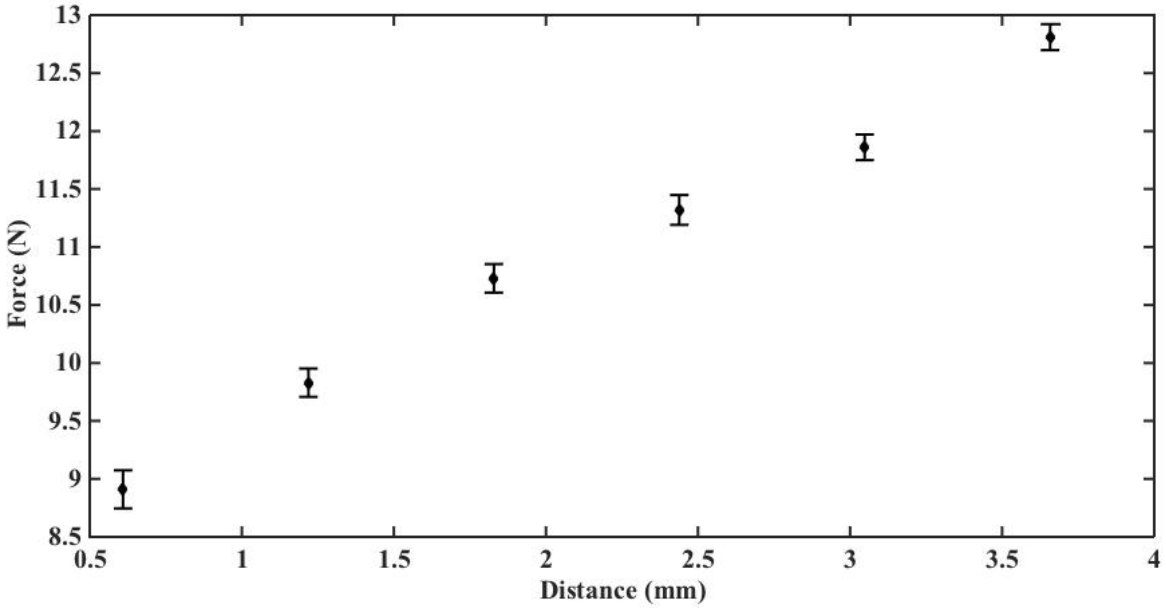

Figure 4.24 Repeatability of force sensor for measuring applied force in simulation test with silicone rubber phantom.

There were some limitations for accuracy measurement due to the limitation of equipment in our laboratory. The absolute value of applied force in this test was not measured because the only reference tools that we had, was a digital scale. When we put this scale under the silicone rubber phantom to measure applied force, the reading value of mass varied over time and it did not remain constant. At this time we do not know why it happened. Then we were not able to measure the true value of applied force for accuracy measurement and the measured accuracy by manufacturer was considered as a reference.

We estimated applied force in each position using force sensor that was calibrated using Vernier force plate as explained in chapter 3 and examined reproducibility of sensor. We

did not have data in position 6 of Fig. 4.5. It could be due to the contact of sensors' wires. So we used data related to positions 0-5 in each measurement cycle. Table 4.7 shows obtained results.

As can be seen from the table 4-7 the percent of RSD, which represents sensor precision does not exceed 1.76% for the force range between 7 ~ 10 N. Based on the manufacturer's user manual repeatability of force sensor for bigger load up to 90 N is less than 2.5%. The applied force in our experiment was only 9% of sensor full range but with this experiment setup it was not possible to increase the amount of load; because the goal of test was to create a displacement of approximately 0.61 mm in the test objects, which is close to the minimum required spatial resolution in for measuring plantar soft tissue mechanical properties (0.62 mm). Besides the positioning device is not made to apply force but to create known displacement and we cannot put too much stress on it.

According to the force sensor manufacturer's information the error of FlexiForce A401 is less than 3% and the repeatability is 2.5% of full range, which is in a good agreement with our results. So based on the results force sensor is good enough to be used in this application.

Table 4-7 Error indexes of FlexiForce A401 for measuring applied force in simulation test with silicone rubber phantom.

Position	Average of Measured Force (N)	Standard Deviation (N)	Percent of RSD
0	7.01	0.1231	1.76
1	7.70	0.0926	1.20
2	8.39	0.0944	1.12
3	8.85	0.0992	1.12
4	9.26	0.0859	0.93
5	10.00	0.0882	0.88

Chapter 5: *In-vivo* Measurement of Mechanical Properties of Plantar Soft Tissue

In this chapter, a method is introduced to extract pressure–displacement curve for plantar soft tissue at heel region during one compression–release cycle while the person is stepping. Force and displacement are measured simultaneously in tests with different conditions, starting the measurements with a near-to-ideal condition and ending with a condition that simulates the real use. In this chapter signal processing is explained in details.

5.1 Measurement Setup

In the tests of the present chapter the PVDF ultrasonic sensor was driven by an ultrasonic pulser/receiver (Model: 5900, Panametrics-NDT, Waltham, MA, USA) while energy and gain was set to 32 μJ and 54.0 dB respectively. The ultrasonic RF signals and output voltage of force sensor were acquired by a PCIe digitizer (Model: ATS9440, AlazarTech, Montreal, QC, Canada) with sampling rate of 125 MS/s and 14-bit resolution with a frame rate of 100 Hz. The maximum number of decimal digits was chosen based on the resolution of digitizer. Force sensor was driven using resistance feedback (R_F) 20kΩ to match the scale. The sensor was calibrated again using new resistance feedback. Following equation was used for force measurement in the further experiments where F and V_{out} are applied force and output voltage of FlexiForce. This equation was obtained according to the procedure that was explained in section 3.2.5.

$$F = 240\ V_{out} + 0.785 \qquad (5.1)$$

5.2 Simultaneous Measurements of Force and Tissue Displacement

In this experiment signals were acquired from the end part of heel. This region was chosen because previous tests showed it provided a stronger echo and with a relative independence of the angle. This can be explained by the size of the bone - big, the bone position - near the surface and shape - round.

To measure the applied force and the resulting tissue displacement simultaneously, the force sensor was fixed on a flat plate using adhesive and the ultrasonic sensor was placed on top of it, as shown in Fig. 5.1. An ultrasonic couplant was applied between the heel and ultrasonic sensor surfaces. A participant put the end part heel of her right foot on top of the sensors. The applied load on the sensor increased and decreased gradually by bending the body forward and backward.

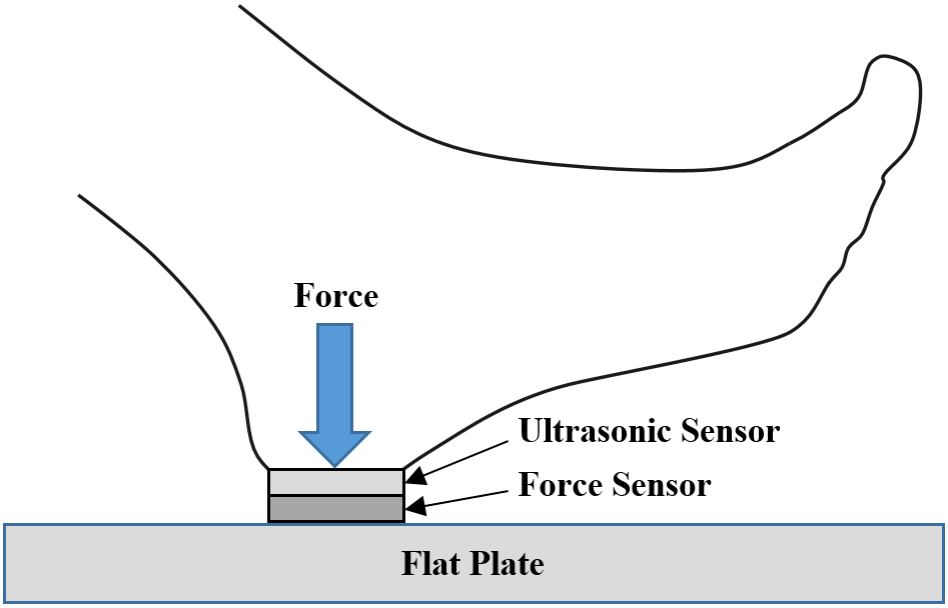

Figure 5.1 Experimental setup and sensor configuration for simultaneous measurements of applied force and tissue displacement at end part of heel.

Force and ultrasonic sensor output were recorded simultaneously. When the PVDF sensor was placed on top of the FlexiForce A401, the noise level increased dramatically and

received echo was not detectable. To solve this problem, the ground of PVDF and drive board of force sensor was connected to each other. In this way noise was reduced to some extent but taking average was essential to reduce the noise level and detect received echo but averaging was not desirable with frame rate of 100 Hz, as it blurs the echo. So extra shield was applied to PVDF transducer and wires to reduce electrical noises. The following picture shows the new PVDF transducer.

Figure 5.2 Thin and flexible PVDF ultrasonic transducer

The output signal of force sensor was recorded and transferred to Matlab environment for processing and display. In this trial approximately 450 frames were recorded for one cycle of force increase and decrease. The sample rate for the force sensor was the same for the ultrasound signal, a constraint of the PCIe digitizer, thus for each frame 10016 samples of the force was acquired. The mean value of the force for each frame was calculated and plotted with respect to the acquiring time. Fig. 5.3 shows the pressure variations during the experiment obtained by the force sensor. The pressure was obtained by dividing force to the sensor's active sensing area. Since this experiment starts with the participant's foot over the sensor, the initial pressure is not zero.

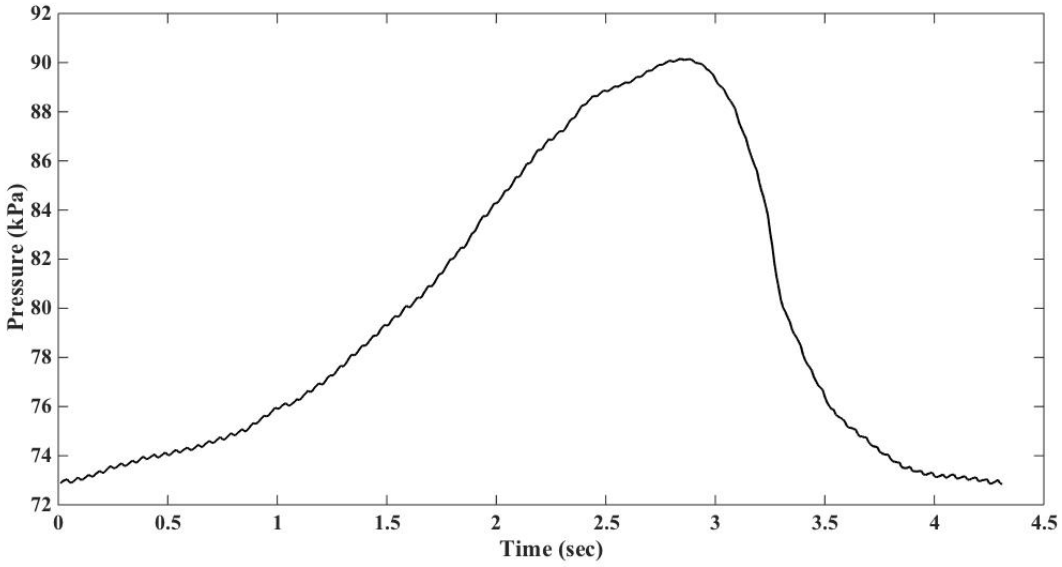

Figure 5.3 Average of measured pressure of plantar soft tissue at heel region during one compression-release cycle.

As explained in chapter 4, we have found that, between the methods we have studied, cross-correlation is the most consistent ultrasonic technique for displacement measuring using PVDF transducer where the amplitude of scattering echoes is very low when comparing to the echo of interest. To obtain the tissue displacement due to the applied force, first a time window containing an echo from the heel bone was selected, as shown in Fig. 5.4, then the time delay change of the bone echo between two consecutive frames was calculated using a cross-correlation method. Defining the position of initial echo is crucial in this method because the time window tracks the desired bone echo using the echo position in the previous frame. So if the position of echo in the first frame were determined falsely, the displacement curve would not be reliable. In addition the window size needs to be carefully selected so that it is large enough to contain a target echo in two consecutive frames. However, a window that is too wide may increase the number of outlier results.

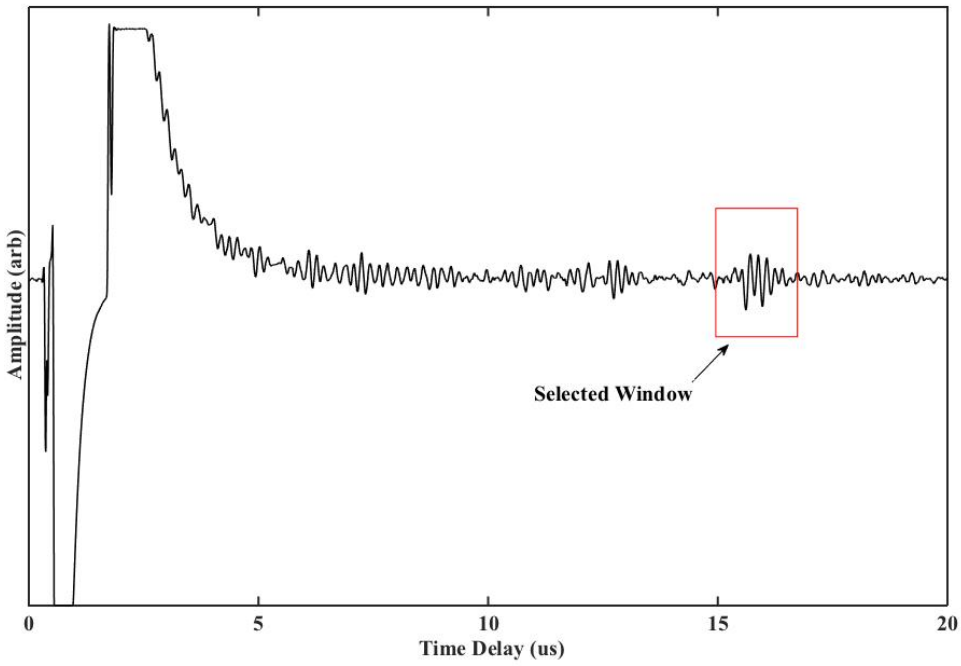

Figure 5.4 RF ultrasonic signal from heel bone and time window for tissue displacement calculation using cross-correlation technique.

In most cases the time delay obtained from cross-correlation method was zero, while manual measurement showed a difference of at least 0.008 ns. To solve this problem, the cross-correlation result was interpolated by ten points between the sample points. In other words the values of the curves was estimated at 10 positions between the known points to increase the time delay estimation resolution. In this study, linear interpolation was used because of its simplicity. We did cross-correlation and then interpolated the results to find the position of largest peak. Taking integral by adding those numerical values yielded the overall displacement as shown in Fig. 5.5. In order to find whether the order of this procedure affects the results or not, the processing of data was repeated by first interpolating the RF ultrasonic signals and then cross-correlating of two consecutive frames of RF ultrasonic signals. The results remained the same.

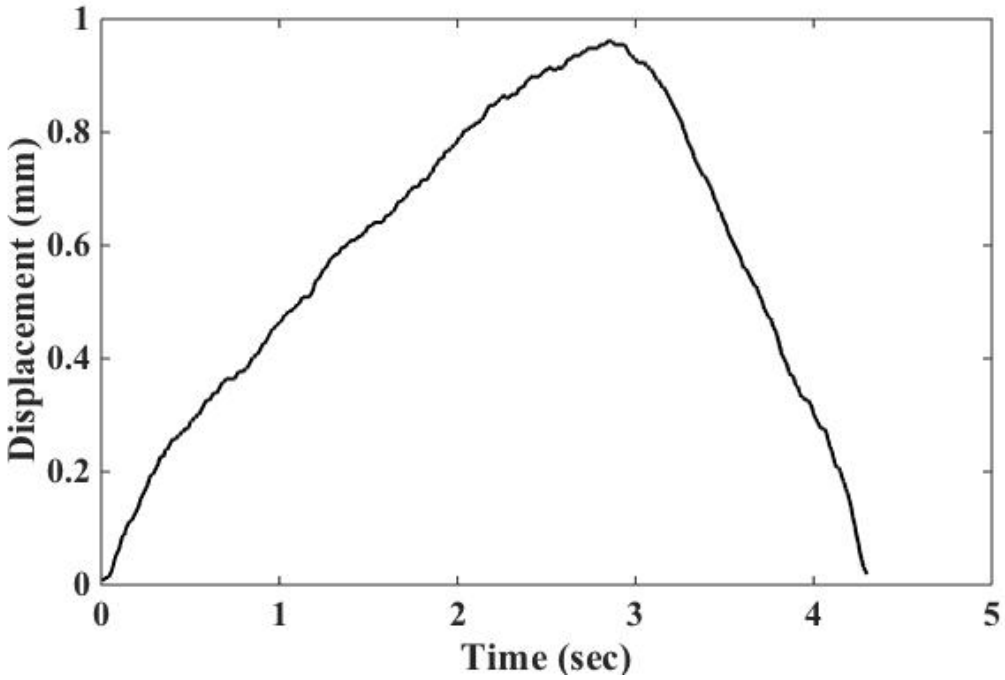

Figure 5.5 Measured displacement of plantar soft tissue at heel region during one compression-release cycle.

As can be seen from the above plot, thickness of plantar tissue has changed as a result of applied load and the form of variation is in concordance with the pressure alteration.

In order to verify the results of displacement measurement obtained by developed algorithm, an M-mode image of plantar soft tissue for one compression-release cycle was plotted in Matlab environment, as shown in Fig. 5.6 to visually check the displacement. The image shows a displacement of 1 mm, which is in good agreement with obtained result from developed method (Fig. 5.5).

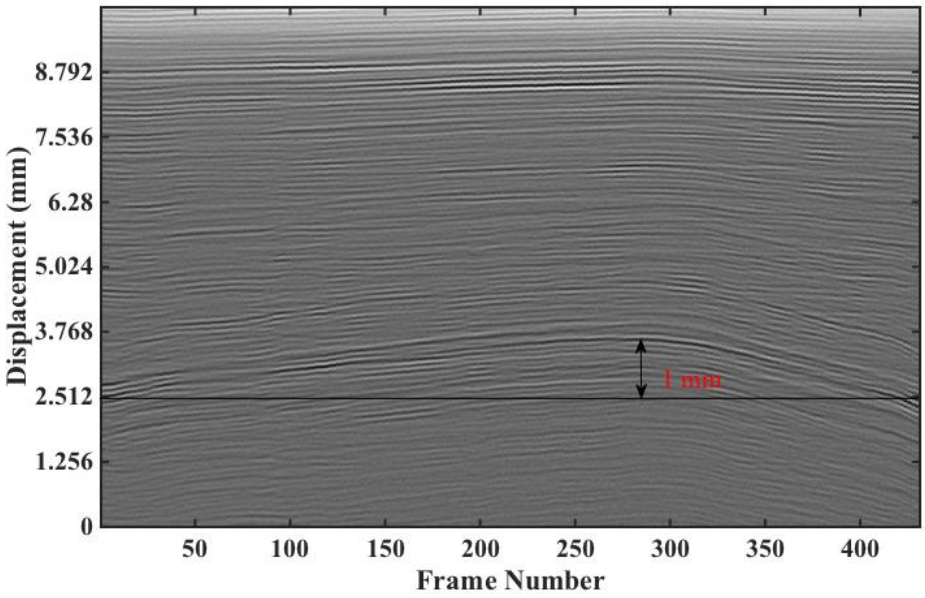

Figure 5.6 M-mode image of plantar soft tissue and maximum of tissue displacement taken during one compression-release cycle.

Having pressure and displacement data for one compression-release cycle, pressure-displacement curve could be plotted as shown in Fig. 5.7.

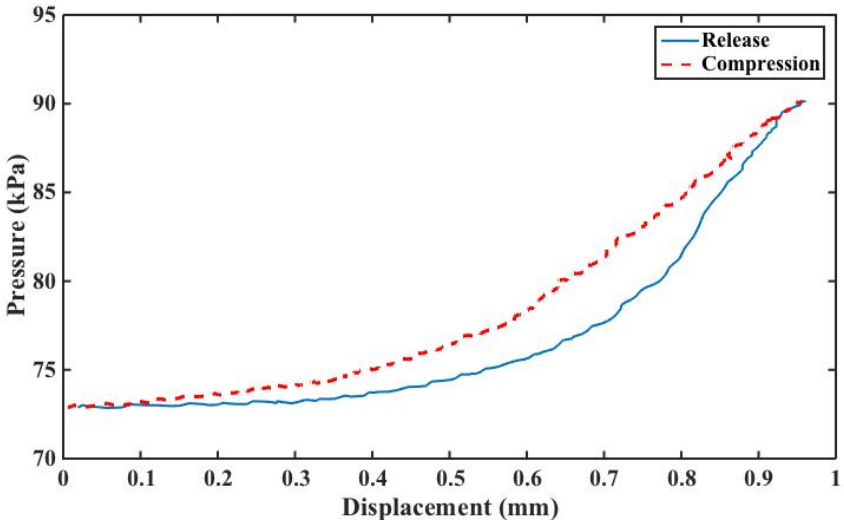

Figure 5.7 Pressure-displacement curves obtained for plantar soft tissue at heel using wearable ultrasonic and force sensors fixed on a flat plate.

Using this curve certain mechanical properties of plantar soft tissue are computable. In this curve the area between loading and unloading pressure-displacement curves defines tissue viscoelasticity (tissue energy loss). This hysteresis may contain the hysteresis of force and ultrasonic sensors. Based on the force sensor manufacturer's information hysteresis of FlexiForce A401 is 4.5% of full range that could be considered in calculation by subtracting this value from the whole hysteresis amount. As indicated in chapter 4, section 4.6 the hysteresis of PVDF transducer is 0.52% that could be applied in computation as well.

By measuring the initial thickness of plantar tissue, strain will be obtained as strain is defined as displacement over initial thickness. In addition in strain-stress curve slope of the loading curve after the inflection point defines the modulus [83]. Moreover other mechanical properties such as stress and strain peak are measureable. Therefore using developed system we are able to extract strain-stress curve, which is a representation of tissue behavior and mechanical properties.

This experiment was repeated and pressure–displacement curves were obtained for two consecutive compression–release cycles as seen in Fig. 5.8.

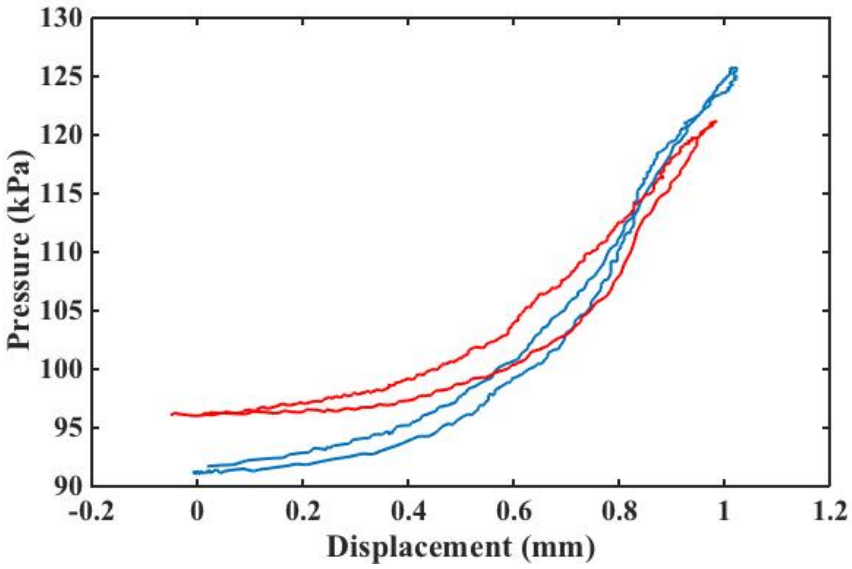

Figure 5.8 Pressure-displacement curves obtained for plantar soft tissue at end part of heel during two consecutive compression-release cycles.

The difference of curves could be justified as a difference of applying load speed and frequency. Pai *et al*. demonstrated that both modulus and energy loss of plantar soft tissue are strain rate dependent and these parameters increase with enhancement of applied force frequency [54]. Also the tissue becomes conditional after several load-unload cycles, which leads to have different pressure-displacement curves. Evaluation of the Effects of Uneven Load on Measurement System and an Algorithm to Remove Outlier Data

An experiment was conducted to investigate the effects of uneven load on the measurement system. In this test both force and PVDF sensors were placed and fixed inside a shoe on heal area and the person (male, 90 Kg) was standing on his right and left foot alternatively. Following picture illustrates test layout.

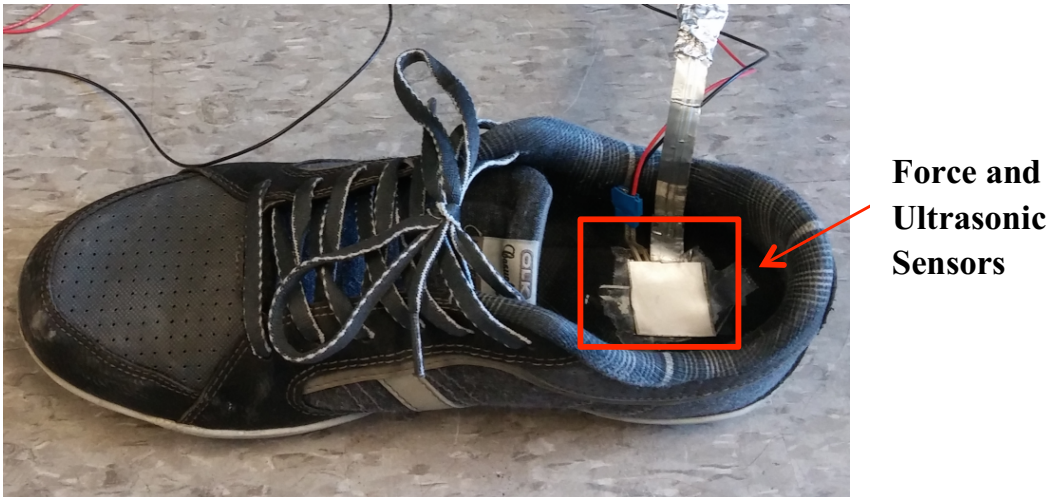

Figure 5.9 Wearable ultrasonic and force sensors attached onto the shoe sole at heel part.

Output signals of force and ultrasonic transducers were recorded simultaneously and test setup was kept as same as previous one. Pressure signal was obtained by taking the average of each frame and plotting the average points with respect to the time. In this experiment the person did the experiment slowly and paused a while when he put his foot on the flat plate. So as can be seen from the Fig. 5.10 there is a flat part in the pressure signal. The results showed that force sensor follow pressure changes well confronting uneven loads and it can be used in next experiments where the real condition of use is simulated.

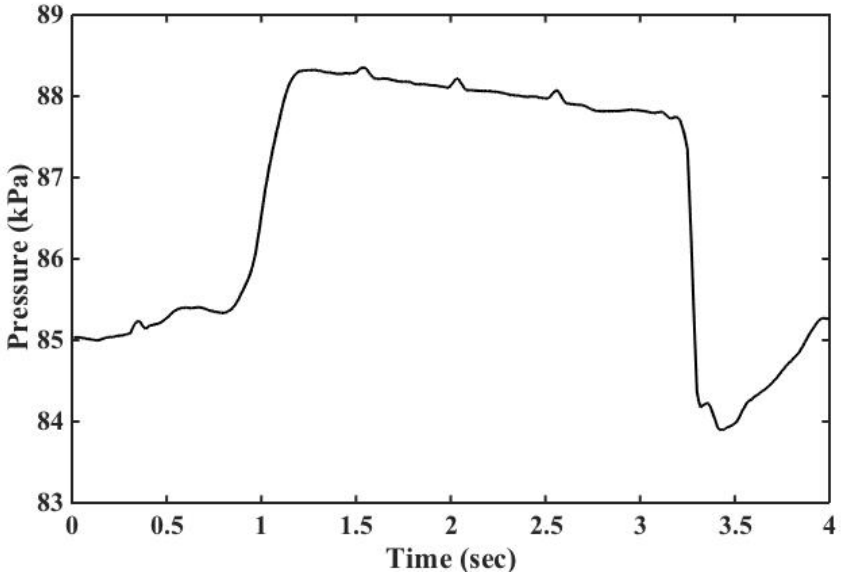

Figure 5.10 Average of measured pressure of plantar soft tissue at heel during one compression-release cycle

For displacement measurement, time delay between two consecutive frames was computed via cross-correlation method as before. Accurate tracking of the desired echo sometimes failed when an uneven force (not normal to the sensor) was applied on the sensors, resulting in outliers as shown in Fig. 5.11.

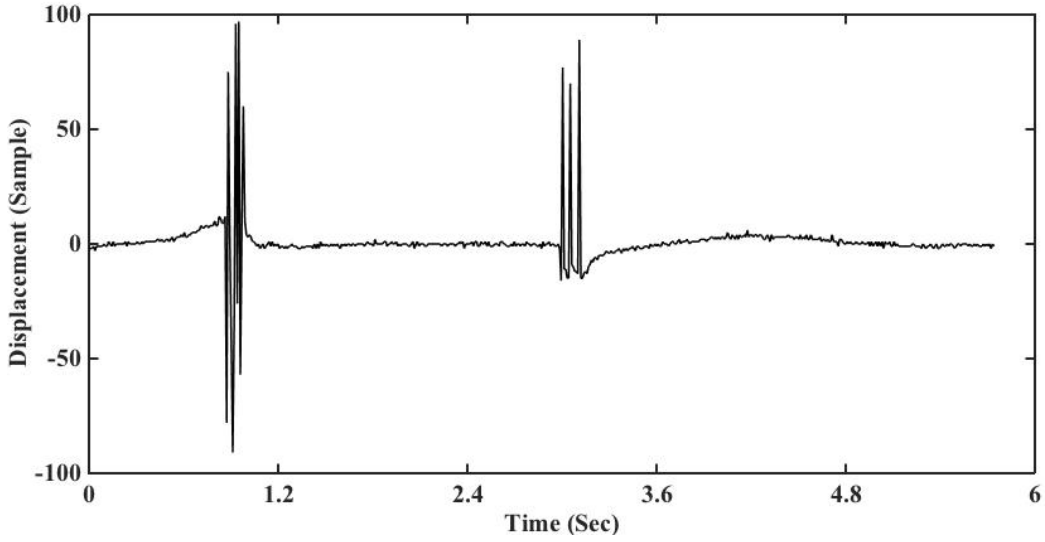

Figure 5.11 Measured displacement between two consecutive frames of ultrasonic RF echo during one compression-release cycle and outliers.

To remove those outliers first, the strength of echo was measured for each frame by examining the peak – peak amplitude of echo to check if outliers could be removed based on the difference of their echo strength with other data. Results demonstrated that outliers couldn't be distinguished based on that parameter; because the peak – peak amplitude of some outliers are higher than true ones and are very close to the mean value as seen from Fig. 5.12, which demonstrates two outlier points and their related amplitude.

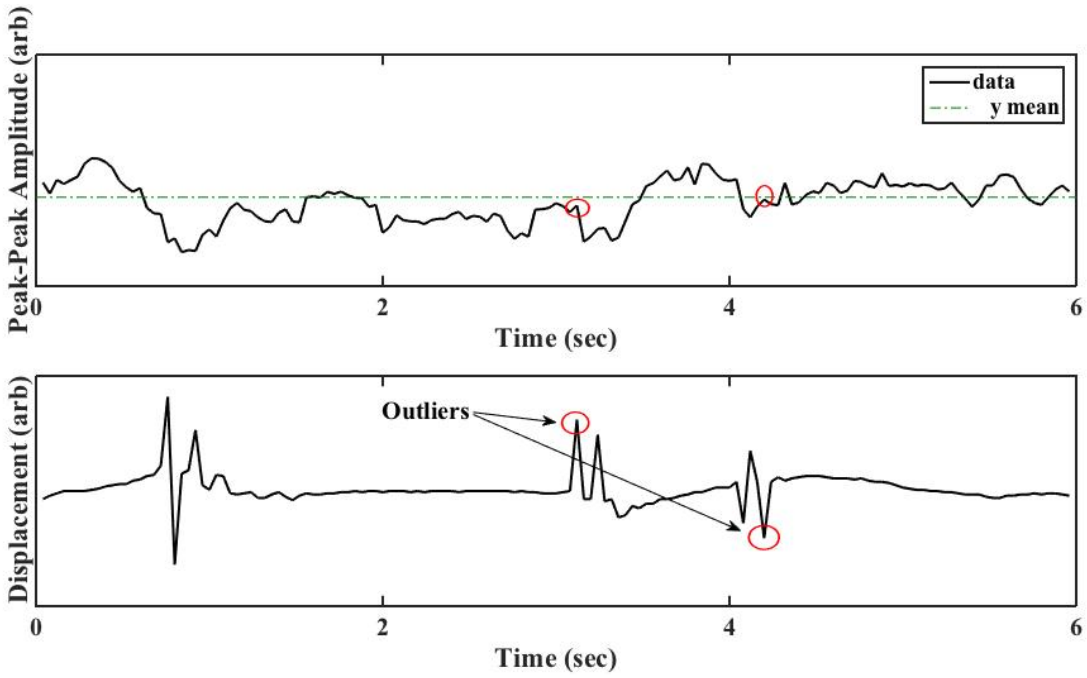

Figure 5.12 Peak-to-peak amplitude of received ultrasonic RF echoes with highligthed corresponding values of outliers during one compression-release cycle (a), measured displacement between two consecutive frames of ultrasonic RF echo during one compression-release cycle and outliers (b).

Therefore another method was used to remove outliers. In this technique, first the time delay between two consecutive frames was measured. Analyzing data revealed that the value of time delay with respect to the subject's movement speed does not exceed 0.056 μs. Thus all frames with bigger time delay were replaced by the average value of two

previous frames. The below graphs illustrate the time delay between two consecutive frames with and without outliers.

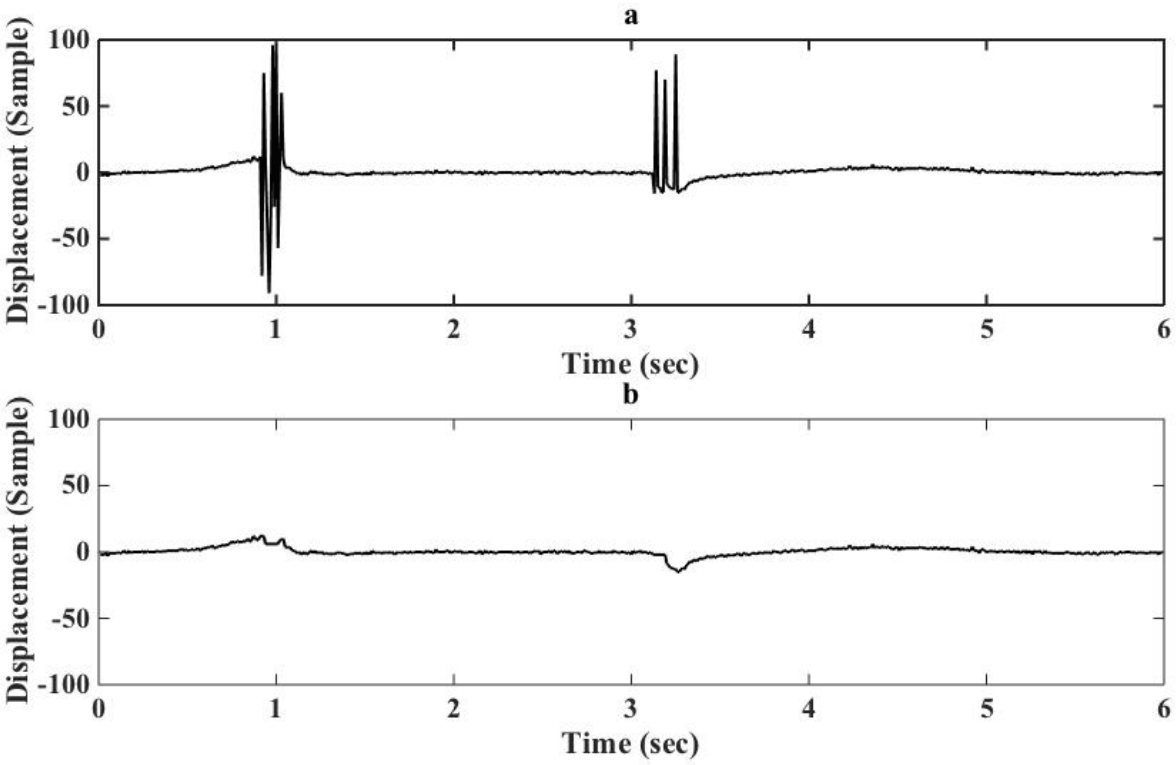

Figure 5.13 Measured displacement between two consecutive frames of ultrasonic RF echo during one compression-release cycle with outliers (a), measured displacement between two consecutive frames of ultrasonic RF echo during one compression-release cycle after removing outliers (b).

Taking the integral from consecutive displacements yields the overall displacement of plantar soft tissue. The overall displacement of the plantar soft tissue for one compression-release cycle is shown in the following figure.

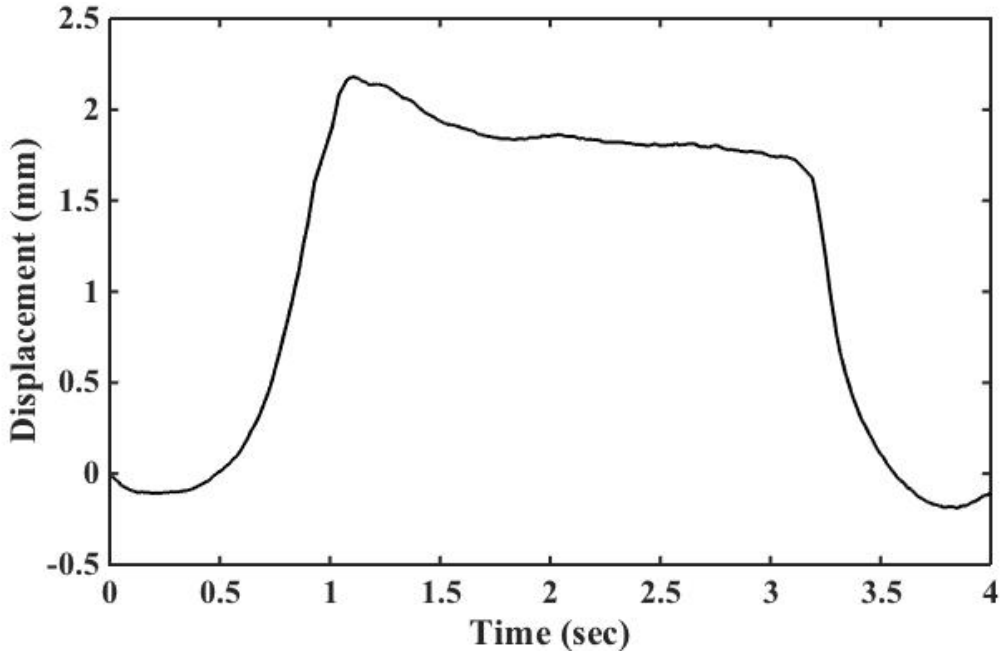

Figure 5.14 Measured displacement of plantar soft tissue at heel during one compression-release cycle.

As can be seen from Fig. 5.14 thickness changes follow the variation of applied pressure in this test (Fig. 5.10). In order to verify the results of displacement measurement obtained by developed algorithm, an M-mode image of plantar soft tissue for one compression-release cycle was plotted in Matlab environment, which is illustrated in Fig. 5.15. The image shows a maximum displacement of approximately 2.3 mm, which is in good agreement with obtained value from developed method (Fig. 5.14).

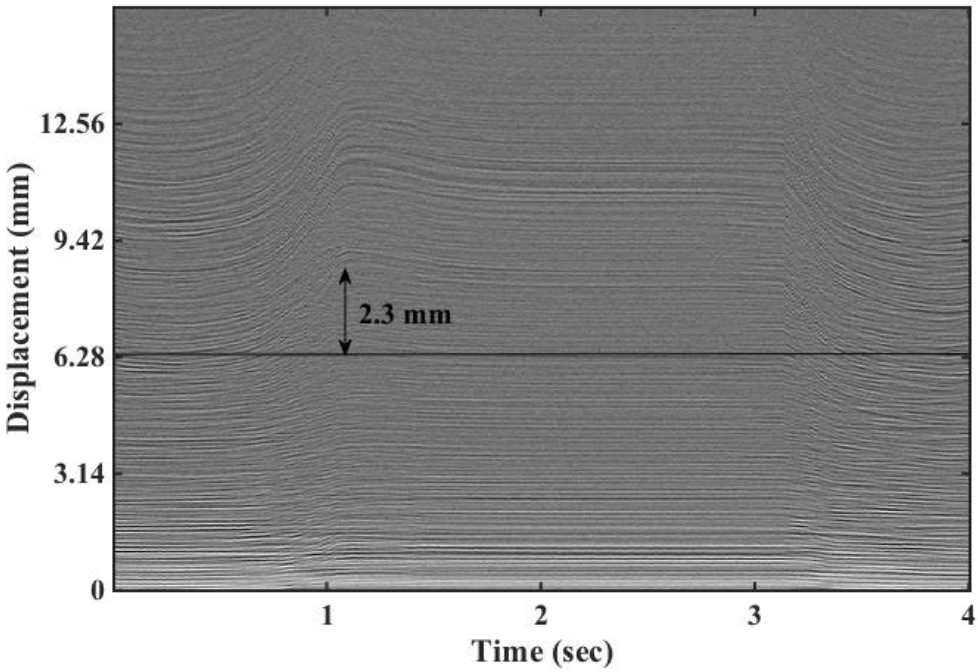

Figure 5.15 M-mode image of plantar soft tissue and the maximum of tissue displacement taken during one compression-release cycle.

The limitation of this method is that this algorithm does work only if the first two frames are not outliers because we are tracking the first echo and outliers are replaced by the average of two previous frames. So the position of initial echo is crucial and determinative. To make sure that the first frame is not outlier, M-mode image of data was plotted in Matlab environment and the position of positive peak was found visually.

Replacing outliers by the average of two previous frames creates artifact and it would be better to use the average of previous and next valid frames but the problem was that in most cases we did not have valid data over a period of time. In other words we had consecutive outliers. So next valid data was available 1 or n frames in the future and the

algorithm was complicated. As the method we used presented a satisfactory result, that algorithm was not used.

5.3 Simulating the Real Condition of Use

In order to verify performance of measuring system in real application, sensors were adhered to a participant's heel before the person donned their shoe as shown in Fig. 5.16. Continuous measurements of pressure and displacement were conducted using the wearable sensors and data acquisition system while a participant was alternating his weight between feet.

Figure 5.16 Wearable ultrasonic and force sensors attached onto the heel (a), and person wearing his shoe and sensors (b).

The following graph illustrates the variation of applied pressure for five steps of the participant (male, 90 Kg).

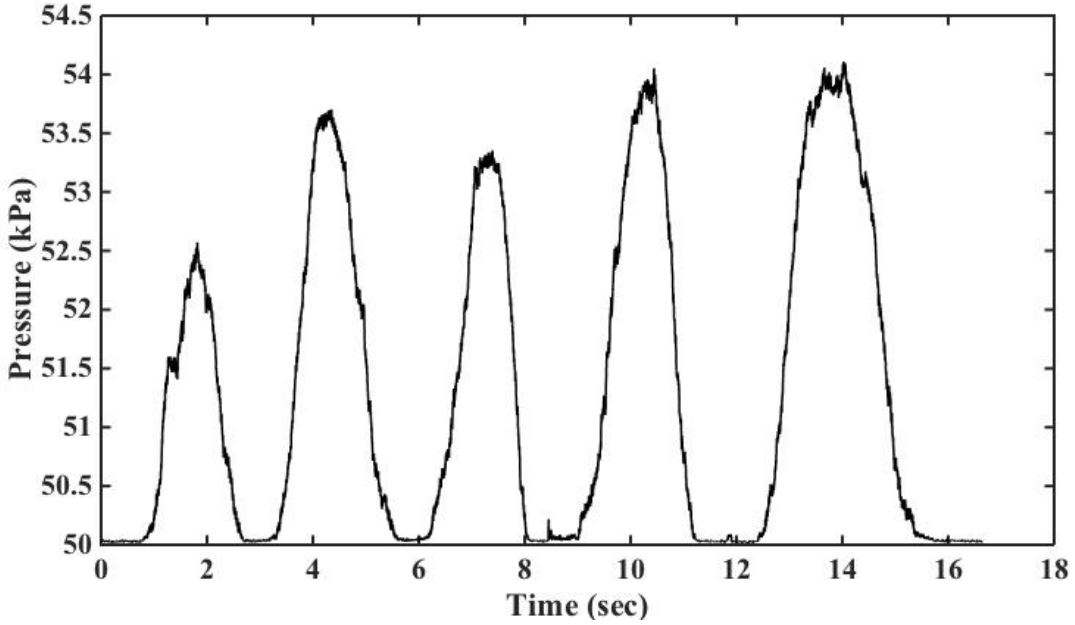

Figure 5.17 Average of measured pressure of the plantar soft tissue at heel during five compression-release cycles.

For measuring tissue displacement, the test region's initial thickness must be estimated; therefore, the received echo from bone's location in the ultrasound RF signal should be specified. Results from this study had more scattered echoes, in comparison with previous research with testing at the end part of heel (Fig. 5.1). The scattered echoes increased the number of outliers. To solve this problem, we raised the frame rate to 1 KHz when obtaining tissue displacement. To analyze data and calculate displacement, first the average of every five frames was calculated to reduce the level of the random noise. Next, the M-mode image was used as a reference for pre-estimating the desired echo's initial location as before. To assure of the position of initial desired echo, the envelope of ultrasonic RF signal was plotted to find the position of strongest echo in the

first frame. Fig. 5.18 demonstrates an M-mode image of ultrasonic RF signals and Fig. 5.19 illustrates the envelope of first frame of second step.

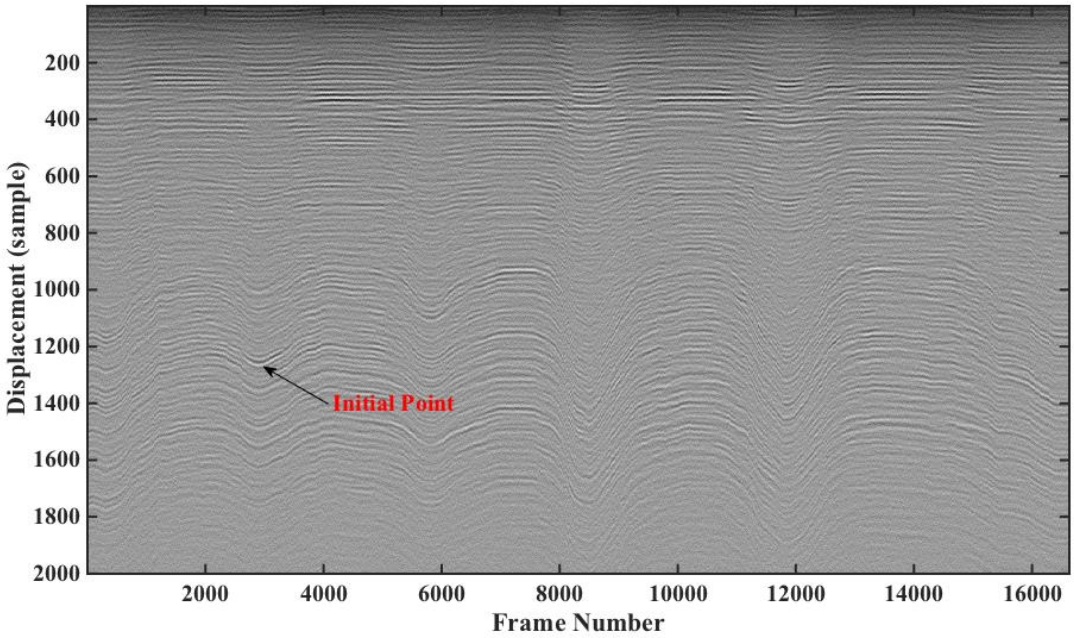

Figure 5.18 M-mode image of plantar soft tissue taken for five compression-release cycles and position of initial point of second cycle.

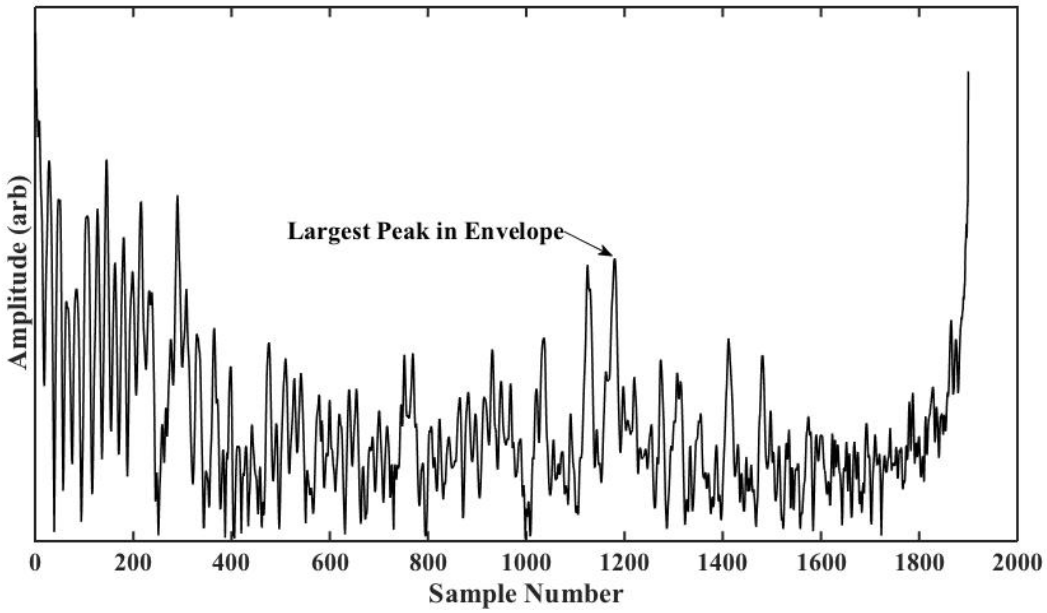

Figure 5.19 Envelope of first frame of ultrasonic RF signal and position of largest peak.

In this experiment data was recorded for 5 steps and second step was considered arbitrarily for mechanical properties estimation. As seen in both figures, on the frame chosen that was the initial frame of the second step, the peak echo is placed at the sample number 1200.

In addition, the size of the time window that included the desired echo was shrunk to avoid interference with scattering echoes. To find the right size of time window the envelope of several frames of RF ultrasonic signals were plotted together and the position of desired echo was tracked visually as demonstrated in Fig. 5.20. It was found that the sample delay between the echoes in two consecutive frames does not exceed 5 samples, which is equal to 0.04 μs, recalling that in this study the sampling rate was 125 MHz. For displacement measurement, we limited the size of time window between 0.048 μs and 0.096 μs, which is equal to sample window of 6 and 12 samples.

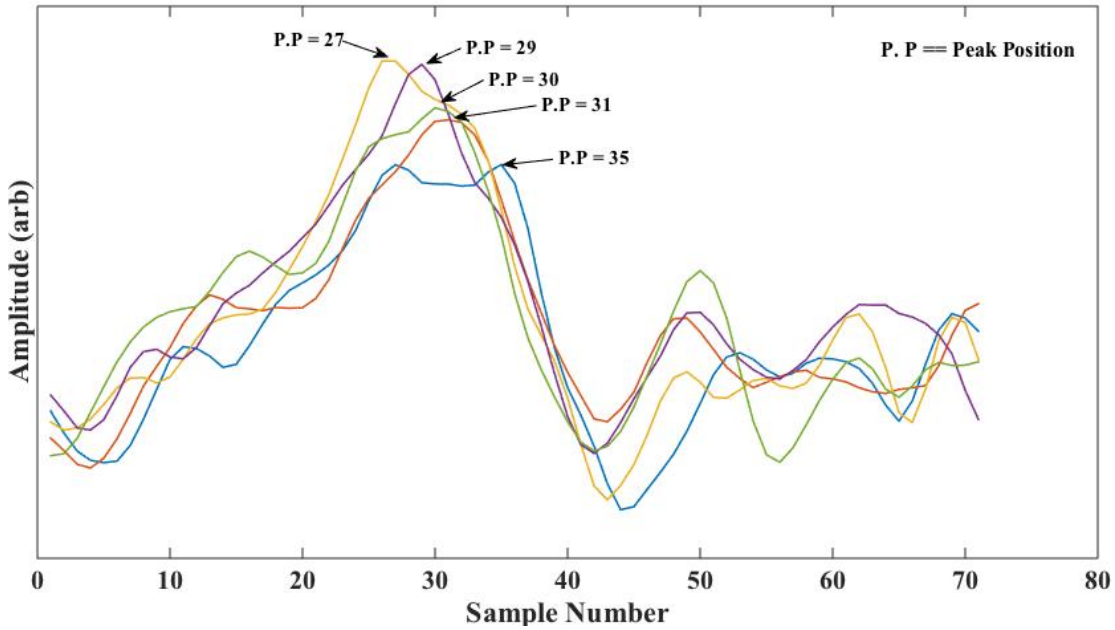

Figure 5.20 Position of the largest peak in the envelope of five consecutive frames of ultrasonic RF signal.

This algorithm was not automatic and for each compression–release cycle we needed to find the desired echo's initial position. Also the size of time window was adjusted by try and error to check what size gives the best results in terms of outlier numbers.

Since the frame rate in this test had been raised, force and displacement curves were smoothed by a moving average filter with the span of five to remove sharp edges. Fig. 5.21 presents the results of pressure-displacement curves obtained from measurement of the force and displacement by the developed sensor and method.

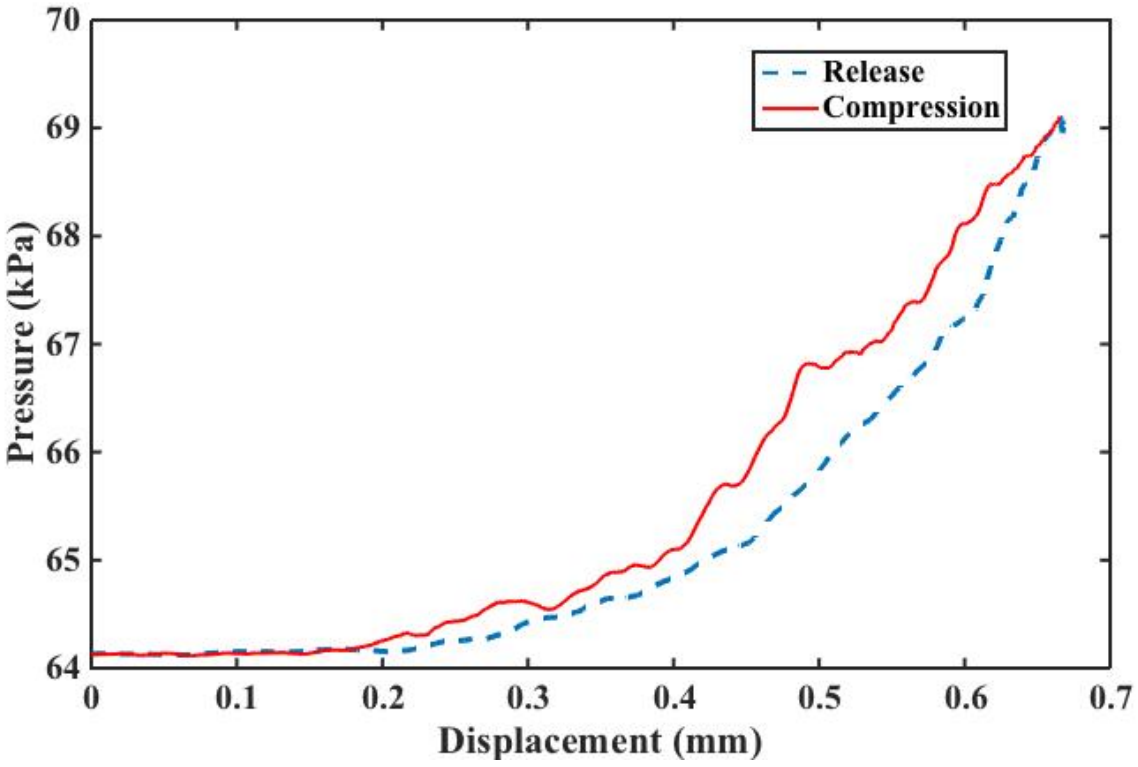

Figure 5.21 Smoothed pressure-displacement curves obtained for plantar soft tissue at heel using wearable ultrasonic and force sensors adhered to the participant's heel.

It seems that the quality of this curve is not as good as previous one. The reason is that in the previous experiment data was acquired from end part of heel, where fewer numbers of scattering echoes existed. Also in previous experiment both sensors were placed on top of a flat plate while in this test sensors were attached to the heel and uneven load was applied on the sensors, which in turns increased the number of outliers. However the developed method worked and pressure-displacement curve was obtained in continuous movement over a period of time.

5.4 Results and Discussion

Using developed system applied force and its resulting displacement was successfully measured while the participant stepping and the pressure-displacement curve was extracted.

In this thesis work the elastic behavior of plantar soft tissue was investigated. Plantar soft tissue nonlinearity is associated with its inelastic behaviour. Once a structure achieves its maximum attainable stress, additional loading will cause response to deviate from the initial elastic behaviour. Since in this study *in-vivo* test was performed on human subjects, all measurements were done in linear range and it was impossible to find the nonlinear span and yield strength of soft tissue but since plantar soft tissue is a tendon, according to the reference handbooks its ultimate tensile strength and strain is 50-100 Mpa and 10-15% respectively [84].

Chapter 6: Conclusion and Future Work

The following chapter concludes the thesis and provides a summary of the results. Some suggestions for future research are presented as well.

6.1 Conclusion

In this research, we have proposed a method, using wearable force and ultrasonic sensors, for continuous monitoring of the mechanical properties of soft tissue over a period of time. A thin and flexible force sensor was selected and calibrated. A proper drive circuit with respect to the required sensitivity, measurement range and linearity for this application was developed to integrate force sensor to the measurement system and an equation was extracted to find a relationship between applied force to the sensor and its output voltage. A PVDF ultrasonic sensor was used for tissue displacement measurement. This sensor is thin and flexible as well. Using this sensor continuous monitoring of tissue displacement is feasible.

The SNR of a commercial ultrasonic transducer and PVDF sensor was measured using soft tissue mimicking phantoms including silicone rubber and pork sirloin. Results revealed that commercial transducer has stronger SNR than PVDF sensor and can be used as a reference for sound speed measurements in phantoms for performance evaluation tests. Also the SNR of PVDF transducer is good enough to separate echo and noise and PVDF could be used for displacement measurement in this application.

Four different ultrasonic methods including, Position of Positive Peak of the Echo, Position of Peak in Absolute Value of Signal, Position of the Largest Peak in Envelope and Cross-Correlation was used for measuring known displacement using PVDF sensor in test with phantoms. Result proved that under quasi-static condition and when the

number of scattering echoes is very low, cross-correlation is the most consistent technique for displacement measurement.

The performance of presented measurement system was evaluated using soft tissue mimicking phantoms by examining the accuracy, precision and hysteresis of force and ultrasonic sensors. Measuring accuracy, reproducibility and hysteresis of developed system showed that our measurement system covers the minimum required spatial resolution and is good enough for measuring soft tissue mechanical properties in this application.

In-vivo experiment was conducted while a participant placed end part of her heel on top of the force and PVDF sensors and bending forward and backward to create time-varying force on the measurement system. A method for simultaneous measurement of force and displacement in continuous mode was developed and pressure-displacement curve for plantar soft tissue at heel region was obtained for one compression-release cycle where mechanical properties of plantar soft tissue such as Young's modulus and stiffness were computable.

The effect of applying uneven load on measurement system was evaluated while both force and PVDF sensors were fixed in the shoe and a participant was stepping. It was found that in this condition the number of outliers increase dramatically. Some DSP technique was applied to remove those outliers and to measure displacement in continuous mode as explained in details in the section 5.4. An M-mode image of plantar soft tissue at heel region was used to verify developed method and algorithm of soft tissue displacement measurement.

The real condition of use was simulated by adhering force and PVDF sensors to the participant's heel and stepping with shoe and sock. In this condition the number of scattering echoes was raised. To solve the problem data was acquired with higher frame rate and averaging filter was applied to reduce the noise. The initial location of echo in each compression-release cycle was pre-estimated using an M-mode image of ultrasonic RF signals to validate displacement measurement. Additionally the size of the time window that included the desired echo was shrunk to avoid interference with scattering echoes during displacement measurement. Therefore using the proposed method and sensors, pressure-displacement curve for plantar tissue over one compression-release cycle was obtained where certain tissue mechanical properties such as Young's modulus and stiffness are computable.

While this research focused on the diabetic foot, the investigated technology can be used to monitor the mechanical properties of any soft tissue in the body, such as within a prosthetic socks or a cast. The presented work has established a basis for future study on the feasibility of real time continuous monitoring of soft tissues that should provide a tool for diabetic foot monitoring and management.

6.2 Future Research

As mentioned before, the main intent of this research was developing a wearable ultrasonic stiffness sensor for continuous monitoring of soft tissue mechanical properties. The research was done to establish a measuring system and method for continuous and simultaneous examination of applied pressure to the soft tissue and its resulting displacement. The following section outlines some suggestions for future work and study.

While in this work, FlexiForce sensor was selected for force measurement and its performance with respect to the required sensitivity, measurement range and linearity was acceptable, it is suggested that different thin and flexible sensor be examined and their performance for continuous and real time monitoring of force be compared to find more accurate and precise sensor with lower hysteresis.

Research indicates that the temperature of in-shoe plantar and FlexiForce sensor increases over time. Force sensor manufacturer recommends that sensors should be calibrated at the same temperature for which testing will occur. So it is suggested to add a temperature sensor to the measuring system and calibrate the sensor at some temperatures and use the proper calibration file for each temperature to ensure more accurate results. It could be beneficial for ulcer formation too. Bernard *et al*. showed that a minimum of 2.2 °C of difference between high-risk area under the foot can occur days before the skin breaks [85]. Foot temperature measurement demonstrates that the average of temperature in no diabetic people and diabetic patients is 29.1 °C and 31.2 °C respectively [86].

The pressure signal in the *in-vivo* test revealed some noise. Processing signal in frequency domain may help to find the source of noise and design a proper digital filter to remove noises and smooth the signal.

Another area that warrants future research is studying the effect of applied load frequency and speed on the mechanical properties of soft tissue.

Also it is recommended to optimize the measurement configuration and perform some clinical trial with diabetic patients to investigate the ability of measurement system for distinguishing between the mechanical properties of healthy and diabetic patients.

A statistical study can be conducted to measure soft tissue stiffness at different area of human body such as breast and back to find other applications for this system and its potential use for cancer prediction or skin injury prevention.

In addition, further investigation is necessary to find the limitations of this method and PVDF transducer for real time monitoring in embedded environment. It is essential to check that if inserting embedded device into the shoe for diabetic patient with neuropathy or into the mattress for motionless patients increase the risk of ulcer formation or not.

Appendices

Appendix A Real Time Measurement of Force

In this study, a digitizer was used as an interface to digitize analog output voltage of force sensor and record data. Since the final goal of this project is to develop an embedded stiffness measuring system, we need to replace interface data acquisition system with microcontroller. A primitive work was performed where a microcontroller board was used for real time monitoring of applied force. This board is Atmel SAM3X8E ARM Cortex-M3 CPU based and has a 32-bit ARM core microcontroller. Based on the required specifications for plantar soft tissue force monitoring, the Arduino Due board was a proper choice.

In the first step, the board was programmed for serial communication to receive the analog data from sensor. Arduino Due has 12 analog inputs and the maximum voltage that I/O pins can tolerate is 3.3V. Applying more than 3.3V will damage the board. Then it is important to choose the proper value for R_F to adjust the maximum gain of FlexiForce sensor less than 3.3V. The resolution of analog pins is 12 bits. It is set to 10 bits by default but it is possible to change it in software [87]. By programming the board the output voltage of sensor was displaying on serial port window continuously.

But for monitoring purpose, it was necessary to send numeric data to computer and graph the results. To end up, the Processing software was chosen. Processing is an open source development tool for writing programs to "talk" with an Arduino. Using the “Processing” it is possible to display or save some data collected by the Arduino.

A program was written in Processing and the force signal was displayed on the computer screen as seen in Fig. A.1.

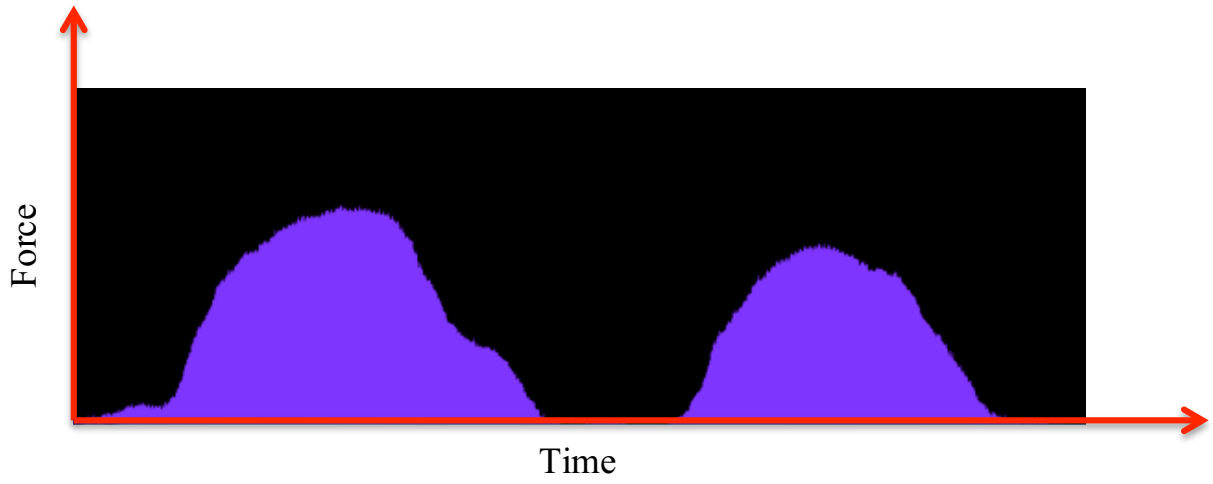

Figure A.1 Real-time display of applied force to the plantar soft tissue at heel during two compression-release cycles

In addition the program was developed to read the data from two analog inputs simultaneously and graph the results.

Below is the source code that was written in Arduino environment to read analog output voltage of force sensor and print them in the serial monitor window.

```
int analogpin1=0;
int analogpin2=1;
void setup() {
Serial.begin(9600);
}
void loop() {
  int val1=analogRead(analogpin1);
  int val2=analogRead(analogpin2);
  float voltage1= val1*(3.3/1023);
  float voltage2= val2*(3.3/1023);
  Serial.print(val1);
  Serial.write(",");
  Serial.print(val2);
  Serial.write(".");
}
```

Following program takes ASCII-encoded strings from the serial port at 9600 baud rate and graphs them.

```
 import processing.serial.*;
Serial port;

String val1 = "";
String val2 = "";
String data = "";
int index = 0;
int xPos1 = 0;
int xPos2 = 900;
PFont font;

void setup(){
 size(1800,950);
 port = new Serial(this, Serial.list()[2], 9600 );
 port.bufferUntil('.');
 font = loadFont("AlNile-70.vlw");
 textFont(font,70);

 background(0);
}
void draw(){

}

void serialEvent (Serial port){

  try{
 data = port.readStringUntil('.');
 data = data.substring (0, data.length() - 1);

 index=data.indexOf(",");

 val1 = data.substring(0 , index);
 val2 = data.substring(index+1 , data.length());

 int inByte1 = int(val1);
 float voltage1 = inByte1*(3.3/1023);
 float force1 = 43*voltage1+2.95;

 int inByte2 = int(val2);
 float voltage2 = inByte2*(3.3/1023);
```

```
float force2 = 43*voltage2+2.95;

stroke(255);
line(900,0,900,950);
stroke(127,34,255);
line(xPos1, height, xPos1, height - inByte1);
line(xPos2, height, xPos2, height - inByte2);

if (xPos1 >= width/2) {
xPos1 = 0;
xPos2 = 900;
background(0);
fill(46,209,2);
text("V1=", 10,75);
text(voltage1,90,75);
text(force1,70,175);
text(voltage2,470,75);
text(force2,470,175);
}
else {
xPos1++;
xPos2++;
}
 }
catch(RuntimeException e) {
   e.printStackTrace();
}
}
```

Appendix B Elastography

Elastography is a relatively new medical imaging modality that maps the elasticity of soft tissue. Development of elastography returns to the 1990s in the purpose of providing more clinical information of internal organs of the human body. Physicians perform palpation to examine the stiffness of some tissues but this technique is limited to the superficial organs. Wherever palpation is used to acquire clinical information, elastography can be used and it can be applied to the deeper organs [19].

In elastography the Young's modulus is imaged quantitatively, which is the physical parameter corresponding to the stiffness. For this purpose, a distortion is created in the soft tissue and the change of mechanical properties is measured to quantify the elasticity of tissue. The main idea for processing the distortion is that soft tissues are more elastic than hard tissues and by a given applied force their mechanical properties such as strain changes more. Also the velocity of mechanical waves in the soft tissue is less in comparison with the stiffer tissues.

Depending on the way the distortion is created and also based on the way that is chosen for observing the distortion, different techniques for elastography have been developed. A mechanical device, ultrasound waves or natural distortion during the physiological process can induce distortion in the soft tissue. Induced distortion can be static or dynamic. At present, the major tools for observing the distortion are ultrasound and magnetic resonance imaging (MRI).

The method that uses MRI for observing the mechanical properties of the tissue is called MRE (Magnetic Resonance Elastography). The most prominent techniques for elastography that use ultrasound are Quasi-static elastography, Transient elastography,

Acoustic Radiation Force Impulse Imaging (ARFI), Shear Wave Elasticity Imaging (SWEI) and Supersonic Shear Imaging (SSI) or Shear Wave elastography (SWE). In the following section each method is explained briefly.

B.1 Magnetic Resonance Elastography (MRE)

In MRE a shear wave is applied to the body to create distortion and the MRI is used to acquire the image depicting the propagation of the induced shear waves. This image is processed to produce quantitative tissue stiffness (Elastogram). MRE is noninvasive, accurate and reproducible method and can be implemented in the conventional MRI by some hardware and software modifications. This technique is limited to the superficial organs, however its application in brain, breast, blood vessels, heart, lung, pancreas and kidney has been reported and it is a safe and reliable alternative for liver biopsy [88].

B.2 Ultrasound Elastography

In this case the ultrasound is used for imaging.

B.2.1 Quasi-static

In this technique a constant stress is applied to the tissue to make compression and the image is taken using ultrasound as shown in Fig. B.1. This image indicates the displacement of the tissue, which is proportional to the external stress. Generated strain is estimated using two-dimensional correlation of ultrasound images and Young's modulus can be calculated through Eq. 2.2. In this method the ultrasound images before and after compression are compared. The areas that deformed more are less stiff and vice versa [89].

Quasi-static ultrasound elastography is easy to implement and is widely spread in the world especially for breast lesions classification but has some disadvantages. When an external force is applied to the tissue, it is likely that the objects move into or out of the image, which cause problem in image interpretation. Also the tissues that are not close to the surface cannot be compressed easily.

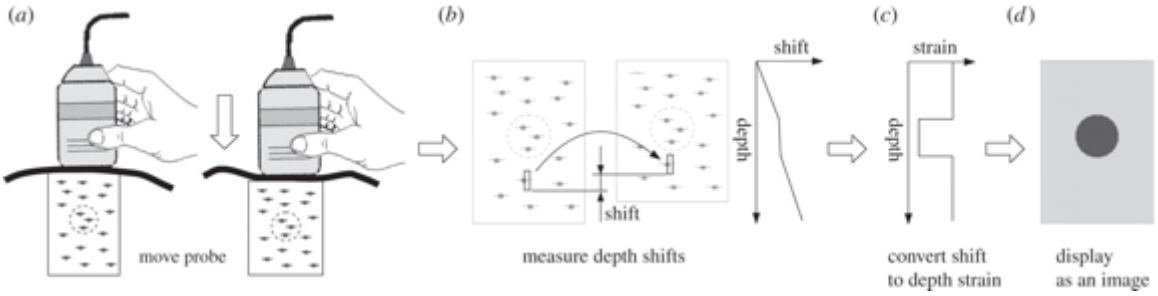

Figure B.1 Overview of Quasi-Static elastography: (a) The scan with a conventional ultrasound probe (b) displacement in the axial direction. (c) Strain estimation in the axial direction (d) Image [90]

B.2.2 Continuous Methods

In this method the applied stress is not constant and changes with time. The time-varying force can be a short transient mechanical force or an oscillatory force with a constant frequency. The produced waves are longitudinal or shear. Shear waves are some kind of elastic waves that do not travel in the flat plane. Longitudinal waves can be generated at high frequencies while shear waves are only generated at low frequencies (10 – 2000 Hz). The longitudinal waves propagate very quickly in the human body (1500 m/s) but shear waves propagate more slowly (1 – 50 m/s) and their speed in the body is related to the medium density and shear modulus.

Continuous methods produce higher resolution images in comparison with quasi-static but required system and processing methods are more complicated.

B.2.2.1 Transient Elastography

This non-invasive method gives a one-dimensional image of tissue stiffness and mostly used for measuring the liver fibrosis. In this technique ultrasound wave in the form of shear waves is applied to the tissue and the Young's modulus is displayed as a one-dimensional image [91].

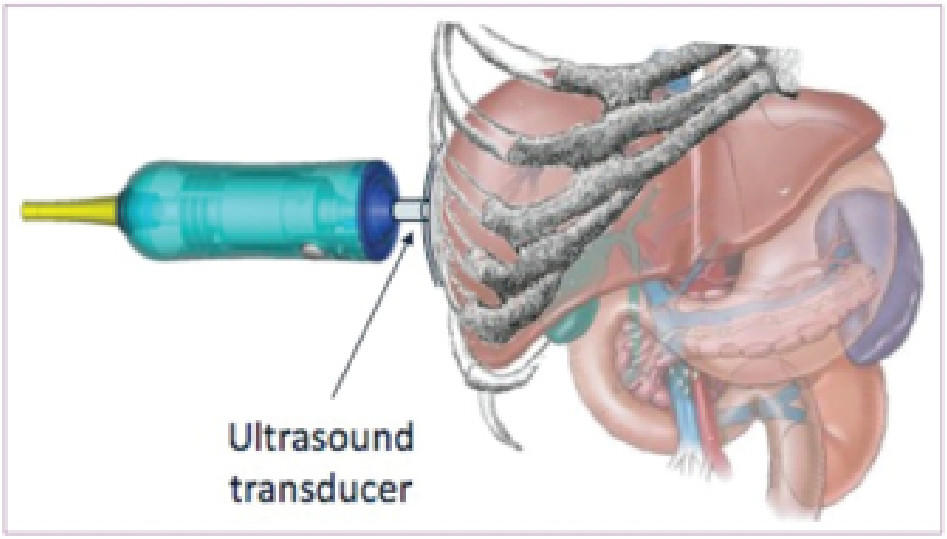

Figure B.2 Transient elastography for the measurement of liver fibrosis [91]

This method is noninvasive and its results are instantaneous, so it has the potential to be replaced with liver biopsy.

B.2.2.2 Acoustic Radiation Force Impulse imaging (ARFI)

In ARFI method, an acoustic wave is applied to the tissue to create a distortion and an image will produced to map the stiffness. In this technique ultrasound beam pushes the tissue along its focused beam and the amount of tissue that push down along this beam, determine the tissue stiffness. By pushing different places, an image is obtained. It is obvious that softer tissues are deformed more than stiffer ones.

B.2.2.3 Shear Wave Elasticity Imaging (SWEI)

This technique is as same as ARFI with the exception that the created distortion waves travel sideways as a shear wave. Using ultrasound, the shear velocity can be measured and be converted to the stiffness. ARFI produces an image, while SWEI indicates the stiffness value in some locations. In comparison with other methods of elastography these two techniques can create stronger distortions and are applicable to the deeper tissues.

B.2.2.4 Supersonic Shear Imaging (SSI)/Shear Wave Elastography (SWE)

In this method, like SWEI, the shear wave is applied to the tissue and using many near simultaneous pushes and ultrafast imaging technique, a two-dimensional image is produced, which reflects the tissue's stiffness.

Appendix C Analyzed Data and Applied Code in Simulation Test with Phantoms

In this section a sample of data obtained in simulation test with phantoms along with source code of software used to program the movement of positioning device are presented.

C.1 Sample of Analyzed Data in Simulation Test with Phantom

Raw data obtained in simulation test with silicone rubber phantom and pork sirloin were analyzed to measure the created displacement in phantoms. Four different ultrasonic methods were used to find the time delay of ultrasonic RF echo.

C.1.1 Position of Positive Peak in the Echo

Following tables show analyzed data related to the measurement cycle #1 of simulation test with silicone rubber phantom and pork sirloin respectively where time delay of ultrasonic RF signal was calculated by finding the position of positive peak.

Table C-1 Sample of data analysis in performance evaluation test with silicone rubber phantom where "Position of Positive Peak" method was used to analyze data.

Measurement Cycle #1							
Ultrasonic Transducer	Position in Movement Pattern	Frames	Position of Positive Peak in the Average of Ultrasonic RF Echo (# Sample)	Time (μs)	Δt (μs)	Sound Speed (m.s-1)	Displacement (mm)
Commercial	P0	1 - 65	4614	36.91			
	P1	70 - 117	4543	36.34	0.5680	1073	0.6096
	P2	120 - 168	4469	35.75	0.5920	1030	0.6096
	P3	174 - 223	4396	35.17	0.5840	1044	0.6096
	P4	226 - 273	4322	34.58	0.5920	1030	0.6096
	P5	280 - 325	4251	34.01	0.5680	1073	0.6096
	P6	330 - 377	4177	33.42	0.5920	1030	0.6096
	Avg.			35.17	0.5827	1047	0.6096
	SD			1.260	0.0118	21.36	0.0000
Ultrasonic Transducer	Position in Movement Pattern	Frames	Position of Positive Peak in the Average of Ultrasonic RF Echo (# Sample)	Round Trip Required Time (μs)	Time (μs)	Δt (μs)	Displacement (mm)
PVDF	P0	1 - 65	9209	73.67	36.84		
	P1	70 - 117	8980	71.84	35.92	0.9160	0.9831
	P2	120 - 168	8828	70.62	35.31	0.6080	0.6261
	P3	174 - 223	8681	69.45	34.72	0.5880	0.6138
	P4	226 - 273	8621	68.97	34.48	0.2400	0.2471
	P5	280 - 325	8392	67.14	33.57	0.9160	0.9831
	P6	330 - 377	8245	65.96	32.98	0.5880	0.6055
	Avg.			69.66	34.83	0.6427	0.6764
	SD			2.657	1.087	0.2525	0.2771

Table C-2 Sample of data analysis in performance evaluation test with pork sirloin where "Position of Positive Peak" method was used to analyze data.

Measurement Cycle #1							
Ultrasonic Transducer	Position in Movement Pattern	Frames	Position of Positive Peak in the Average of Ultrasonic RF Echo (# Sample)	Time (μs)	Δt (μs)	Sound Speed (m.s-1)	Displacement (mm)
Commercial	P0	1 - 60	4018	32.14			
	P1	70 - 115	3975	31.80	0.3440	1772	0.6096
	P2	120 - 165	3931	31.45	0.3520	1732	0.6096
	P3	170 - 220	3887	31.10	0.3520	1732	0.6096
	P4	225 - 270	3844	30.75	0.3440	1772	0.6096
	P5	275 - 320	3802	30.42	0.3360	1814	0.6096
	P6	330 - 375	3761	30.09	0.3280	1859	0.6096
	Avg.			31.11	0.3427	1780	0.6096
	SD			0.6415	0.0094	49.22	0.0000
Ultrasonic Transducer	Position in Movement Pattern	Frames	Position of Positive Peak in the Average of Ultrasonic RF Echo (# Sample)	Round Trip Required Time (μs)	Time (μs)	Δt (μs)	Displacement (mm)
PVDF	P0	1 - 60	7925	63.4	31.7		
	P1	70 - 115	7899	63.19	31.60	0.1040	0.1843
	P2	120 - 165	7811	62.49	31.24	0.3520	0.6096
	P3	170 - 220	7723	61.78	30.89	0.3520	0.6096
	P4	225 - 270	7635	61.08	30.54	0.3520	0.6238
	P5	275 - 320	7553	60.42	30.21	0.3280	0.5951
	P6	330 - 375	7469	59.75	29.88	0.3360	0.6245
	Avg.				30.866	0.3040	0.5411
	SD				0.6441	0.0985	0.1752

C.1.2 Position of Peak in the Absolute Value of Signal

Following tables show analyzed data related to the measurement cycle #1 of simulation test with silicone rubber phantom and pork sirloin respectively where time delay of ultrasonic RF signal was calculated by finding the position of positive peak in absolute value of signal.

Table C-3 Sample of data analysis in performance evaluation test with silicone rubber phantom where "Position of Largest Peak in Absolute Value" method was used to analyze data.

Measurement Cycle #1							
Ultrasonic Transducer	Position in Movement Pattern	Frames	Position of Peak in the Absolute Value of Average of Ultrasonic RF Echo (# Sample)	Time (μs)	Δt (μs)	Sound Speed (m.s-1)	Displacement (mm)
Commercial	P0	1 - 65	4614	36.91			
	P1	70 - 117	4543	36.34	0.5680	1073	0.6096
	P2	120 - 168	4469	35.75	0.5920	1030	0.6096
	P3	174 - 223	4396	35.17	0.5840	1044	0.6096
	P4	226 - 273	4322	34.58	0.5920	1030	0.6096
	P5	280 - 325	4251	34.01	0.5680	1073	0.6096
	P6	330 - 377	4177	33.42	0.5920	1030	0.6096
	Avg.			35.17	0.5827	1047	0.6096
	SD			1.260	0.0118	21.36	0.0000
Ultrasonic Transducer	Position in Movement Pattern	Frames	Position of Peak in the Absolute Value of Average of Ultrasonic RF Echo (# Sample)	Round Trip Required Time (μs)	Time (μs)	Δt (μs)	Displacement (mm)
PVDF	P0	1 - 65	9156	73.25	36.62		
	P1	70 - 117	9015	72.12	36.06	0.5640	0.6053
	P2	120 - 168	8870	70.96	35.48	0.5800	0.5972
	P3	174 - 223	8716	69.73	34.86	0.6160	0.6430
	P4	226 - 273	8574	68.59	34.30	0.5680	0.5849
	P5	280 - 325	8427	67.42	33.71	0.5880	0.6311
	P6	330 - 377	8276	66.21	33.10	0.6040	0.6220
	Avg.			69.75	34.88	0.5867	0.6139
	SD			2.538	1.105	0.0203	0.0219

Table C-4 Sample of data analysis in performance evaluation test with pork sirloin where "Position of Largest Peak in Absolute Value" method was used to analyze data.

Measurement Cycle #1							
Ultrasonic Transducer	Position in Movement Pattern	Frames	Position of Peak in the Absolute Value of Average of Ultrasonic RF Echo (# Sample)	Time (μs)	Δt (μs)	Sound Speed (m.s-1)	Displacement (mm)
Commercial	P0	1 - 60	4018	32.14			
	P1	70 - 115	3975	31.80	0.3440	1772	0.6096
	P2	120 - 165	3931	31.45	0.3520	1732	0.6096
	P3	170 - 220	3887	31.10	0.3520	1732	0.6096
	P4	225 - 270	3844	30.75	0.3440	1772	0.6096
	P5	275 - 320	3802	30.42	0.3360	1814	0.6096
	P6	330 - 375	3761	30.09	0.3280	1859	0.6096
	Avg.			31.11	0.3427	1780	0.6096
	SD			0.6415	0.0094	49.22	0.0000
Ultrasonic Transducer	Position in Movement Pattern	Frames	Position of Peak in the Absolute Value of Average of Ultrasonic RF Echo (# Sample)	Round Trip Required Time (μs)	Time (μs)	Δt (μs)	Displacement (mm)
PVDF	P0	1 - 60	7962	63.696	31.848		
	P1	70 - 115	7873	62.98	31.49	0.3560	0.6309
	P2	120 - 165	7811	62.49	31.24	0.2480	0.4295
	P3	170 - 220	7697	61.58	30.79	0.4560	0.7897
	P4	225 - 270	7635	61.08	30.54	0.2480	0.4395
	P5	275 - 320	7553	60.42	30.21	0.3280	0.5951
	P6	330 - 375	7469	59.75	29.88	0.3360	0.6245
	Avg.				30.857	0.3287	0.5848
	SD				0.6121	0.0775	0.1349

C.1.3 Position of Largest Peak in the Echo's Envelope

Following tables show analyzed data related to the measurement cycle #1 of simulation test with silicone rubber phantom and pork sirloin respectively where time delay of ultrasonic RF signal was calculated by finding the position of largest peak in the signal envelope.

Table C-5 Sample of data analysis in performance evaluation test with silicone rubber phantom where "Position of Largest Peak in Envelope of Signal" method was used to analyze data.

Measurement Cycle #1							
Ultrasonic Transducer	Position in Movement Pattern	Frames	Position of Peak in the Envelope of Average of Ultrasonic RF Echo (# Sample)	Time (μs)	Δt (μs)	Sound Speed (m.s-1)	Displacement (mm)
Commercial	P0	1 - 65	4617	36.94			
	P1	70 - 117	4545	36.36	0.5760	1058	0.6096
	P2	120 - 168	4472	35.78	0.5840	1044	0.6096
	P3	174 - 223	4398	35.18	0.5920	1030	0.6096
	P4	226 - 273	4324	34.59	0.5920	1030	0.6096
	P5	280 - 325	4252	34.02	0.5760	1058	0.6096
	P6	330 - 377	4178	33.42	0.5920	1030	0.6096
	Avg.			35.18	0.5853	1042	0.6096
	SD			1.266	0.0079	14.06	0.0000
Ultrasonic Transducer	Position in Movement Pattern	Frames	Position of Peak in the Envelope of Average of Ultrasonic RF Echo (# Sample)	Round Trip Required Time (μs)	Time (μs)	Δt (μs)	Displacement (mm)
PVDF	P0	1 - 65	9182	73.46	36.73		
	P1	70 - 117	9042	72.34	36.17	0.5600	0.5927
	P2	120 - 168	8889	71.11	35.56	0.6120	0.6388
	P3	174 - 223	8731	69.85	34.92	0.6320	0.6508
	P4	226 - 273	8600	68.80	34.40	0.5240	0.5396
	P5	280 - 325	8455	67.64	33.82	0.5800	0.6138
	P6	330 - 377	8310	66.48	33.24	0.5800	0.5972
	Avg.			69.95	34.98	0.5813	0.6055
	SD			2.518	1.089	0.0381	0.0395

Table C-6 Sample of data analysis in performance evaluation test with pork sirloin where "Position of Largest Peak in Envelope of Signal" method was used to analyze data.

Measurement Cycle #1							
Ultrasonic Transducer	Position in Movement Pattern	Frames	Position of Peak in the Envelope of Average of Ultrasonic RF Echo (# Sample)	Time (μs)	Δt (μs)	Sound Speed (m.s-1)	Displacement (mm)
Commercial	P0	1 - 60	4020	32.16			
	P1	70 - 115	3976	31.81	0.3520	1732	0.6096
	P2	120 - 165	3933	31.46	0.3440	1772	0.6096
	P3	170 - 220	3889	31.11	0.3520	1732	0.6096
	P4	225 - 270	3846	30.77	0.3440	1772	0.6096
	P5	275 - 320	3804	30.43	0.3360	1814	0.6096
	P6	330 - 375	3764	30.11	0.3200	1905	0.6096
	Avg.			31.12	0.3413	1788	0.6096
	SD			0.6372	0.0120	65.11	0.0000
Ultrasonic Transducer	Position in Movement Pattern	Frames	Position of Peak in the Envelope of Average of Ultrasonic RF Echo (# Sample)	Round Trip Required Time (μs)	Time (μs)	Δt (μs)	Displacement (mm)
PVDF	P0	1 - 60	7962	63.696	31.848		
	P1	70 - 115	7883	63.06	31.53	0.3160	0.5473
	P2	120 - 165	7800	62.40	31.20	0.3320	0.5883
	P3	170 - 220	7712	61.70	30.85	0.3520	0.6096
	P4	225 - 270	7629	61.032	30.516	0.3320	0.5883
	P5	275 - 320	7542	60.34	30.17	0.3480	0.6314
	P6	330 - 375	7468	59.74	29.87	0.2960	0.5639
	Avg.				30.855	0.3293	0.5881
	SD				0.6270	0.0208	0.0303

C.1.4 Cross-Correlation

Following tables show analyzed data related to the measurement cycle #1 of simulation test with silicone rubber phantom and pork sirloin respectively where time delay of ultrasonic RF signal was calculated using cross-correlation method.

Table C-7 Sample of data analysis in performance evaluation test with silicone rubber phantom where "cross-correlation" method was used to analyze data.

Ultrasonic Transducer	Position in Movement Pattern	Frames	Position of Largest Lag in the Cross-Correlation of Two Consecutive Echoes (# Sample)	Time Lag between two Consecutive Stages of Positioning Device (μs)	Sound Speed (m.s-1)	Displacement (mm)
Commercial	P0	1 - 65				
	P1	70 - 117	72	0.5760	1058	0.6096
	P2	120 - 168	73	0.5840	1044	0.6096
	P3	174 - 223	74	0.5920	1030	0.6096
	P4	226 - 273	73	0.5840	1044	0.6096
	P5	280 - 325	72	0.5760	1058	0.6096
	P6	330 - 377	73	0.5840	1044	0.6096
	Avg.			0.5827	1046	0.6096
	SD			0.0060	10.79	0.0000
Ultrasonic Transducer	Position in Movement Pattern	Frames	Position of Largest Lag in the Cross-Correlation of Two Consecutive Echoes (# Sample)	Time Lag between two Consecutive Stages of Positioning Device (μs)	Sound Speed (m.s-1)	Displacement (mm)
PVDF	P0	1 - 65				
	P1	70 - 117	141	0.5640	1081	0.5969
	P2	120 - 168	142	0.5680	1073	0.5929
	P3	174 - 223	143	0.5720	1066	0.5890
	P4	226 - 273	143	0.5720	1066	0.5971
	P5	280 - 325	140	0.5600	1089	0.5927
	P6	330 - 377	143	0.5720	1066	0.5971
	Avg.			0.5680	1073	0.5943
	SD			0.0051	9.61	0.0033

Table C-8 Sample of data analysis in performance evaluation test with pork sirloin where "cross-correlation" method was used to analyze data.

Ultrasonic Transducer	Position in Movement Pattern	Frames	Position of Largest Lag in the Cross-Correlation of Two Consecutive Echoes (# Sample)	Time Lag between two Consecutive Stages of Positioning Device (μs)	Sound Speed (m.s-1)	Displacement (mm)
Commercial	P0	1 - 60				
	P1	65 - 110	45	0.3600	1693	0.6096
	P2	115 - 160	44	0.3520	1732	0.6096
	P3	170 - 215	44	0.3520	1732	0.6096
	P4	220 - 265	44	0.3520	1732	0.6096
	P5	270 - 315	42	0.3360	1814	0.6096
	P6	325 - 370	40	0.3200	1905	0.6096
	Avg.			0.3453	1768.01	0.6096
	SD			0.0147	77.99	0.0000
Ultrasonic Transducer	Position in Movement Pattern	Frames	Position of Largest Lag in the Cross-Correlation of Two Consecutive Echoes (# Sample)	Time Lag between two Consecutive Stages of Positioning Device (μs)	Sound Speed (m.s-1)	Displacement (mm)
PVDF	P0	1 - 60				
	P1	65 - 110	92	0.3680	1657	0.6231
	P2	115 - 160	89	0.3560	1712	0.6165
	P3	170 - 215	86	0.3440	1772	0.5957
	P4	220 - 265	86	0.3440	1772	0.5957
	P5	270 - 315	84	0.3360	1814	0.6096
	P6	325 - 370	80	0.3200	1905	0.6096
	Avg.			0.3447	1772	0.6084
	SD			0.0165	85.29	0.0110

C.2 Source Code Used to Program Positioning Device

The following codes were used to create the movement pattern of Figs. 4.5 and 4.22 in the positioning device respectively. This program is developed by Dr. Bruno M. Trindade.

Program 1
C
P70
I3M96
P50
I3M96
P50
I3M96
P50
I3M96
P50
I3M96
P50
I3M96
P50
I3M-576
L7
R

Program 2
C
P50
I3M96
P50
I3M96
P50
I3M96
P50
I3M96
P50
I3M96
P50
I3M96
P50

I3M-96
P50
I3M-96

P50
I3M-96
P50
I3M-96
P50
I3M-96
P50
I3M-96
P50
I3M576
I3M-576
L7
R

REFERENCES

[1] Duck FA, Physical Properties of Tissues—A Comprehensive Reference Book, 6th ed., UK: Academic Press, 1990.

[2] Sarvazyan A., "Shear acoustic properties of soft biological tissues in medical diagnostics," J. Acoust. Soc. Am., vol. 93, no. 4, pp. 2329-2330, 1993.

[3] Jia-Hui Sun, Benson K. Cheng, Yong-Ping Zheng, Yan-Ping Huang, Jenny Y. Leung, Gladys L. Cheing, "Changes in the Thickness and Stiffness of Plantar Soft Tissues in People With Diabetic Peripheral Neuropathy," Archives Phys. Medic. Rehab., vol. 92, no. 9, pp. 1484-1489, 2011.

[4] Andrew J.M. Boulton, Robert S. Kirsner and Loretta Vileikyte, "Neuropathic diabetic foot ulcers," New Engl. J. Medic., vol. 351, no. 1, pp. 48– 55, July 2004.

[5] American podiatric medical association, Diabetic wound care, [Online]. Available: http://www.apma.org

[6] Shruti Pai, "Changes in the Mechanical Properties of the Plantar Soft Tissue with Diabetes," Ph.D. Dissertation, Dept. Mech. Eng., Univ. Washington, USA.

[7] C.Y.L. Chao, Y.P. Zheng, and G.L.Y. Cheing, "Epidermal thickness and biomechanical properties of plantar tissues in diabetic foot," Ultrason. Med. Biol., vol. 37, no. 7, pp. 1029–1038, July 2011.

[8] I. AlMohimeed, H. Turkistani, and Y. Ono, "Development of wearable and flexible ultrasonic sensor for skeletal muscle monitoring," in Proc. IEEE Int. Ultrason. Symp. Of

Conf., Prague, 2013, pp. 1137–1140.

[9] Bruno M. Trindade, Yuu Ono, Edward D. Lemaire and Ibrahim AlMohimeed, "Development of a Wearable Ultrasonic Sensor and Method for Continuous Monitoring of Mechanical Properties of Plantar Soft Tissue for Diabetic Patients," *in Proc. IEEE Int. Ultrason. Symp. of Conf.*, Chicago, IL, 2014, pp. 2112-2115.

[10] William J Jeffcoate and Keith G Harding, "Diabetic Foot Ulcers", The Lancet, vol. 361, no. 9368, pp. 21-24, May 2003.

[11] John J. Swierzewski, (2015, Sep. 15), *Muscles, Tendons & Ligaments of the Foot & Ankle* [Online]. Available: http://www.healthcommunities.com

[12] WebMD, Pain Management Health Center, [Online]. Available: http://www.webmd.com

[13] Medspace, Foot Bone Anatomy, [Online]. Available: http://emedicine.medscape.com

[14] Chad Simmons. (2013), [Online]. Available: http://elitefootandanklecenter.com

[15] Harold B. Kitaoka, Zong Ping Luo, Eric S. Growney, Lawrence J. Berglund and Kai-Nan An, "Material Properties of the Plantar Aponeurosis," Foot & anckle Int., vol. 15. No. 10, pp. 557-560, Oct. 1994.

[16] Arturo N. Natali, Piero G. Pavan and Carla Stecco, "A constitutive model for the mechanical characterization of the plantar fascia," Connective Tissue Research, vol. 51, no. 5, pp. 337-346, Oct. 2010

[17] Shelbourne Physiotherapy. (2015), What to do about Plantar Fasciitis?, [Online]. Available: http://www.massagevictoria.com

[18] Docpods. (2016), The Windlass Mechanism in the Foot, [Online]. Available:

http://www.docpods.com

[19] Bellefleur physiotherapy. (2016), plantar-fasciitis-pain-in-the-arch, [Online]. Available: http:// http://www.bellefleurphysio.com

[20] Warren, B.L., "Plantar fasciitis in runners," J. Sport Medic., vol. 10, no. 5, pp. 338–345, Nov. 1990.

[21] J. Greenleaf, "Selected Methods for Imaging Elastic Properties of Biological Tissues," Annu. Review Biomed. Eng., vol. 5, no. 1, pp. 57-78, Aug. 2003.

[22] F. Baumgart, "Stiffness - an unknown world of mechanical science?," Injury, vol. 31, pp. S-B14, S-B23, 2000.

[23] Armen P. Sarvazyan, Oleg V. Rudenko, Scott D. Swanson, J. Brian Fowlkes and Stanislav Y. Emelianov, "Shear wave elasticity imaging: a new ultrasonic technology of medical diagnostics," Ultrason. Med. Biol., vol. 24, no. 9, pp. 1419–1435, 1998.

[24] Mostafa Fatemi and James F. Greenleaf, "Ultrasound-Stimulated Vibro-Acoustic Spectrography," Science, vol. 280, no. 5360, pp. 82-85, Apr. 1998.

[25] R. Muthupillai, D. J. Lomas, P. J. Rossman, J. F. Greenleaf, A. Manduca and R. L. Ehman, "Magnetic resonance elastography by direct visualization of propagation acoustic strain waves," Science, vol. 269, no. 5232, pp. 1854–1857Sep. 1995.

[26] Ophir J, Céspedes I, Ponnekanti H, Yazdi Y and Li X, “Elastography: a quantitative method for imaging the elasticity of biological tissues,” Ultrason. Imag., vol. 13, no.2, pp.111–134. 1991.

[27] Dickinson RJ and Hill CR., “Measurement of soft tissue motion using correlation between A-scans,” Ultrason. Med. Biol., vol. 8, no. 3, pp.263–271, 1982.

[28] Wilson LS and Robinson DE., “Ultrasonic measurement of small displacements and deformation of tissue,” Ultrason. Imag., vol. 4, no. 1, pp.71-82, 1982.

[29] Bjaerum S, Torp H and Kristoffersen K., “Clutter filters adapted to tissue motion in ultrasound color flow imaging,” IEEE Trans. Ultrason. Ferroelec. Freq. Contr., vol. 49, no. 6, pp.693–704, 2002.

[30] Kevin J. Glaser, Armando Manduca and Richard L. Ehman, “Review of MR Elastography applications and recent developments,” J. MRI, vol. 36, no. 4, pp.757–774, Oct. 2012.

[31] Garra BS, Cespedes EI, Ophir J, Spratt SR, Zuurbier RA, Magnant CM and Pennanen MF, “Elastography of breast lesions: initial clinical results,” Radiology, vol. 202, no. 1, pp.79–86, 1997.

[32] Korte Chris L de, Steen Anton F W van der, Céspedes E Ignacio, Pasterkamp Gerard, Carlier Stephane G, Mastik F, Schoneveld Arjen H, Serruys Patrick W and Bom Nicolaas, “Characterization of plaque components and vulnerability with intravascular ultrasound elastography,” Phys. Med. Biol., vol. 45, no. 6, pp.1465–1475, June 2000.

[33] Hoeks APG, Brands PJ, Willigers JM and Reneman RS, “Non-invasive measurement of mechanical properties of arteries in health and disease,” Proc. Inst. Mech. Eng., vol. 213, no. 3, pp.195–202, Mar. 1999.

[34] Levinson SF, Shinagawa M and Sato T., “Sonoelastic determination of human skeletal muscle elasticity,” J. Biomech., vol. 28, no. 10, pp.1145–1154, 1995.

[35] Adler Rs, Rubin Jm, Bland Ph and Carson Pl, “Quantitative tissue motion analysis of digitized M-mode images: gestational differences of fetal lung,” Ultrason. Med. Biol., vol. 16, no. 6, pp.561–569, 1990.

[36] Emelianov SY, Lubinski MA, Skovoroda AR, Erkamp RQ, Leavey SF, Wiggins RC and O'Donnell M., “Reconstructive ultrasound elasticity imaging for renal transplant diagnosis: kidney ex-vivo results,” Ultrason. Imag., vol. 22, no. 3, pp.178–194, 2000.

[37] Kentaro Yoshioka, Naoto Kawabe and Senju Hashimoto, “Transient elastography: Applications and limitations,” Hepatology Research, vol. 38, no. 11, pp.1063–1068, Nov. 2008.

[38] Kyu Sik Jung and Seung Up Kim, “Clinical applications of transient elastography,” Clinic. Molecular Hepatology, vol. 18, no. 2, pp.163-173, June 2012.

[39] Palle Lalitha, Balaji Reddy and K.Jagannath Reddy, “Musculoskeletal applications of elastography: a pictorial essay of our initial experience,” Korean J. Radiology, vol. 12, no. 3, pp. 365 – 375, June 2011.

[40] Drakonaki EE, Allen GM and Wilson DJ., "Ultrasound elastography for musculoskeletal applications," British J. Radiology, vol. 85, no. 1019, pp.1435–1445, Nov. 2012.

[41] Itoh A, Ueno E, Tohno E, Kamma H, Takahashi H, Shiina T, Yamakawa M and Matsumura T, "Breast disease: clinical application of US elastography for diagnosis," Radiology, vol. 239, no. 2, pp. 341-350, May 2006.

[42] Sarah Ostadabbas, Mehrdad Nourani and Adnan Saeed, "A Knowledge-Based Modeling for Plantar Pressure Image Reconstruction," IEEE Trans. Biomed. Eng.,vol. 61, no. 10, pp. 2538 - 2549 , Oct. 2014.

[43] Zhang XF, Zhao YL, Duan ZY and Liu Y, "Design and Test of a Soft Plantar Force Measurement System for Gait Detection," Sensors, vol. 12, no. 12, pp.16628-16640, Dec. 2012.

[44] Susan Stacpoole-Shea,Graeme Shea, and Lawrence Lavery, "An Examination of Plantar Pressure Measurements to Identify the Location of Diabetic Forefoot Ulceration," J. Foot & Ankle Surgery, vol. 38, no. 2, pp. 109-115, 1999.

[45] Rahman Muhammad Afiq, Aziz Zulkarnain, Rajendra Acharya U, Ha Tan Peck, Kannathal N, Ng E.Y.K, Law Chelsea, Subramaniam Tavintharan, Shuen Wong Yue and Fang Sum Chee, "Analysis of plantar pressure in diabetic type 2 subjects with and without neuropathy," ITBM-RBM, vol. 27, no. 2, pp.46–55, 2006.

[46] Jee Chin Teoh, V.P.W. Shim and Taeyong Lee, "Quantification of plantar soft tissue changes due to aging in various metatarsophalangeal joint angles with realistic tissue

deformation," J. Biomech., vol. 47, no. 12, pp. 3043–3049, Oct. 2012.

[47] Jan YK, Lung CW, Cuaderes E, Rong DQ and Boyce K, "Effect of viscoelastic properties of plantar soft tissues on plantar pressures at the first metatarsal head in diabetics with peripheral neuropathy," Physiolog. Measure., vol. 34, no. 1, pp. 53-66, Jan. 2013.

[48] David G. Armstrong, Lawrence A. Larvey, "Diabetic Foot Ulcers: Prevention, Diagnosis and Classification," vol. 57, no. 6, pp. 1325-1332, Mar. 1998.

[49] Best Practice Advocacy Centre New Zealand (bpaz^{nz}). (2010), Screening and management of "The Diabetic Foot" [Online]. Available: http://www.bpac.org.nz.

[50] Oyer DS, Saxon D and Shah A., " Quantitative assessment of diabetic peripheral neuropathy with use of the clanging tuning fork test," PubMed, vol. 13, no. 1, pp. 5-10, Jan. 2007.

[51] Evan D. Williams, "Quantifying Patient-Specific Plantar Soft Tissue Stiffness using Magnetic Resonance Imaging and a Hydraulic Loading Device", Ph.D. dissertation, Dept. Mech. Eng., Univ. Washington, Wash. 2015.

[52] Zheng YP, Huang YP, Zhu YP, Wong M, He JF and Huang ZM, "Development of a foot scanner for assessing the mechanical properties of plantar soft tissues under different bodyweight loading in standing," Med. Eng. Phys., vol. 34, no. 4, pp. 506–511, May 2012.

[53] Parker D, Cooper G, Pearson S, Crofts G, Howard D, Busby P and Nester C, "A device for characterising the mechanical properties of the plantar soft tissue of the foot," Med. Eng. Phys., vol. 37, no. 11, pp. 1098–1104, Nov. 2015.

[54] S. Pai and W. R. Ledoux, "The compressive mechanical properties of diabetic and non-diabetic plantar soft tissue," J. Biomech., vol. 43, no. 9, pp. 1754–1760, June 2010.

[55] S. Pai and W. R. Ledoux, "The shear mechanical properties of diabetic and non-diabetic plantar soft tissue," J Biomech, vol. 45, no. 2, pp. 364–370, Jan. 2012.

[56] S. Pai and W. R. Ledoux, "The quasi-linear viscoelastic properties of diabetic and non-diabetic plantar soft tissue," Ann. Biomed. Eng., vol. 39, no. 5, pp. 1517–1527, May 2011.

[57] Chao Clare Y.L, Zheng Yong-Ping, Huang Yan-Ping and Cheing Gladys L.Y, "Biomechanical properties of the forefoot plantar soft tissue as measured by an optical coherence tomography-based air-jet indentation system and tissue ultrasound palpation system," Clinical Biomech., vol. 25, no. 6, pp. 594–600, 2010.

[58] Rachel Lai-Chu Kwan, Yong-Ping Zheng and Gladys Lai-Ying Cheing, "The effect of aging on the biomechanical properties of plantar soft tissues," Clinic. Biomech., vol. 25, no. 6, pp. 601–605, July 2010.

[59] J. L. Prince and J. M. Links, "The Physics of Ultrasound," in Medical Imaging: Signals and Systems, 2nd ed. Pearson, 2006.

[60] P.R. Hoskins, A. Thrush, K. Martin and T.A. Whittingham, Diagnostic Ultrasound Physics and Equipment, London, England: Greenwich Medical Media Limited, 2003.

[61] W. R. Hedrick, D. L. Hykes, and D. E. Starchman, Ultrasound Physics and Instrumentation, 4th ed., Missouri, U.S.A: Elesvier Mosby, 2005.

[62] W. R. Hedrick, D. L. Hykes, and D. E. Starchman, Ultrasound Physics and Instrumentation, 4 ed. Missouri, U.S.A: Elesvier Mosby, 2005.

[63] Mathworks. (2016), Envelope Detection [Online]. Available: http://www.mathworks.com.

[64] Reza Zahiri-Azar and Septimiu E. Salcudean, "Motion Estimation in Ultrasound Images Using Time Domain Cross-correlation With Prior Estimates," IEEE Trans. Biomed. Eng., vol. 53, no. 10, pp. 1990 – 2000, 2006.

[65] Jacques Riviere, Sylvain Haupert, and Pascal Laugier, "Nonlinear ultrasound: Potential of the cross-correlation method for osseointegration monitoring," J. Acoust. Soc. Am., vol. 132, no. 3, pp- EL202 - EL207, Sep. 2012.

[66] Che-Chou Shen, Yi-Hong Chou and Pai-Chi Li, "Pulse Inversion Techniques in Ultrasonic Nonlinear Imaging," J Med Ultrasound, vol. 13, no. 1, pp. 3-17, 2005.

[67] Colette Ridehalgh, Ann Moore and Alan Hough, "Repeatability of measuring sciatic nerve excursion during a modified passive straight leg raise test with ultrasound imaging," Manual Therapy, vol. 17, no. 6, pp. 572-576, Dec. 2012.

[68] Tekscan. FlexiForce A401 sensor, [Online]. Available: http://www.tekscan.com

[69] Vernier. (2016), Logger Pro 3, Quick Reference Manual, [Online]. Availabe: http://www.vernier.com

[70] Vernier. (2016), Force Plate, [Online]. Availabe: http://www.vernier.com

[71] Rick S. Hall, Geoffrey T. Desmoulin and Theodore E. Milner, "A technique for conditioning and calibrating force-sensing resistors for repeatable and reliable measurement of compressive force," J. Biomech., vol. 41, no. 16, pp. 3492–3495, 2008.

[72] Andrew G. Herbert-Copley, Emily H. Sinitski, Edward D. Lemaire and Natalie Baddour, "Temperature and measurement changes over time for F-Scan sensors," in *Proc. IEEE Int. Symp. Med. Measur. App. Of Conf.*, Gatineau, QC, 2013, pp. 265-267.

[73] Microchoip. MCP6001/1R/1U/2/4, 1 MHz, Low-Power Op Amp, [Online]. Available: http://www.microchip.com

[74] Sarah Ostadabbas, Adnan Saeed, Mehrdad Nourani and Matthew Pompeo, "Sensor architectural tradeoff for diabetic foot ulcer monitoring," in *Proc. IEEE Eng Med Biol Soc of Conf.*, San Diego, CA, 2012, pp. 6687–6690.

[75] Ostadabbas Sarah, Nourani Mehrdad, Saeed Adnan, Yousefi Rasoul and Pompeo Matthew, "A knowledge-based modeling for plantar pressure image reconstruction", IEEE Trans. Biomed. Eng., vol. 61, no. 10, pp. 2538–2549, 2014.

[76] H. Ohigashi, "Ultrasonic transducers in the megahertz range," in The Application of Ferroelectric Polymers, Glasgow, UK: Blackie, 1987, Chap. 11, pp. 237-273.

[77] L. F. Brown, "Design considerations for piezoelectric polymer ultrasound transducers," IEEE Trans. Ultrason. Ferroelectr. Freq. Control., vol. 47, no. 6, pp. 1377-1396, 2000.

[78] A. Lanatà, E. P. Scilingo, and D. De Rossi, “A multimodal transducer for cardiopulmonary activity monitoring in emergency,” IEEE Trans. Inf. Technol. Biomed., vol. 14, no. 3, pp. 817-825, 2010.

[79] Koch Tim, Lakshmanan Sannachi, Brand Sebastian, Wicke Michael, Raum Kay and Mörlein Daniel, “Ultrasound velocity and attenuation of porcine soft tissues with respect to structure and composition: I. Muscle”, Meat Sci., vol. 88, no. 1, pp. 51–58, 2011.

[80] Velmex (2016), Motor-Driven BiSlide, [Online]. Available:http://www.velmex.com.

[81] Don H. Johnson (2006), Signal-to-niose ratio, [Online]. Available: http://Scholarpedia.org

[82] Shruti Pai, “The shear mechanical properties of diabetic and non-diabetic plantar soft tissue,” J Biomech., vol. 54, no. 2, pp. 364 – 370, Jan. 2012.

[83] Shruti Pai, WilliamR.Ledoux, “The compressive mechanical properties of diabeti cand non-diabetic plantar soft tissue,” J Biomech., vol. 43, no. 9, pp. 1754 – 1760, 2010

[84] Gerhard A. Holzapfel, “Biomechanics of Soft Tissue,” in *Computational Biomechanics,* Graz, Austria, 2000, ch. 2, pp. 3

[85] T. Bernard, “ An early detection system for foot ulceration in diabetic patients,” in *Proc. IEEE 35th Ann. Northest Bioeng. Of Conf*., Boston, MA, pp. 1-2, 2009.

[86] J. Gutiérrez Martínez, F.J., “Development of an electronic equipment for the pre medical diagnose in the progress of diabetic foot disease,” *in Proc. Int. Control, Decision IT of Conf*., Metz, 2014, pp. 679-683.

[87] Arduino (2016), Arduino Due, [Online]. Available: http://www.arduino.cc

[88] Sudharshan Parthasarathy, Bradley D. Bolster and Frank H. Miller (2012, Jan.),

Magnetic Resonance Elastography: Proven Indications, Challenges and Future Considerations, [Online]. Available: http://static.healthcare.siemens.com

[89] Gennisson J-L, Deffieux T, Fink M and Tanter M, "Ultrasound elastography: Principles and techniques", Diagnos. Intervent. imag., vol. 94, no. 5, pp. 487 – 495, May 2013.

[90] Treece G, Lindop J, Chen LJ, Housden J, Prager R and Gee A., "Real-time quasi-static ultrasound elastography," Interface Focus, vol. 1, no. 4, pp- 540-552, Aug. 2011.

[91] Nezam H. Afdhal, "Fibroscan (Transient Elastography) for the Measurement of Liver Fibrosis," Gastroenterol Hepatol, vol. 8, no. 9, pp.605-607, Sep. 2012.